NEW THERAPIES FOR CREB3L1-DEFICIENT TRIPLE NEGATIVE BREAST CANCER

A Thesis Submitted to the
College of Graduate and Postdoctoral Studies
In Partial Fulfillment of the Requirements
For the Degree of Master of Science
In the Department of Pharmacology
University of Saskatchewan
Saskatoon

By

Riley Brianna Plett

PERMISSION TO USE

In presenting this thesis/dissertation in partial fulfillment of the requirements for a Postgraduate degree from the University of Saskatchewan, I agree that the Libraries of this University may make it freely available for inspection. I further agree that permission for copying of this thesis/dissertation in any manner, in whole or in part, for scholarly purposes may be granted by the professor or professors who supervised my thesis/dissertation work or, in their absence, by the Head of the Department or the Dean of the College in which my thesis work was done. It is understood that any copying or publication or use of this thesis/dissertation or parts thereof for financial gain shall not be allowed without my written permission. It is also understood that due recognition shall be given to me and to the University of Saskatchewan in any scholarly use which may be made of any material in my thesis/dissertation.

DISCLAIMER

Reference in this thesis/dissertation to any specific commercial products, process, or service by trade name, trademark, manufacturer, or otherwise, does not constitute or imply its endorsement, recommendation, or favoring by the University of Saskatchewan. The views and opinions of the author expressed herein do not state or reflect those of the University of Saskatchewan, and shall not be used for advertising or product endorsement purposes.

Requests for permission to copy or to make other uses of materials in this thesis/dissertation in whole or part should be addressed to:

Head of the Anatomy, Physiology and Pharmacology Department
GA20 Health Sciences Building, 107 Wiggins Road
University of Saskatchewan
Saskatoon, Saskatchewan S7N 5E5 Canada

OR

Dean
College of Graduate and Postdoctoral Studies
University of Saskatchewan
116 Thorvaldson Building, 110 Science Place
Saskatoon, Saskatchewan S7N 5C9 Canada

ABSTRACT

The lack of targeted therapies for triple-negative breast cancer (TNBC) contributes to their high mortality rates and high risk of relapse compared to other subtypes of breast cancer. Developing targeted therapies for TNBC is an unmet clinical need. Our lab has described metastasis suppressor cAMP-responsive element-binding protein 3- like protein 1 (CREB3L1) deficiency as a novel molecular feature of TNBCs. CREB3L1 has been shown to function as a metastasis suppressor in breast cancer, downregulating genes involved in tumorigenesis, angiogenesis, migration and invasion.

In this project, inhibitors that selectively block the growth and/or survival of metastatic CREB3L1-deficient breast cancer cells have been identified and validated as new treatments for CREB3L1-deficient breast cancers. A global drug discovery approach was used to screen 1,818 FDA-approved drugs for their ability to kill CREB3L1-deficient TNBC cells at 1μM. Of the 47 drugs identified, 27 drugs were then confirmed as killing CREB3L1-deficient TNBC cells in validation experiments. The 27 drugs were then titrated out over a range of concentrations to determine their ability to selectively kill CREB3L1-deficient TNBC cells at concentrations lower than 1 μM.

Four compounds, palbociclib isethionate, cladribine, isolanid and homoharringtonine, were validated as selectively killing CREB3L1-deficient TNBC cells significantly more than CREB3L1 re-expressing cells at concentrations lower than 1 μM. The majority of these drugs also killed non-tumorigenic control normal breast cells (MCF10A cells) at these same concentrations, with the exception of cladribine. Importantly, three of the four promising drugs identified, with the exception of isolanid, displayed synergistic interactions when combined with standard of care chemotherapeutic reagent doxorubicin, reducing the dose required to achieve the desired cytotoxic response. Furthermore, the selective CREB3L1-deficient effects of these compounds were exhibited across multiple CREB3L1-deficient TNBC cell lines, suggesting they may be broadly applicable for the treatment of TNBCs.

The top four compounds identified in this project show promise as more selective therapies for CREB3L1-deficient TNBC and their further evaluation *in vivo* and possible future clinical implementation would address the unmet clinical need of designing targeted therapies for TNBC.

ACKNOWLEDGEMENTS

Firstly, I would like to thank Dr. Deborah Anderson, my supervisor, for her many years of guidance and encouragement. Her brilliance, composure, and dedication to science has been an example to me of the health professional I hope to one day become. The time I have spent learning from her over the past 5 years has formed me into a better student, researcher and person.

I would like to thank my advisory committee, Dr. Franco Vizeacoumar, Dr. Stanley Bardal and Dr. Kaushik Desai for their insightful feedback over the course of my graduate studies. Thank you for investing your time in my academic growth and in this project.

I would like to thank our wonderful collaborators, Dr. Franco Vizeacoumar and Frederick Vizeacoumar for their exceptional experimental and analytical assistance in performing the initial drug screen at the Phenogenomic Imaging Centre of Saskatchewan (a facility established by Dr. Vizeacoumar).

Next, I would like to thank the Anderson Lab, past and present members, for their patience, support and teachings. Especially, I would like to thank Dr. Paul Mellor and Stephanie Kendal. I would like to thank Stephanie for always having the answers to my questions, and for sharing her vast knowledge and expertise. I am extremely grateful to Dr. Mellor for his exceptional mentorship throughout my studies, for providing crucial feedback as I developed my thesis and his experimental work in the initial drug screen. Thank you as always for your thorough instruction, patient affirmation and kind guidance.

Thank you to Austin Hammond for his extraordinary analytical assistance. Thank you for sharing your talents and careful computational explanations. Specifically, thank you for performing the synergy analysis on the combination data in this project.

Finally, I am thankful for the scholarship support I have received from: Canadian Graduate Scholarship – Master's (CIHR); the College of Graduate and Postdoctoral Studies and the department of Anatomy, Physiology and Pharmacology. As well, I am thankful to the sponsor of this study, the College of Medicine (CoMRAD, 421028).

DEDICATION

I dedicate this thesis to my family who always listen to me and assure me. To my husband, Maxton, my parents, Kevin and Nadine, and my siblings, Kolton and Charis.

LIST OF TABLES

LIST OF FIGURES

LIST OF ABBREVIATIONS

1 x PBS	1 x phosphate buffered saline
AB	ApexBio
AChE	acetylcholinesterase
AG	AdipoGen
AQ	AdooQ Bioscience
ATCC	American Type Culture Collection
BCL-2	B cell lymphoma-2
BL	basal-like
CC	Cayman Chemical
CKD 4/6	cyclin dependent kinase 4/ cyclin dependent kinase 6
CREB3L1	cAMP-responsive element-binding protein 3-like protein 1
DCK	deoxycytidine kinase
DMF	Dimethylformamide
DMSO	Dimethyl Sulfoxide
EGF	epidermal growth factor
EGFR	epidermal growth factor receptor
ER	estrogen receptor
ERK	extracellular signal regulated kinase 1/2
ETOH	ethanol
FBS	fetal bovine serum
G418	geneticin
HA	hemagglutinin
HCS	High content screening
HDACs	histone deacetylases
HER2	human epidermal growth factor receptor 2
HSA	highest simple agent
HTS	High-throughput screening
IM	immunomodulatory
J&K	J&K Scientific
JAK	Janus kinase
LAR	luminal androgen receptor
LC	LC Laboratories
M	mesenchymal
MAO-A	monoamine oxidase-A
MCE	MedChemexpress CO. Ltd

MEK1	MAP (Mitogen-Activated Protein) Kinase/ERK (Extracellular Signal-Regulated Kinase) Kinase 1
MMPs	matrix metalloproteinases
MSL	mesenchymal stem-like
mTOR	mammalian target of rapamycin
PARP	poly (ADP-ribose) polymerase
PDE	Phosphodiesterase
PenStrep	Penicillin-Streptomycin
PERK	protein kinase-like endoplasmic reticulum kinase
PI3K	phosphatidylinositol 3-kinases
PKC	protein kinase C
PR	progesterone receptor
PTEN	phosphatase and tensin homolog
RAR	retinoic acid receptor
Rb	retinoblastoma
RFP	red fluorescent protein
RNR	ribonucleotide reductase
ROS	reactive oxygen species
SA	Sigma Aldrich
SC	Selleckchem
SE	standard error
SMBS	StressMarqBioSciences Inc.
STAT	signal transducer and activator of transcription
STAT3	signal transducer and activator of transcription 3
THR	thyroid hormone receptor
TNBC	triple negative breast cancer
ZIP	zero interaction potency

Table of Contents

1. BACKGROUND

1. 1 Breast Cancer

Breast cancer is the 2nd leading cause of death from cancer in Canadian women, affecting approximately 1 in 8 (Canadian Cancer Society, 2018). The four major subtypes of breast cancer are: luminal A, luminal B, human epidermal growth factor receptor 2 positive (HER2+) and triple negative breast cancer (TNBC) (Canadian Cancer Society, 2015). Breast cancer is not a single disease, but a heterogenous group of many diseases, characterized by clinical parameters and molecular entities (Eroles, Bosch, Pérez-Fidalgo & Lluch, 2012). The current best standards for treatment of different breast cancers depends on the subtype and stage of the cancer. Early stage breast cancer treatment plans often include surgery and/or radiotherapy (Di Leo et al., 2015). Breast cancer subtypes are distinguished using immunohistochemical analysis which identifies tissue-based biomarkers estrogen receptor (ER) progesterone receptor (PR) and HER2. Luminal A breast cancers express hormone receptors (ER+, PR±). Luminal B breast cancers express hormone receptors (ER+, PR±) and HER2 (HER2+). HER2+ breast cancers express HER2 (HER2+). TNBCs lack the receptors that characterize the other 3 major subtypes of breast cancer (ER-, PR-, HER2-) (Fig 1.1).

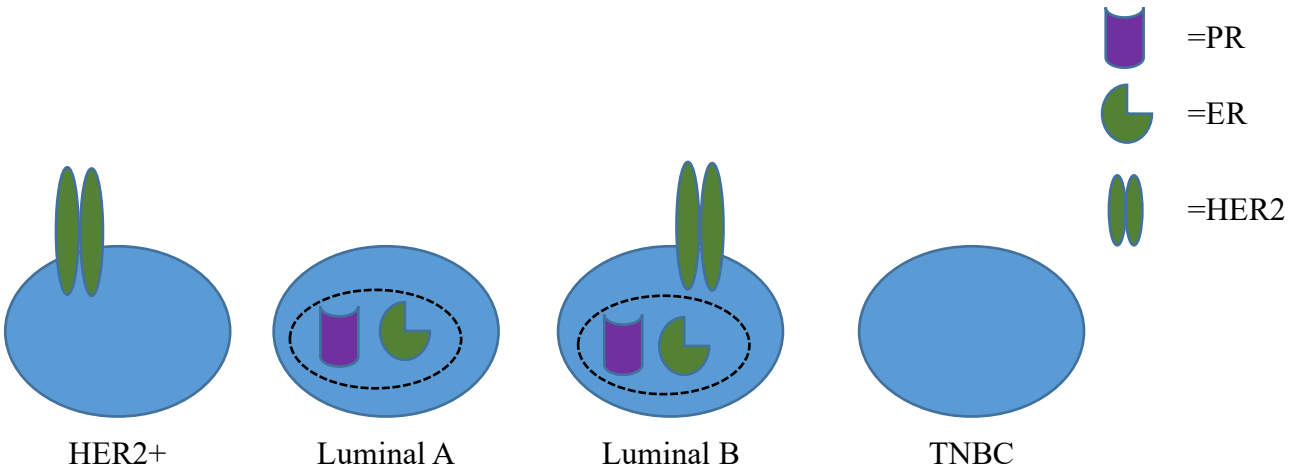

Fig. 1.1: The four major clinical subtypes of breast cancer and the receptors they express. PR = Progesterone receptor; ER = estrogen receptor; HER2 = human epidermal growth factor receptor 2; TNBC = triple negative breast cancer.

Identifying intrinsic molecular subtypes would complement tissue-based biomarker analyses, and this is currently under investigation for clinical implementation in breast cancer management (De Laurentiis et al., 2010; Rossing et al., 2018).

1. 2 Approaches to HER2+ Breast Cancer

The HER2+ subtype encompasses 10-15% of all breast cancers (Canadian Cancer Society, 2015). HER2 is overexpressed in this subtype and is a direct driver of pathogenesis (Perou et al., 2000; Slamon et al., 2001; Sørlie et al., 2001). Targeted therapies such as monoclonal antibodies have been developed to interfere with HER2 dimerization and activation of downstream pathways and/or cause degradation of the receptor (Eroles, Bosch, Pérez-Fidalgo & Lluch, 2012). Trastuzumab is a monoclonal antibody commonly used to treat the HER2+ subtype (Eroles, Bosch, Pérez-Fidalgo & Lluch, 2012). The use of this targeted therapy greatly improved survival outcomes over the course of 1 year in early stage HER2+ breast cancer in an adjuvant setting, with no additional benefit seen after 2 years use (Cameron et al., 2017). Survival outcomes were also improved in locally advanced and inflammatory breast cancer settings (Gianni et al., 2010). However, advanced, metastatic HER2+ breast cancer patients almost always progress due to resistance. Additional therapies such as immune checkpoint inhibitors, cyclin dependent kinase 4/ cyclin dependent kinase 6 (CDK4/6) inhibitors and phosphatidylinositol 3-kinases/Akt/mammalian target of rapamycin (PI3K/Akt/mTOR) pathway inhibitors are being investigated in clinical trials and could potentially improve patient outcomes (Pernas & Tolaney, 2019).

1. 3 Approaches to Luminal A and Luminal B Breast Cancers

Breast cancers of the luminal A subtype account for 40% of all breast cancers and those of the luminal B subtype account for 20% (Canadian Cancer Society, 2015). Luminal A and B breast cancers can be treated with endocrine (hormone) therapy due to the presence of hormone receptors (Eroles, Bosch, Pérez-Fidalgo & Lluch, 2012). They express progesterone (PR+) and/or estrogen (ER+) receptors.

Luminal A breast cancers (ER+, PR±, HER2-) can usually be targeted with therapies that target their ER function due to their estrogen dependency. These endocrine therapies include aromatase inhibitors, selective ER modulators, and in some instances, selective ER degraders (Bardia et al., 2019; Cardoso et al., 2018; Coates et al., 2015). Aromatase inhibitors (e.g.

letrozole/Femara) block the synthesis of estrogen (Coates et al., 2015). Selective ER modulators (e.g. tamoxifen) prevent estrogen from acting on the estrogen receptor (Cardoso et al., 2018). The use of selective ER degraders (e.g. fulvestrant) can be used to treat postmenopausal women (that already naturally produce less estrogen) with disease progression and these compounds bind the ER protein and cause proteasomal degradation of the receptor (Bardia et al., 2019). However, resistance often develops to these therapies and estrogen dependency is often lost (Angus, Beije, Jager, Martens & Sleijfer, 2017; Fribbens et al., 2016; Reinert, Gonçalves & Bines, 2018). For metastatic luminal A breast cancers, a combination of CDK4/6 inhibitors and aromatase inhibitors can be given depending on whether the patient is pre or post-menopausal (Jacquet et al., 2018). Chemotherapy can also be used to treat metastatic luminal A breast cancer (Jacquet et al., 2018). Additionally, newer, more selective therapies have been emerging to overcome the resistance and evolution of ER+HER2- metastatic disease, that target the cell cycle (CDK inhibitors and PI3K pathway inhibitors) and DNA repair pathways (poly (ADP-ribose) polymerase, or PARP inhibitors) (Robson, Goessl & Domchek, 2017; Turner, Neven, Loibl & Andre, 2017).

Luminal B breast cancers (ER+, PR±, HER2+) usually have high expression of proliferative marker and prognostic predictor, Ki67, and typically respond to trastuzumab therapy (which selectively targets HER2) as well as endocrine therapies and variably to chemotherapy (Eroles, Bosch, Pérez-Fidalgo & Lluch, 2012).

1. 4 Approaches to TNBC and Reoccurring Metastatic Breast Cancer - Chemotherapy

The TNBC subtype accounts for 15-20% of all breast cancers (Canadian Cancer Society, 2015). TNBC, unlike the other subtypes, currently lacks validated clinically actionable molecular markers (Eroles, Bosch, Pérez-Fidalgo & Lluch, 2012). TNBCs (ER-, PR-, HER2-) do not express the biological markers that characterize the other clinical breast cancer subtypes. Therefore, targeted therapies are not available to treat breast cancers of this subtype.

Targeted therapies for the other breast cancer subtypes are initially effective, however, patients often relapse. Unfortunately, chemotherapy is currently the best clinical option to treat reoccurring metastatic breast cancer and TNBC (Eroles, Bosch, Pérez-Fidalgo & Lluch, 2012).

Chemotherapy can be used as an adjuvant or neoadjuvant therapy (given before or after surgery) in early and locally advanced stages of breast cancer (American Cancer Society, 2019). Chemotherapeutic treatment regimens for reoccurring metastatic and TNBC rely on a number of

currently recommended cytotoxic therapies approved for the general breast cancer population (André & Zielinski, 2012). Selection of chemotherapeutic reagents is based on a number of factors including the patient's age, the size of the tumor, whether or not the cancer is present in axillary nodes, the ability of the cancer to invade lymph nodes and vasculature, and histological characteristics of the cancer (Griffiths & Olin, 2012).

Adjuvant and neoadjuvant chemotherapy (for early and locally advanced breast cancers) typically involves treating with combinations of chemotherapeutic drugs, whereas advanced breast cancers are usually treated with chemo monotherapy, unless the course of action is to give dose dense chemotherapy, where certain cycles of chemotherapeutic reagents are given closer together (American Cancer Society, 2019). For example, in Saskatchewan, the current standard of care for reoccurring metastatic breast cancer and TNBC is to give doxorubicin (an anthracycline) with cyclophosphamide (an alkylating agent) once every 2 weeks for four cycles, followed by paclitaxel (a taxol that suppresses microtubule dynamics during mitosis) once per week for 12 cycles, whereas traditionally, cycles of chemotherapy are given 3 weeks at a time. Giving dose-dense therapy to HER2 negative patients has been shown to improve survival outcomes (Citron, 2008).

The chemotherapeutic mechanism of action differs across classes of agents and is better characterized in some more than others. Major chemotherapy breast cancer drug classes target: DNA synthesis and repair complexes (alkylating compounds, platinum compounds, and taxanes), p53 (taxanes), or cell proliferation (anthracyclines). For any current chemotherapy employed in metastatic reoccurring and TNBC, the clinical response to certain compounds is variable, likely due to the molecular complexity and heterogeneity of breast cancer.

Anthracyclines like hallmark chemotherapeutic reagent doxorubicin have greatly improved survival outcomes in metastatic breast cancer and TNBC (Gennari & D'Amico, 2011; Isakoff, 2010). These drugs exert their anti-cancer effects by interfering with cell replication on many levels, like by inhibiting DNA topoisomerase II (Minotti, Menna, Salvatorelli, Cairo & Gianni, 2004). Despite many neoadjuvant trials demonstrating the efficacy of anthracyclines in metastatic breast TNBC, there is evidence to suggest that this may depend on the heterogenous intrinsic TNBC subtypes. Subgroup analyses yield mixed results for anthracycline-based therapies. In some molecular TNBCs there has been lack of benefit, whereas basal-like TNBCs have typically seen favorable outcomes (Wahba & El-Hadaad, 2015). Alternatively, other subgroup analyses have

suggested basal-like TNBCs might not receive a particular benefit from anthracycline treatments over other cytotoxic treatments within TNBC (Glendenning, Irshad & Tutt, 2012).

Alkylating agents, like hallmark chemotherapeutic reagent cyclophosphamide have provided improvements in response rates to chemotherapy and the best rates of therapeutic success with these agents occur in BRCA1 mutation carriers (Bergin & Loi, 2019). These compounds covalently modify DNA (often by cross-linking DNA) and repair attempts result in DNA breaks and eventually cell death (Chaney & Sancar, 1996). It is likely the success these agents have shown in TNBC is due to the DNA damage induced by the alkylating agent itself combined with the frequent presence of the BRCA1 mutation in TNBC which leads to insufficient DNA repair (Bergin & Loi, 2019; Kondo, Takahashi, Ono & Ohnishi, 2010).

Taxanes arrest cells in the G2 and M phases of the cell cycle through the inhibition of microtubules, which leads to cell death (Gradishar, 2012). Taxanes are important drugs used in metastatic breast cancer and TNBC, but their use in TNBC has not shown benefit over their use in non-TNBC (Carey et al., 2007; Ghersi, Wilcken, Simes & Donoghue, 2005; Griffiths & Olin, 2012). As well, *in vitro* evidence has reported BRCA1 mutations might convey resistance to taxanes (Tassone et al., 2003). However, a paper by Prat *et al.*, comparing the benefits of docetaxel (a taxane – derivative) vs carboplatin (a platinum containing agent) in basal-like vs non-basal like TNBC, showed no benefit of one over the other for basal-like patients, and there was increased sensitivity to docetaxel in non-basal like metastatic TNBC (2015). Given these different responses to taxanes within TNBC, categorizing patients by gene expression when deciding which of these chemotherapeutic reagents to prescribe would be beneficial.

There is a high level of evidence of increased toxicity and little-to-no survival benefit with the use of platinum agents within metastatic breast cancer (Egger et al., 2017). However, platinum agents have recently regained interest as treatments for TNBC. Cisplastin is one of the representative platinum-containing drugs of choice. New preclinical data and improved methods for managing side effects suggest that platinum agents might be of particular use in TNBC due to their shared characteristics with BRCA1 mutated breast cancers, with the caveat being that not all TNBCs have this mutation (Wahba & El-Hadaad, 2015). There is also some evidence for the benefit of these agents specifically within the TNBC metastatic setting (Glendenning, Irshad & Tutt, 2012).

Unfortunately, despite the benefit of chemotherapy in metastatic reoccurring and TNBC

(with the exception of certain molecular contexts) chemotherapeutic reagents also induce significant cellular damage, and as a result, numerous iatrogenic complications. Chemotherapies are not targeted therapies and are cytotoxic to all rapidly dividing cells (cancerous or non-cancerous). Chemotherapeutic drugs are toxic pharmaceuticals and are not well tolerated (Clark, Finkel, Rey & Whalen, 2012). Chemotherapy drugs typically have a narrow therapeutic index (Clark, Finkel, Rey & Whalen, 2012). Acute and long-lasting adverse effects associated with chemotherapy largely impacts the quality of life of patients. Acute side effects can often include severe vomiting, bone marrow suppression, alopecia, stomatitis, and predisposition to infection (Clark, Finkel, Rey & Whalen, 2012). Certain chemotherapy drugs cause specific adverse reactions, like bladder toxicity, cardiotoxicity and pulmonary fibrosus (Clark, Finkel, Rey & Whalen, 2012). In addition, psychological distress has also been shown to be related to chemotherapy and is a major issue facing breast cancer patients (Milanti, Metsälä & Hannula, 2016). Chemotherapy is a challenging therapy for patients to endure that can weaken, and in some ways, harm patients while helping fight the cancer.

Resistance is another challenging issue within chemotherapy. Many breast cancer cell types are inherently resistant to anti-cancer drugs and others can develop resistance due to the cytotoxic effects of the treatment (Martin, Smith & Tomlinson, 2014). There are multiple mechanisms by which this can occur, and many are still unknown. In addition, cancer cells can acquire multi-drug resistance (Martin, Smith & Tomlinson, 2014).

Clinically, molecular markers that are predictive of treatment effectiveness have not yet been characterized and validated in metastatic reoccurring and TNBC. It is possible that this lack of information on biomarkers within metastatic reoccurring and TNBC could explain the high percentage of patients that do not have a complete response to chemotherapy and eventually relapse. This knowledge gap has also prevented the development of novel treatment plans for patients and the development of targeted therapies for metastatic reoccurring and TNBC making it an unmet clinical need.

Our lab has previously identified a transcription factor, cAMP-responsive element-binding protein 3-like protein 1 (CREB3L1), whose expression is lost in metastatic human and rat breast cancer but is endogenously expressed in non-metastatic cells. Recently, our lab has shown that in breast cancer CREB3L1 acts as a metastasis suppressor and that its loss directly contributes to the metastatic properties of breast cancer cells (Mellor, Deibert, Calvert, Bonham, Carlsen & Anderson, 2013; Ward

et al., 2016). Since CREB3L1 is lost in highly metastatic breast cancer cells, it cannot be directly targeted for therapy. However, CREB3L1-deficiency can be used as a novel molecular signature to identify metastatic reoccurring and TNBC cells and to develop new therapies specifically effective against these metastatic cells.

1. 5 CREB3L1

CREB3L1 belongs to the family of CREB/ATF transcription factors and functions to regulate gene expression (Ward et al., 2016). Under normal conditions, CREB3L1 is ubiquitously expressed and is located in the endoplasmic reticulum (Fig. 1.2). It traffics to the Golgi complex in response to cell stress and is cleaved by regulated intramembrane proteolysis, yielding a mature protein that translocates to the nucleus and regulates gene expression (Kondo et al., 2012).

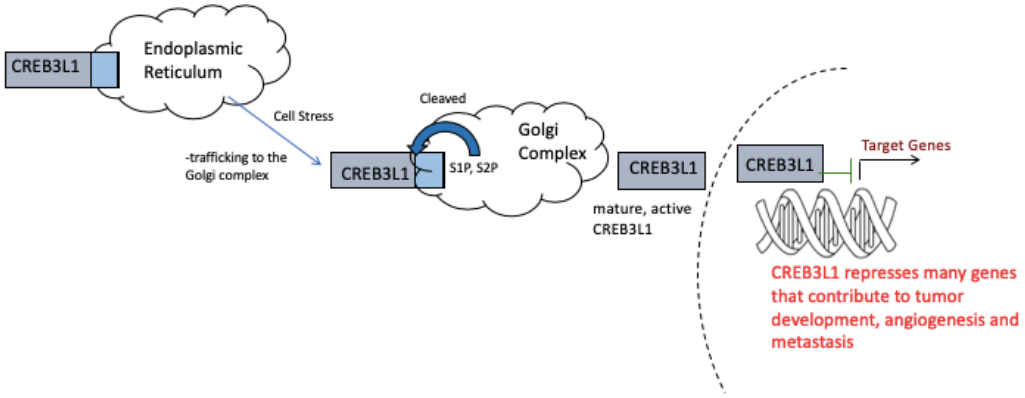

Figure 1.2: CREB3L1 and its role in gene regulation.

CREB3L1 is a unique endoplasmic reticulum stress response protein (Honma et al., 1999). Endoplasmic reticulum stress can occur due to a number of factors, including hypoxia, oxidative stress, depleted nutrients, mutant proteins or even viral infections (Dufey, Sepúlveda, Rojas-Rivera & Hetz, 2014; Pahl, 1999). Stress in the endoplasmic reticulum results in the accumulation of unfolded proteins, which can disrupt the function of the cell. The general role of stress response proteins is to restore normal protein folding, by increasing the folding capacity of the endoplasmic reticulum, reducing the translation of new proteins and increasing the degradation of misfolded proteins to alleviate the accumulation of unfolded proteins (Wang & Kaufman, 2012). A lengthened response to endoplasmic reticulum stress can result in apoptosis (Dufey, Sepúlveda, Rojas-Rivera & Hetz, 2014). In response to endoplasmic reticulum stress CREB3L1 is activated and suppresses metastasis by repressing the expression of genes involved in promoting breast cancer progression, angiogenesis, migration, invasion and metastasis (Fig. 1.2) (Mellor, Deibert,

Calvert, Bonham, Carlsen & Anderson, 2013).

Our laboratory has shown that expression of CREB3L1 suppresses the metastatic properties of breast cancer cells, including cell migration and invasion (Mellor, Deibert, Calvert, Bonham, Carlsen & Anderson, 2013). Re-expressing CREB3L1 in highly metastatic CREB3L1-deficient breast cancer cells inhibited migratory and invasive properties of the cells, as well as the ability of the cells to form colonies in soft agar. Reciprocally, the knockdown of CREB3L1 in poorly metastatic, CREB3L1-expressing cells increased the migratory and invasive properties of the breast cancer cells and the ability of the cells to form colonies in soft agar. Additionally, in rats, re-expression of CREB3L1 in metastatic breast cancer cells has been shown to block tumor progression, angiogenesis and metastasis (Mellor, Deibert, Calvert, Bonham, Carlsen & Anderson, 2013). Rats injected with CREB3L1-deficient cells formed large primary tumors that metastasized to the popliteal lymph node. In contrast, for cells re-expressing CREB3L1, all metastasis was inhibited in all rats injected. Further, while 70% of the animals injected with cells re-expressing CREB3L1 initially formed primary tumors, many of these primary tumors regressed in size. Upon completion of the experiment, only 30% of the animals in this group had primary tumors. The regression was shown to be the result of a decrease in angiogenesis as the tumors in animals formed from cells re-expressing CREB3L1 had a significant ($P<0.001$) reduction in the total number of blood vessels, particularly large blood vessels (>2 mm diameter), compared to the control CREB3L1-deficient tumors (Mellor, Deibert, Calvert, Bonham, Carlsen & Anderson, 2013).

Re-expressing CREB3L1 in highly metastatic CREB3L1-deficient human TNBC cells significantly reduced metastasis and anchorage-independent growth and had no impact on cell proliferation (Smith et al., unpublished results). In female immune compromised (NOD/SCID/γ) mice models where mice were injected via mammary fat pad with human CREB3L1-deficient TNBC cells and those same cells re-expressing CREB3L1, the CREB3L1 expression caused a significant reduction in tumor growth over time (Smith et al., unpublished results). These results suggest that CREB3L1 acts as a metastasis suppressor in human TNBC.

In low-grade human breast tumors CREB3L1 expression is initially upregulated (Ward et al., 2016). This is in response to the stressful conditions that exist within the tumor environment and allows CREB3L1 to block the transcription of genes that promote cell growth, survival, migration, invasion, angiogenesis and metastasis (Mellor, Deibert, Calvert, Bonham, Carlsen & Anderson, 2013). In contrast, CREB3L1 expression is low in advanced breast tumors (Ward et al.,

2016). This is consistent with our previous work that suggests the loss of CREB3L1 is required for the development of a metastatic phenotype (Mellor, Deibert, Calvert, Bonham, Carlsen & Anderson, 2013; Ward et al., 2016). Approximately 30% of breast cancers have decreased CREB3L1-expression (including ~90% of TNBCs) and these patients usually have a poor prognosis (Ward et al., 2016). Luminal A and TNBC patients with low CREB3L1 expression have a shorter relapse-free survival time (Ward et al., 2016). CREB3L1 therefore has a direct effect on the phenotypes of breast cancer cells and targeting CREB3L1-deficient breast cancer cells shows promise as a new strategy for the development of breast cancer therapies.

1.6 Using Chemotherapy to Treat CREB3L1-Deficient Breast Cancers

Finding new therapies for CREB3L1-deficient breast cancers, which are typically the most metastatic, is an unmet clinical need. The expression of CREB3L1 has also been reported to influence the effectiveness of some chemotherapy agents, specifically doxorubicin (Denard, Lee & Ye, 2012; Denard et al., 2015). The chemotherapeutic reagent doxorubicin is an anthracycline and is used to treat many different types of cancer. In breast cancer, it has been demonstrated that for doxorubicin to exert its effects, CREB3L1 expression is needed (Denard, Lee & Ye, 2012; Denard et al., 2015). CREB3L1-deficient breast cancers (MCF7, ER+) are insensitive to doxorubicin, but when CREB3L1 is re-expressed in these cells, they can become sensitized (Denard, Lee & Ye, 2012). Liver (Huh7) and human fibroblast cells (SV589) endogenously expressing CREB3L1 can become resistant to doxorubicin if CREB3L1 is knocked down within these cells (Denard, Lee & Ye, 2012).

Doxorubicin is thought to be more effective at killing cancer cells that express CREB3L1. This drug induces proteolysis of CREB3L1 in a ceramide-dependent manner, liberating the transcription factor to regulate anti-proliferative genes (Denard, Lee & Ye, 2012; Reynolds, Maurer & Kolesnick, 2004; Senchenkov, Litvak & Cabot, 2001). Doxorubicin increases the production of ceramide, a component of lipid membranes (Reynolds, Maurer & Kolesnick, 2004). Excess ceramide is predicted to trigger the trafficking of CREB3L1 from the endoplasmic reticulum to the Golgi complex where it is processed further to its active form (Fig 1.2) (Denard, Lee & Ye, 2012). It is predicted that CREB3L1 ultimately inhibits cell growth by the regulation of gene expression (Chen, Denard, Lee, Han, Ye & Ye, 2016).

1.7 TNBC Heterogeneity

The heterogeneity of TNBC also presents a challenge for chemotherapy treatment success. 'Unselected' therapies disregard the molecular variety that exists within this subtype. Some reports suggest that TNBC is more chemo-sensitive than other subtypes, but still these patients typically have a poor prognosis (Wahba & El-Hadaad, 2015). This might be attributed to the fact that more than 50-60% of TNBC have intrinsic chemo-resistance (De Laurentiis et al., 2010). These chemo resistant subsets of TNBC need to be characterized so that molecular markers might be identified for more targeted and novel therapeutic approaches. Six different molecular subtypes of TNBC have been identified that each exhibit their own particular gene expression profile. These subtypes include two basal-like (BL1 and BL2) subtypes, compromising 50-75% of TNBCs, and immunomodulatory (IM), mesenchymal (M), mesenchymal stem-like (MSL) and luminal androgen receptor (LAR) subtypes, compromising a much lower percentage of TNBCs, (Hubalek, Czech & Müller, 2017; Lehmann et al., 2011).

One unique feature of the less common mesenchymal subtype of TNBC is that in this cellular context, CREB3L1 does not function as a metastasis suppressor. Instead, CREB3L1 switches to promote metastasis activity through effects of the protein kinase-like endoplasmic reticulum kinase (PERK) signaling pathway (Feng, Jin, Sokol, Reinhardt, Miller & Gupta, 2017). In their study involving the ability of PERK to promote metastasis through the downstream effector CREB3L1, Feng *et al.* found that the metastasis promoting activity of CREB3L1 was specific to the mesenchymal subtype of TNBC and only present in this context because PERK was activated (2014). Mesenchymal TNBCs make up a small percentage of TNBCs. PERK activation is necessary for cancer cells to undergo dissemination once an epithelial to mesenchymal transition has taken place (Feng et al., 2014). In this context, the action of CREB3L1 downstream of PERK signaling favors the development of metastases (Feng et al., 2014).

It is interesting to note that breast cancers with amplified HER2, including both the HER2+ subtype and luminal B breast cancers (ER+, PR±, HER2+), are not impacted by CREB3L1 expression in terms of patient prognosis as determined by progression-free survival (Ward et al., 2016). Thus, as with many molecular features in cancer cells, the impact and function of CREB3L1 expression or deficiency can be modified by the genetic background or cellular context.

1.8 Cancer Drug Discovery

The completion of the Human Genome Project prompted amplified genomic work within cancer research and has resulted in an explosion of targeted cancer drug discovery (Lander et al., 2001). There has been a fundamental shift over the past couple decades in the way cancer target identification is approached. In the past, a much smaller number of oncogenes were known, and a major goal of cancer research was understanding the way in which these gene products functioned. Now, advances in molecular biology have allowed a shift from identifying and understanding single cancer genes and gene products to understanding the more complex web of molecular mechanisms underlying the heterogenous disease (Gibbs, 2000). This altered focus within cancer therapy development could provide insight into the shortcomings of current therapies like "unselected" chemotherapies currently employed in metastatic reoccurring and TNBC.

Through understanding of the biological roles of genes, pathological roles of genes have also been revealed accompanied by many new molecular targets. Development of targeted drugs like Herceptin® (for HER2), Glivec® (for BCR-Abl) and Iressa® (for EGFR) within genomic cancer research exemplifies the success of molecularly targeted approaches to cancer therapy (Workman, 2001). Selective therapies that consider mechanistic targets within breast cancer are expected to be more effective and less cytotoxic than traditional chemotherapeutic approaches. Many new drugs are being developed in preclinical and clinical settings in this post-genome era. This is especially significant within the subtype of TNBC, as selective therapies are needed.

However, while there is great promise within genomic cancer research, the process of developing new targeted therapies is not easy. Defining new cancer genes as molecular targets is only the beginning of a long and expensive endeavor to deliver therapeutic benefit within a clinical setting. Developing a new cancer compound and bringing it to market takes approximately 10-15 years and upwards of $500 million USD (Aherne, McDonald & Workman, 2002).

1.9 High-throughput Drug Screening

High-throughput screening (HTS) is an efficient and effective approach to apply the high throughput technologies and sensitive assays that use small sample sizes to cancer research. HTS, such as the NCI-60 screens (John & John, 2000), can generate a large amount of information about promising compounds including their mechanism of action and selectivity, supporting the goal of precision medicine within cancer research. Thousands of compounds can be screened in a

miniaturized format, in 384-well plates or 1536-well plates with volumes of approximately 50 and 10 μL respectively (Aherne, McDonald & Workman, 2002). This miniaturized format is made more robust and reliable by automated technologies. Furthermore, screening compounds that are already FDA-approved for other non-cancer indications can speed up the otherwise lengthy drug development and testing process. This is especially appealing in TNBC research, where new targeted therapies are an unmet clinical need.

1.10 Research Approach

In this project, a global drug discovery approach was taken by using cutting edge HTS technologies to identify new selective therapies for CREB3L1-deficient TNBC cells (ER-, PR-, HER2-). A library of 1,818 FDA-approved compounds was tested in a human TNBC cell line ±CREB3L1 where the absence of CREB3L1 was employed as a novel molecular signature to identify compounds that selectively killed CREB3L1-deficient metastatic breast cancer cells. The efficacy and potency of the most promising compounds was further evaluated *in vitro* in additional cell lines. Inhibitors that selectively blocked the growth and/or survival of metastatic CREB3L1-deficient breast cancer cells were identified and validated. With further preclinical testing, one or more of these could become a new treatment for CREB3L1-deficient breast cancer, including ~90% of TNBCs that are CREB3L1-deficient.

2. MATERIALS AND METHODS

2.1 Cell Culture

TNBC cell lines HCC1806, HCC38, BT549 and control non-tumorigenic breast cell line MCF10A were obtained from the American Type Culture Collection (ATCC, Manassas, Virginia, USA 30-4500 K) (American Type Culture Collection, 2016). HCC1806 and HCC38 TNBC cell lines were cultured in RPMI 1640 medium containing 10% fetal bovine serum (FBS; 31800022, Gibco, Grand Island, NY, USA). BT549 TNBC cell line was cultured in RPMI 1640 medium (31800022, Gibco, Grand Island, NY, USA) containing 10% FBS and 0.023 U/mL bovine insulin (I6634, Sigma Aldrich). Control non-tumorigenic breast cell line MCF10A was cultured in Advanced DMEM/F12 (12634-010, Gibco, Grand Island, NY, USA) containing 5% horse serum (30-2040, ATCC), 20 ng/mL epidermal growth factor (EGF, E9644, Sigma Aldrich), 10 μg/mL bovine insulin (I6634, Sigma Aldrich), 0.5 μg/mL hydrocortisone (H0135, Sigma Aldrich), and 100 ng/mL cholera toxin (C8052, Sigma Aldrich). Cells were cultured according to ATCC recommendations for fewer than six months from the time of resuscitation. All cell lines were authenticated by the supplier.

Previously, triple-hemagglutinin (HA)-tagged CREB3L1 was re-expressed in CREB3L1-deficient TNBC cells (HCC1806). Additionally, the clonal cell line (HCC1806 +HACREB3L1 Cl3) had been characterized as stably expressing high levels of CREB3L1. The clonal cell line has reduced metastatic properties as compared to the CREB3L1-deficient TNBC HCC1806 cell line, including decreased migration and anchorage-independent growth (Smith et al., unpublished results). The clonal cell line was maintained in RPMI 1640 medium containing 400 μg/mL Geneticin (G418; 11811-031, Gibco).

2.2 Drug Screen

A high-throughput drug screen of an FDA-approved drug library consisting of 1,818 compounds (TargetMol, L1000) was carried out on the TNBC cell line HCC1806 ± HACREB3L1 at the Phenogenomic Imaging Centre of Saskatchewan. Due to the expense of these high throughput screens, the initial drug library screen was carried out at a single drug concentration (1 μM) using one TNBC cell line pair (HCC1806 and HCC1806 HACREB3L1 Cl3), then validated over a larger ranges of drug concentrations using additional cell lines.

2.2.1 Generation of RFP-Expressing Cells

For the purposes of a high-throughput drug screen, HCC1806 cells and HCC1806 +HACREB3L1 Cl3 cells were engineered to express red-fluorescent protein (RFP). Each cell line was transduced with an RFP-encoding lentivirus that also confers hygromycin-resistance (pLJM5). A hygromycin B (10687-010, Invitrogen) kill-curve was carried out to determine the appropriate concentration needed to kill untransduced cells (12.5 µg/mL), allowing the stably-expressing RFP cells to be selected. This allowed live cells, still adhered to the plate to be imaged and counted by the automated imaging fluorescence microscope system, ImageXpress Micro XLS Widefield.

2.2.2 Cell Titration to Determine Optimal Numbers

Since different cell lines can have different proliferation rates and plating efficiencies, the optimum number of cells to plate in each well for each cell line was determined. We had previously determined that HCC1806 cells and HCC1806 +HACREB3L1 Cl3 cells had the same rate of proliferation (Smith et al., unpublished results), so this experiment focused on confirming proliferation rates of RFP-expressing HCC1806 and HCC1806 +HACREB3L1 Cl3 cells and determining the plating efficiency. Cell numbers were titrated in a 384-well black-walled plate (142761, NUNC) so that an optimal number of cells could be identified where on day 5 the wells of the 384-well plates would be ~90% confluent. The RFP-expressing HCC1806 and HCC1806 +HACREB3L1 Cl3 cells were then imaged and counted using the automated imaging microscope, on days 1-5. Cell proliferation was decreased in the both RFP-expressing cell lines compared to numbers previously determined for non-RFP-expressing HCC1806 and HCC1806 +HACREB3L1 Cl3 cell lines, so it was necessary to plate greater numbers of RFP-expressing cells. This could be due to the presence of hygromycin B in the RFP-expressing cell media. The doubling times for non-RFP-expressing and RFP-expressing HCC1806 and HCC1806 +HACREB3L1 Cl3 cells were 24 (Smith et al., unpublished results) and 96 hours, respectively. Generally, there was no difference in the proliferation rate between HCC1806 and HCC1806 +HACREB3L1 Cl3 cells (both RFP-expressing and non-RFP-expressing), although the RFP-expressing HCC1806 cells had a better plating efficiency. Therefore, it was necessary to plate greater numbers of RFP-expressing HCC1806 +HACREB3L1 Cl3 cells.

2.2.3 Initial Drug Library Screen

Utilizing a Biomek FX liquid handling system (A31843), high-throughput dispensing of cells was accomplished in 384-well black-walled plates. On day 0, HCC1806 cells or HCC1806 +HACREB3L1 Cl3 cells (both RFP-expressing) were each seeded in six 384-well plates. In addition, to account for cytotoxicity typically present after the addition of drugs, cell-seeding numbers were increased by an additional 30%. HCC1806 cells were seeded at 1300 cells per well in a total volume of 50 µL per well. HCC1806 +HACREB3L1 Cl3 cells were seeded at 2600 cells per well in a total volume of 50 µL. The two cell lines were plated at different densities due to differences in plating efficiencies as determined above. Cells were allowed to attach overnight at 37ºC and 5% CO_2.

The original concentration of drug (10 mM in Dimethyl Sulfoxide [DMSO]) in each stock drug plate was initially diluted to a working drug concentration of 250 µM using the Biomek FX liquid handling system. On Day 1, drugs from the 250 µM working drug plates were added to each set of six 384-well plates (containing either HCC1806 or HCC1806 +HACREB3L1 Cl3 cells). A volume of 0.2 µL of drug was added to each well using the Biomek FX liquid handling system, resulting in a final concentration of 1 µM of drug. Initial assessment of drugs at 1 µM is similar to the approach used for the NCI-60 screens used to identify new anti-cancer compounds effective in the nanomolar range (Holbeck, Collins & Doroshow, 2010). Each working drug plate also contained DMSO control wells, so that each 384-well plate would also have DMSO only control wells equal to the concentration of DMSO present in the drugs being tested. These controls were used to account for the effects of DMSO alone on the cells in the absence of added drug.

On days 1-5, each of the 384-well plates was imaged using an automated imaging fluorescence microscope system, ImageXpress Micro XLS Widefield (Molecular Devices) at the Phenogenomic Imaging Centre of Saskatchewan. From these images the total number of RFP-labeled fluorescent cells attached to the bottom of the well (total cell count per well) was determined.

The total cell counts for each test well (those wells that contained a drug/inhibitor), were adjusted to account for any cytotoxic effects due to the solvent DMSO. The % Viability for each test well on a particular plate was then calculated by dividing the total cell count of the test well by the average total cell count of the DMSO control wells (in the same plate) and then multiplying by 100. The difference in viability between test wells in the HCC1806 plate and HCC1806

+HACREB3L1 Cl3 plate was calculated to compare the effects of each drug/inhibitor on cell viability between the two lines.

There were a number of possible results each drug could produce at the drug screen test concentration of 1 μM (Fig. 2.1). A drug could cause little to no effect on either cell line (A), affect the "wrong", cells (i.e. CREB3L1 re-expressing cells) (B) or, show promise, by being cytotoxic to only the CREB3L1-deficient cells (C). A drug could also be cytotoxic to both CREB3L1+ and CREB3L1- cells at 1 μM (D, E, F). However, once titrated over a range of concentrations, these drugs could possibly be selectively cytotoxic towards CREB3L1-deficient cells (D), be cytotoxic to the CREB3L1-expressing cells (E), or affect both cells similarly at lower concentrations (F).

The drugs/inhibitors that caused a difference in survival between the two cell lines greater than 40% (Fig. 2.1C) and the drugs that killed both cell lines with similar efficacy at 1 μM were focused on for further target validation experiments (Fig. 2.1D-F). A survival difference of greater than 40% was selected in order to focus on a feasible number of potential drugs. Drugs that were cytotoxic to both cell lines at 1 μM were also prioritized for validation experiments because at lower concentrations these drugs may selectively kill the CREB3L1-deficient cells.

2.3 Target Validation Experiments

The 47 most promising drugs/inhibitors identified in the high-throughput drug screen were further validated using expanded cell viability assays.

2.3.1 Drugs/Inhibitors

The most promising drugs from the high-throughput drug screen were obtained from the supplier CEDARLANE, which distributes compounds to Canada from various companies. For the validation assays these drugs were reconstituted using the appropriate solvent suggested by the supplier. Solvents utilized include: DMSO, Dimethylformamide (DMF), Ethanol (ETOH) or 1 x Phosphate Buffered Saline (1 x PBS). Drugs were reconstituted to the highest concentration possible, constrained by the solubility of each drug in its suggested solvent. Drugs were then aliquoted in 5 μL 10 mM aliquots, with the exception of those drugs whose original reconstituted concentration was lower than 10 mM (Table 2.1). All reconstituted drugs were then stored at -80°C.

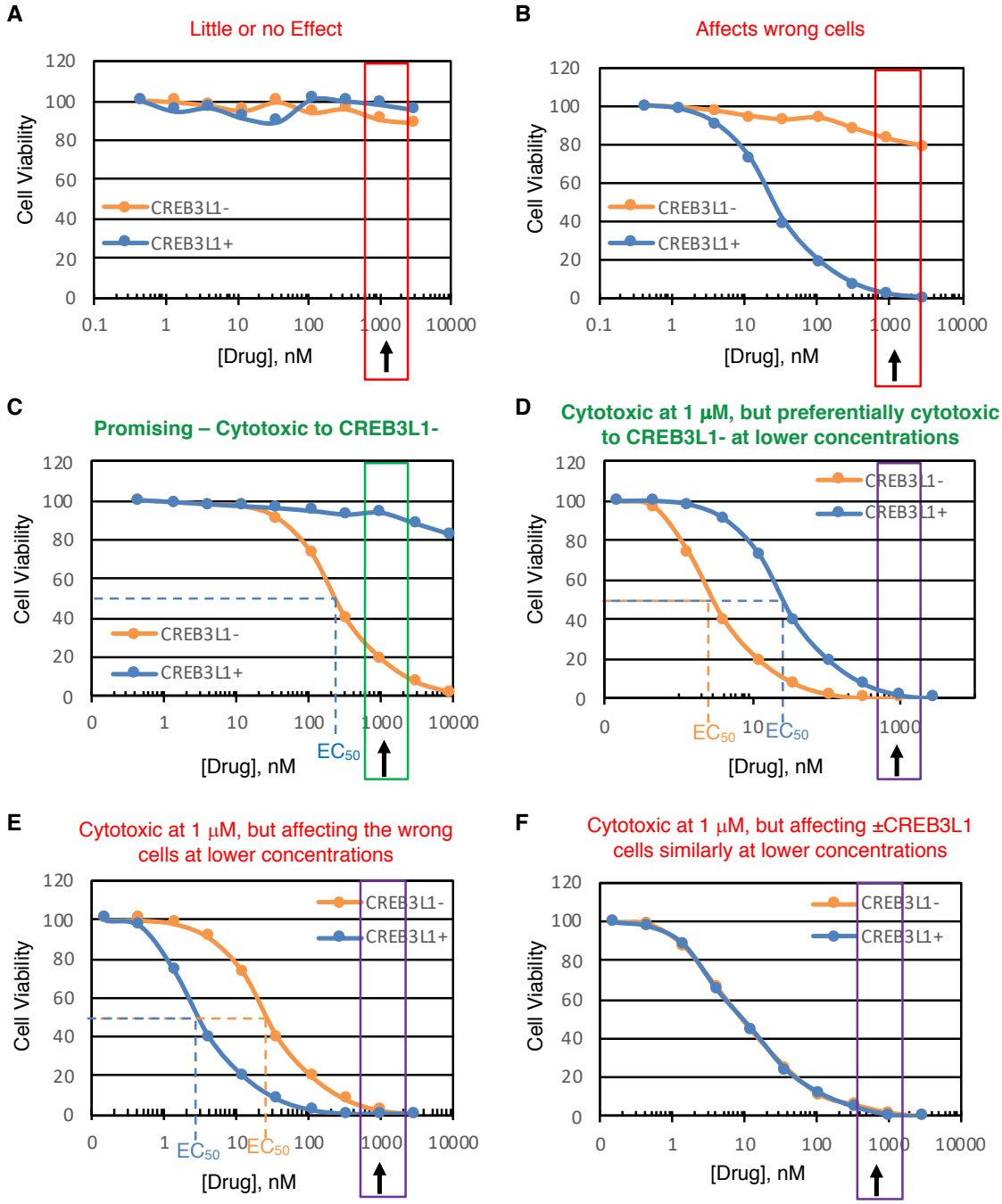

Figure 2.1: Possible drug effects on cell viability for CREB3L1- compared to CREB3L1+ cells. Arrows and boxes indicate the 1 µM (or 1000 nM) drug concentration used for the initial drug library screens. Drugs showing little or no effect at 1000 nM (A) or affecting the wrong cell type (B) were not pursued. Drugs that caused reduced cell number (due to cell death or decreased rates of cell division) for the parental HCC1806 cell lines, but not the HCC1806 + HACREB3L1 cells (C) were analyzed further. Drugs that were cytotoxic to CREB3L1-deficient HCC1806 cells at 1 µM (panels D-F) were further tested in drug titration curves (EC50) to determine if they exhibited the desired selective cytotoxicity towards CREB3L1-deficient cells (shown in panel D). Drugs with profiles similar to panels E and F were not pursued. Drug profiles similar to panels C and D were the most favorable.

Table 2.1: Drugs tested in validation experiments. *

#	Inhibitor	Target	Solvent	Stock Concentration, mM	Working Stock Concentration, mM	Catalogue #	Company
1	MLN9708	20S Proteasome	DMF	9.7	9	18386	CC
2	MLN2238 (Ixazomib)	20S Proteasome	DMF	415.9	10	18385	CC
3	Erlotinib HCl	EGFR	DMSO	41.8	10	SIH-444	SMBS
4	Icotinib HCl	EGFR	DMSO	199.5	10	A3482	AB
5	Aminophylline	PDE	1 x PBS	47.6	10	22235	CC
6	Tadalafil	PDE	DMF	64.2	10	14024	CC
7	Cobimetinib	MEK1	DMSO	47.1	10	19563	CC
8	Raberprazole Sodium	ERK1/2	DMSO	65.6	10	14939	CC
9	Acitretin	RAR	DMF	15.3	10	20853	CC
10	Bexarotene	RAR	DMF	57.4	10	11571	CC
11	Climbazole	Anti-infective	DMSO	45.3	10	B1706	AB
12	Thioctamide	Anti-oxidant	DMSO	243.5	10	HY-B1142	MCE
13	Moxifloxacin HCl	Antibiotic	DMSO	198.6	10	S1465	SC
14	Quinacrine Dihydrochloride	Anti-malarial	DMSO	93.2	10	HY-13735A	MCE
15	Moclobemide	MAO-A	ETOH	37.2	10	24361-1(CA)	CC
16	Tolazoline HCl	β-Adrenergic receptor	ETOH	127.0	10	18865	CC
17	Benorilate	Anti-inflammatory	DMSO	399.0	10	HY-107795	MCE
18	Cisatracurium Besylate	Neuromuscular blocking agent	DMSO	24.1	10	22959-25	CC
19	Felypressin	Vasoconstrictor	DMSO	10.0	10	HY-A0182	MCE
20	Liothyronine	THR	DMSO	51.7	10	16028	J&K
21	Alcaftadine	Histamine Receptor	ETOH	97.6	10	21290	CC
22	Sanguinarine Chloride	STAT3, MMPs	DMSO	13.6	10	1695	CC
23	Zinc Pyrithione	Anti-infective	DMSO	42.3	10	B2201	AB
24	Digitoxin	Na+/K+ ATPase	DMSO	10.0	10	HY-B1357	MCE
25	Doxorubicin HCl	Anthracycline	DMSO	4.0	4	S1208	SC
26	Digoxin	Na+/K+ ATPase	DMSO	38.4	10	22266	CC
27	Ouabain octahydrate	Na+/K+ ATPase	DMSO	13.7	10	O3125	SA
28	Bortezomib (PS-341)	20S Proteasome	DMSO	52.0	10	AG-CR1-3602-M005	AG
29	Nocodazole	Microtubules	DMSO	16.6	10	13857	CC
30	Cladribine	Nucleotide analog	DMF	56.0	10	12085	CC
31	Doxorubicin	Anthracycline	DMSO	50.0	10	A3966	AB
32	Teniposide	Topoisomerase II	DMSO	7.6	3	14425	CC
33	Cyclocytidine HCl	Nucleotide analog	DMSO	95.5	10	HY-N0093	MCE
34	Carfilzomib (PR-171)	Proteasome	DMSO	41.7	10	AG-CR1-3669-M001	AG
35	Isolanid	Na+/K+ ATPase	ETOH	2.1	2	HY-B1030	MCE
36	Daunorubicin HCl	Anthracycline	DMSO	4.0	4	14159	CC
37	Cephalomannine	Microtubules	DMSO	120.2	10	A11632	AQ
38	Panobinostat	HDACs	DMSO	4.0	4	S1030	SC
39	Irinotecan	Topoisomerase I	DMSO	4.0	4	I-4122	LC
40	Palbociclib (PD0332991) Isethionate	CDK 4/6	DMSO	50.0	50	A8335	AB
41	Verteporfin	vascular occlusion	DMF	4.2	3	17334	CC
42	Belinostat (PXD101)	HDACs	DMSO	50.0	10	A4096	AB
43	Homoharringtonine	Protein translation	DMSO	100.0	10	14531	CC
44	Hydroxy Camptothecine	Topoisomerase I	DMSO	79.6	10	S3898	SC
45	Romidepsin	HDACs	DMSO	50.0	10	A8173	AB
46	Octenidine	Anti-infective	DMSO	13.1	10	HY-B2170A	MCE
47	Malathion	AChE	DMSO	11.5	10	22998	CC

* EGFR = epidermal growth factor receptor; PDE = Phosphodiesterase; MEK1 = MAP (Mitogen-Activated Protein) Kinase/ERK (Extracellular Signal-Regulated Kinase) Kinase 1; ERK1/2 = extracellular signal-regulated protein kinase 1/2; RAR = retinoic acid receptor; MAO-A = monoamine oxidase-A; THR = thyroid hormone receptor; STAT3 = signal transducer and activator of transcription 3; MMPs = matrix metalloproteinases; HDACs = histone deacetylases; CDK = cyclin dependent kinase; AChE = acetylcholinesterase; DMSO = Dimethyl Sulfoxide; DMF = N,N-Dimethylformamide; ETOH = 95% Ethanol; 1xPBS = 1x phosphate buffered saline; CC = Cayman Chemical; SMBS = StressMarqBioSciences Inc.; AB = ApexBio; MCE = MedChemexpress CO. Ltd; SC = Selleckchem; J&K = J&K Scientific; LC = LC Laboratories. SA = Sigma Aldrich; AG = AdipoGen; AQ = AdooQ Bioscience.

2.3.2 1 µM Validation Assay

Validation viability assays were performed utilizing two approaches. Initially, a 1 µM validation assay was performed using a single test concentration to confirm, in an expanded format, the 47 drugs identified in the initial drug screen were genuine hits.

On day 0, cells were seeded in a volume of 50 µL in a sterile 384-well black-walled optical bottom plate (6007558, PerkinElmer) using an ASSIST PLUS pipetting robot and a 16-channel VIAFLO pipette (4505 and 4642, INTEGRA Biosciences AG). The cells were seeded in RPMI +10% FBS + 100 µg/mL Penicillin-Streptomycin (PenStrep, 15140122, Gibco). The media included 100 µg/mL PenStrep to prevent bacterial infection of the cells, as the ASSIST PLUS system could not be used while inside a biosafety cabinet. Cell numbers were previously titrated for each cell line such that on day 5, the wells of the 384-well plate were ~90-95% confluent. Cell lines HCC1806 and HCC1806 +HACREB3L1 Cl3 were plated at 500 cells/well and 600 cells/well, respectively (Fig. 2.2). Cells were incubated at 37°C with 5% CO_2 for 24 hours.

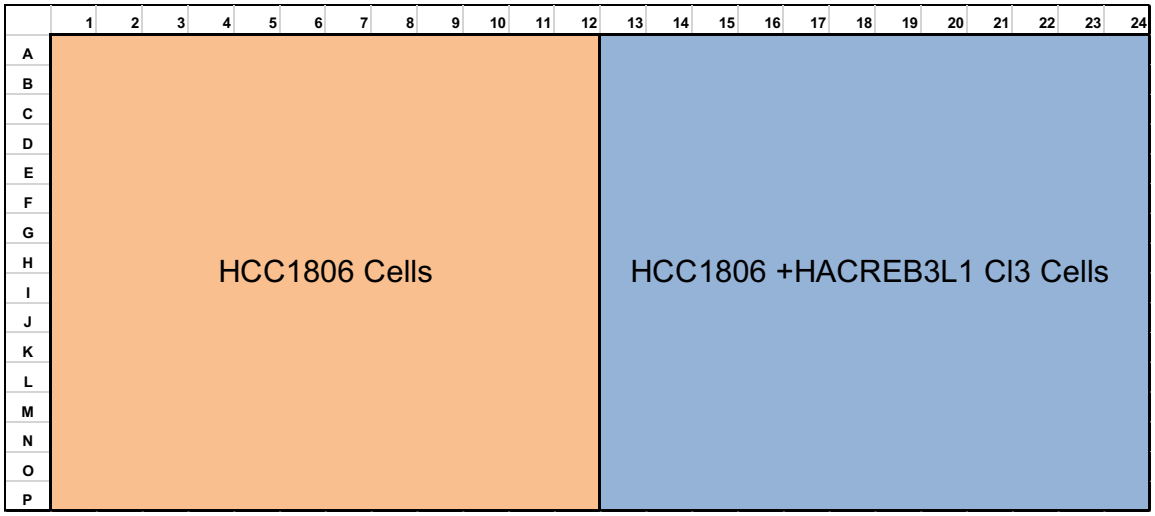

Figure 2.2: 1 µM Validation Experiment: Day 0, 384-well plate. Cells were seeded in a volume of 50 µL. HCC1806 cells were plated at 500 cells/well and HCC1806 +HACREB3L1 Cl3 were plated at 600 cells/well.

On day 1, all of the 47 drugs (Table 2.1) were diluted to a final concentration of 1 µM, in a volume of 300 µL, in duplicate, over two 96 deep-well plates (780261, Grenier; Fig. 2.3). These drug dilutions were carried out in media, so that the final % of the appropriate solvent in the RPMI +10% FBS + 100 µg/mL PenStrep media was less than 0.1%. Concentrations of DMSO and ETOH below 0.5% have been demonstrated to show little to no toxicity to breast cancer cells, and concentrations below 0.5% of DMF have showed some toxicity (Jamalzadeh et al., 2016).

However, the impact of these solvents on cell growth and survival may be cell line dependent, rendering solvent controls necessary, even at low concentrations (Jamalzadeh et al., 2016). Therefore, solvent controls (<0.1%) corresponding to the final % of each solvent in the diluted drugs were used to account for any background cytotoxic effects due to the solvent and not the compound itself.

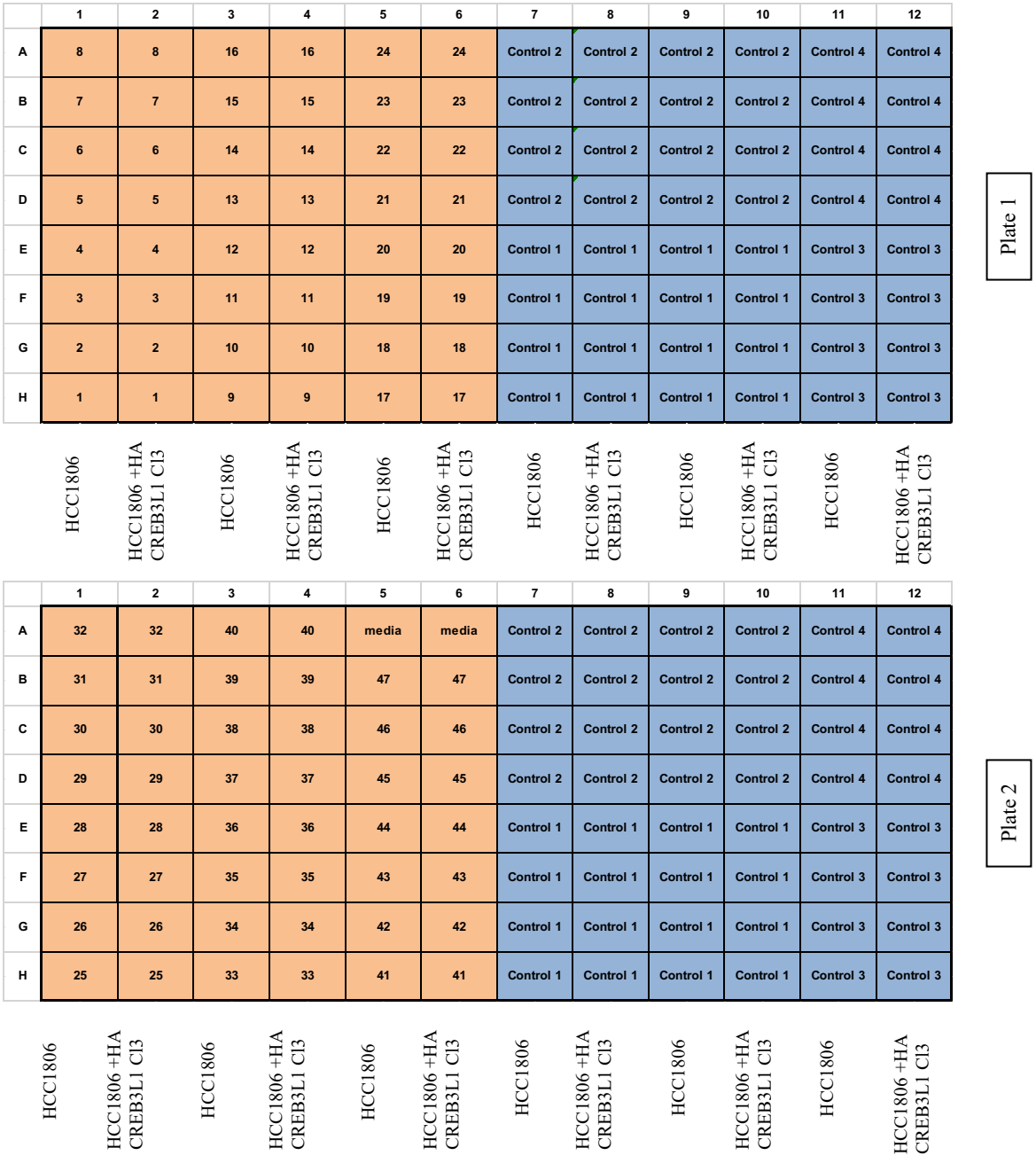

Figure 2.3: 1 µM Validation Experiment: Day 1, 96-well plates 1 and 2. 300 µL of each of the 47 drugs was added, in duplicate, to deep 96-well plates. 300 µL of 0.1% solvent controls were also added. Control 1 = 0.1% DMSO. Control 2 = 0.1% DMF. Control 3 = 0.1% ETOH. Control 4 = 1 x PBS.

The media was removed from the cells of the 384-well plate from day 0 (Fig. 2.3) using the ASSIST PLUS pipetting robot and 16-channel VIAFLO pipette. The 1 µM dilution of each drug, and solvent controls, were then transferred from the deep 96-well plate to the 384-well plate (from day 0), in triplicate, in a volume of 50 µL per well, using the ASSIST PLUS pipetting robot and an 8-channel VOYAGER pipette (4722, INTEGRA Biosciences AG) (Fig. 2.4). Cells were incubated for 4 days (96 hours) at 37°C with 5% CO_2.

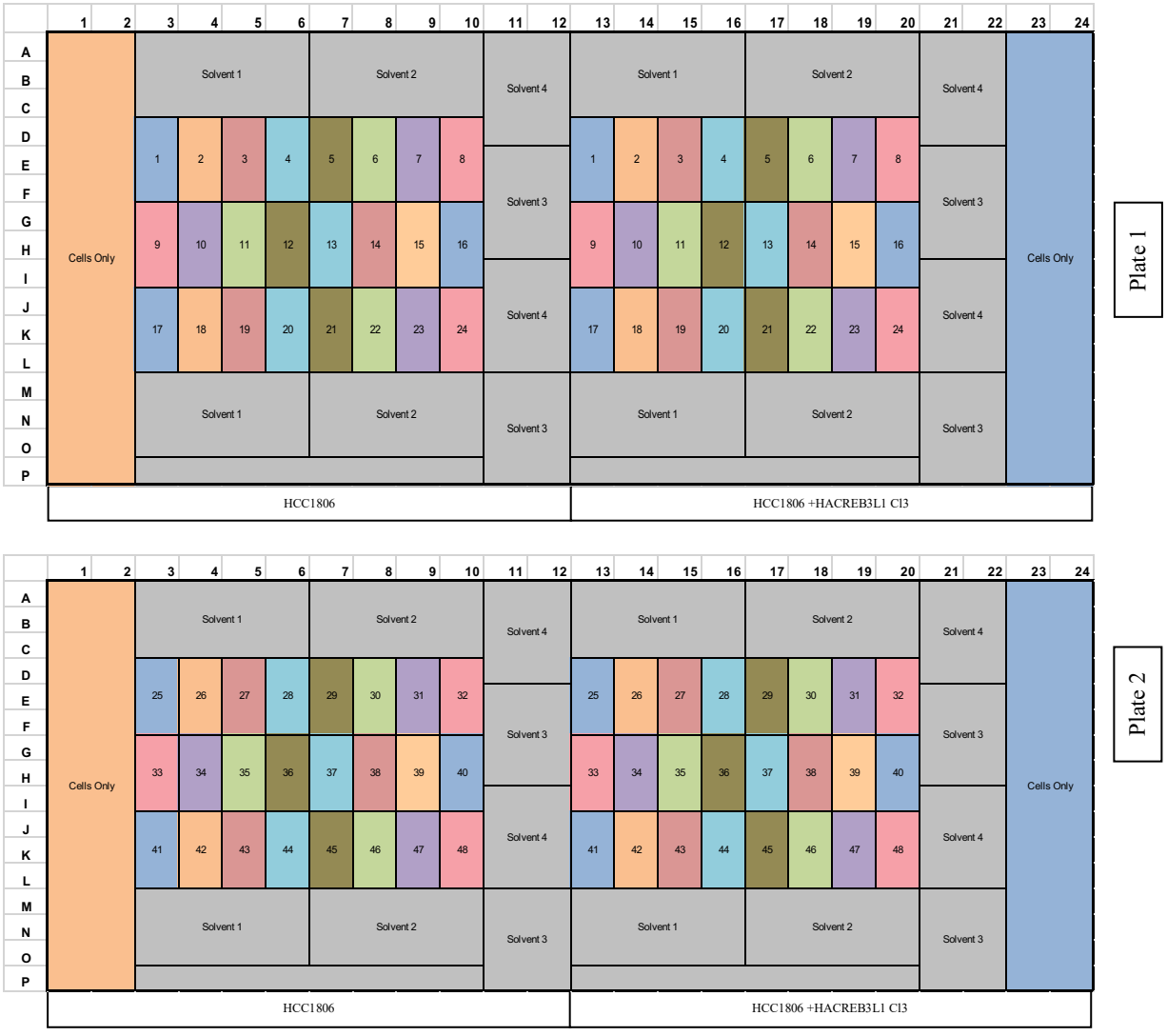

Figure 2.4: 1 µM Validation Experiment: Day 1, 384-well plate. 47 drugs were added, in triplicate, at 1 µM with a final volume of 50 µL in each well. Solvent 1 = 0.1% DMSO; Solvent 2 = 0.1% DMF; Solvent 3 = 0.1% ETOH; Solvent 4 = 0.1% 1xPBS.

The media was removed from the cells of the 384-well plate using the ASSIST PLUS pipetting robot and 16-channel VIAFLO pipette. Media containing Hoechst 33324 dye (5 µM;

ThermoFisher Scientific, 62249) and ImageIT Dead Green dye (100 nM; ThermoFisher Scientific, I10291) was added and incubated for 30 min at 37°C with 5% CO_2. The Hoechst 33324 dye stained the cell nuclei, and allowed the identification of the nuclei of every cell. The ImageIT Dead Green dye permeated compromised plasma membranes and then stained the cytoplasm of dead cells. Images of each well of the 384-well plates were acquired using a Thermo Scientific™ CellInsight™ CX7 High Content Screening (HCS) Platform. Nine fields of view were captured using a 10x (0.4 NA) air objective lens and quantified using the Thermo Scientific™ HCS Studio™ Cell Analysis (Cellomics) software.

Images were analyzed using Thermo Scientific™ HCS Studio 3 Cell Analysis Software using the Spot Detector bio-application. The protocols were pre-designed within the Spot Detector application to specifically identify cells, alive and dead, using criteria such as shape, area and intensity. Cells (alive or dead) were identified by their Hoechst stained nuclei at 386 nm (blue) channel 1 (Ch1) using the preset CX7 software criteria. This allowed identified objects (cell nuclei) to be quantified using the Spot Detector bio-application, yielding a total cell count in nine fields per well.

From the total cell count in nine fields per well, the percentage of viable cells was given as an output value based on the intensity of ImageIT Dead Green on the 485 nm wavelength (green) channel 2 (Ch2). Live cells had very little to no intensity in Ch2 as their membranes were not compromised, and the ImageIT Dead Green dye was unable to permeate into the cytoplasm. A cut-off for live cells was set at a very low intensity on Ch2. Any of the cells lower than the low intensity Ch2 cut-off were deemed alive. This yielded the percentage of live cells in nine fields per well. The % of live cells (determined from Ch2), in decimal form, was multiplied by the total cell count to determine the total live cell count in each well.

The total live cell count for each well containing a drug/inhibitor (determined from Ch1), was adjusted for the total live cell count for each control well. This was to account for any dead cells that had lifted off of the plate in test wells. The test well total live cell count was divided by the average of the corresponding control (DMSO, DMF, or ETOH) total live cell count, giving the percentage cell viability (% Viability). The average % Viability of each set of triplicate wells was calculated, along with the standard error (SE) for each mean.

This analysis enabled impacts on cell survival due to the drug/inhibitor to be quantified, as well as differences between parental, CREB3L1-deficient metastatic cell lines and those same cells re-expressing CREB3L1.

2.3.3 Drug Titration Experiments

From the 1 μM validation experiment, 27 drugs were confirmed as potentially promising compounds. Most of the 27 drugs were similarly cytotoxic to both cell lines at 1 μM while a few were preferentially cytotoxic to CREB3L1-deficient cells. Drug titration experiments were then performed to determine if these compounds were preferentially cytotoxic to CREB3L1-deficient cells at lower concentrations and to determine their EC_{50} values. An EC_{50} value is the concentration of a drug/inhibitor necessary to reach half of the maximum response (Clark, Finkel, Rey & Whalen, 2012). In the context of this experiment, the maximal response was the lowest percentage of cell survival for each cell line. It was essential that dose response curves with a well-defined slope were produced for the accurate determination of the drug EC_{50} value, since the slope is the portion of the curve from which the parameter is derived.

As described in the 1 μM validation experiment, on day 0, HCC1806 and HCC1806 +HACREB3L1 cells were seeded at 500 cells/well and 600 cells/well, respectively, in a volume of 50 μL in a sterile 384-well black-walled optical bottom plate (6007558, PerkinElmer, Fig. 2.2). Each of the 27 promising compounds were diluted in the RPMI +10% FBS + 100 μg/mL PenStrep media to a final concentration of 9 μM and the final % of the appropriate solvent in the RPMI +10% FBS + 100 μg/mL PenStrep media was less than 0.5%. Due to the poor solubility of some compounds, the final concentration of solvent in the 9 μM dilution for these compounds was greater than 0.1% (and higher than the percentage of solvent used in the first 1 μM validation experiment), increasing the likelihood of cytotoxic effects due to the solvent (Jamalzadeh et al., 2016). However, solvent controls corresponding to the highest concentration of solvent used for diluted drug (<0.5%) were found to have little to no effect on the cell growth/number.

A number of serial dilutions were performed in a deep 96-well plate using the ASSIST PLUS pipetting robot and an 8-channel VOYAGER pipette (Grenier; 4723, INTEGRA Biosciences AGm, Fig. 2.5). Drugs were serially diluted 1:3 as follows: 9000 nM, 3000 nM, 1000 nM, 333.33 nM, 111.11 nM, 37.04 nM, 12.35 nM, and 4.12 nM, such that each dilution was in a volume of 240 μL. Four drugs were serially diluted in each 96 deep-well plate.

	Drug 1		Drug 2		Drug 3		Drug 4					
	1	2	3	4	5	6	7	8	9	10	11	12
A	4 nM	4 nM	4 nM	4 nM	4 nM	4 nM	4 nM	4 nM	Control 1	Control 1	Control 2	Control 2
B	12 nM	12 nM	12 nM	12 nM	12 nM	12 nM	12 nM	12 nM	Control 1	Control 1	Control 2	Control 2
C	37 nM	37 nM	37 nM	37 nM	37 nM	37 nM	37 nM	37 nM	Control 1	Control 1	Control 2	Control 2
D	111 nM	111 nM	111 nM	111 nM	111 nM	111 nM	111 nM	111 nM	Control 1	Control 1	Control 2	Control 2
E	333 nM	333 nM	333 nM	333 nM	333 nM	333 nM	333 nM	333 nM	Control 1	Control 1	Control 2	Control 2
F	1000 nM	1000 nM	1000 nM	1000 nM	1000 nM	1000 nM	1000 nM	1000 nM	Control 1	Control 1	Control 2	Control 2
G	3000 nM	3000 nM	3000 nM	3000 nM	3000 nM	3000 nM	3000 nM	3000 nM	Control 1	Control 1	Control 2	Control 2
H	9000 nM	9000 nM	9000 nM	9000 nM	9000 nM	9000 nM	9000 nM	9000 nM	Control 1	Control 1	Control 2	Control 2
	HCC1806	HCC1806 +HA CREB3L1 Cl3	HCC1806	HCC1806 +HA CREB3L1 Cl3	HCC1806	HCC1806 +HA CREB3L1 Cl3	HCC1806	HCC1806 +HA CREB3L1 Cl3	HCC1806	HCC1806 +HA CREB3L1 Cl3	HCC1806	HCC1806 +HA CREB3L1 Cl3

Figure 2.5: Drug Titration Experiment: Day 1, 96-well plate. 360 µL of 4 drugs 9 µM were added, in duplicate, to row H of a deep 96-well plate. 240 µL of media was added to rows A-G and columns 1-8. 1:3 Serial dilutions were made vertically up the plate so that the final concentrations in each wells H-A are as follows: 9000 nM, 3000 nM, 1000 nM, 333.33 nM, 111.11 nM, 37.04 nM, 12.35 nM, and 4.12 nM. 240 µL of <0.5% solvent controls were also added.

The media was removed from the cells of the 384-well plate from day 0 using the ASSIST PLUS pipetting robot and 16-channel VIAFLO pipette. The serial dilution of each drug was then transferred in triplicate, in a volume of 50 µL per well, to the 384-well plate for each cell line using the ASSIST PLUS pipetting robot and an 8-channel VOYAGER pipette (4722, INTEGRA Biosciences AG; Fig. 2.6). Solvent control wells containing media and DMSO, DMF or ETOH were also added to the plate (Fig. 2.6). Cells were incubated for 96 hours at 37°C with 5% CO_2.

Finally, the media was removed and the cells were stained with both Hoechst 33324 and ImageIT Dead Green dye as before. Cells were imaged and quantified as detailed above.

Additional drug titration experiments were performed on drugs for which the previous 1:3 serial dilutions were inappropriate to develop dose response curves. For example, some drugs were cytotoxic to both cell lines even at the lowest concentration of 4.12 nM. For these drugs, serial dilutions were performed at lower concentrations within the nanomolar range to better characterize the dose response curves. Additionally, for some drugs, the initial concentration range of 0-9 µM was inappropriate because there were not enough points to clearly establish the slope of the curve.

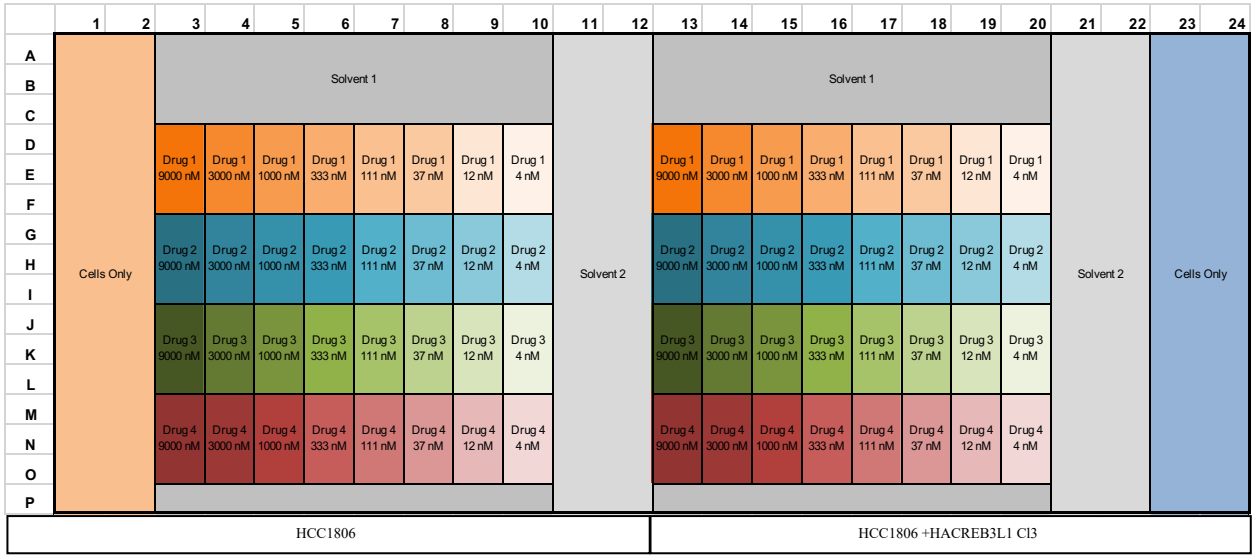

Figure 2.6: Drug Titration Experiment: Day 1, 384-well plate. Drugs were added in triplicate at concentrations ranging from 0-9 µM in a final volume of 50 µL in each well. Solvent controls (<0.5%) were also added in a final volume of 50 µL in each well.

Additional drug titrations in this case were performed using 1:2 serial dilutions to increase the number of points defining the slope and increase the quality of the EC_{50} determinations for these drugs. At the best concentration range for each promising drug, three independent biological replicates were performed, each with triplicate measurements.

Image and data analysis were performed as described in the 1 µM validation experiment. Briefly, the CX7 CellInsight identified and validated cells, live and dead, to give a total cell count for each well. The CX7 also calculated the percentage of live cells in each well based on a low-intensity cut-off. Then, the total cell count of each well was multiplied by the percentage of live cells in that particular well to yield the total live cell count for each well. Then, each test well total live cell count was adjusted to the average total live cell count of the solvent control wells to give % Viability.

PRISM Graphpad software (Version 8.3) was used to perform non-linear regression analysis on each cell line data set and calculate the EC_{50} value for each drug. Two-way ANOVA tests were conducted using the PRISM software to calculate the significance of the difference of means between the two drug titration curves for the two cell lines.

2.3.4 Control Non-tumorigenic Breast Cell Line (MCF10A) Drug Titration Experiments

To determine whether the drugs would be cytotoxic to normal breast tissue, drug titration experiments were performed comparing drug cytotoxicity in CREB3L1-deficient TNBC cell line

HCC1806 to control non-tumorigenic breast cell line MCF10A. Three biological replicates for each of the top 4 promising compounds (homoharringtonine, isolanid [e.g. lanatoside C], cladribine and palbociclib isethionate) were performed.

In a similar way to previous drug titration experiments, although using different cell lines now, on day 0, HCC1806 and MCF10A cells were seeded at 500 cells/well and 200 cells/well, respectively, in a volume of 50 µL in a sterile 384-well black-walled optical bottom plate (6007558, PerkinElmer, Fig. 2.2). The HCC1806 cells were seeded in RPMI +10% FBS + 100 µg/mL Penicillin-Streptomycin (PenStrep, 15140122, Gibco) and the MCF10A cells were seeded in Advanced DMEM/F12 containing 5% horse serum, 20 ng/mL EGF, 10 µg/mL bovine insulin, 0.5 µg/mL hydrocortisone, and 100 ng/mL cholera toxin and 100 µg/mL PenStrep.

In a similar way to previous drug titration experiments performed, although using the appropriate media for each cell line, on day 1, the top four promising compounds were diluted to a final concentration of 9 µM (or lower depending on the titration curve profile for the specific compound) and added to the deep 96-well plate (Fig. 2.5). 1:3 serial dilutions (or 1:2 depending on the titration curve profile for the specific compound) were made vertically up the deep 96-well plate, and then transferred to the 384-well plate from day 0 (Fig. 2.6). As in other drug titration experiments, on day 5 the cells were stained, imaged and quantified using the CX7 CellInsight. % Viability for each test well was calculated by determining the number of live cells in each well and adjusting these for the number of live cells in solvent control wells. Using the PRISM software, the EC_{50} values were determined for each drug in each cell line that responded to the drug, and significant differences between dose response curves were evaluated by two-way ANOVA analysis.

2.3.5 Additional CREB3L1-Deficient TNBC Drug Titration Experiments

To confirm that the impacts of the most promising drugs were not a cell line dependent effect and applicable across other CREB3L1-deficient breast cancers, drug titration experiments were carried out on additional CREBL3L1-deficient TNBC cell lines. Three biological replicates for each of the top 4 promising compounds (homoharringtonine, isolanid, cladribine and palbociclib isethionate) were performed. Additionally, 3 biological replicates for doxorubicin were performed to determine the general sensitivity of the additional cell lines to drug.

In a similar way to previous drug titration experiments, although using different cell lines now, on day 0, HCC38 and BT549 cells were seeded (1000 cells/well) in a volume of 50 µL in a

sterile 384-well black-walled optical bottom plate (6007558, PerkinElmer, Fig. 2.2). The HCC38 cells were seeded in RPMI +10% FBS + 100 µg/mL PenStrep (15140122, Gibco) and the BT549 cells were seeded in RPMI +10% FBS + 0.023 U/mL bovine insulin (I6634, Sigma Aldrich) + 100 µg/mL PenStrep (15140122, Gibco).

In a similar way to previous drug titration experiments performed, although using the appropriate media for each cell line, on day 1, the top four promising compounds were diluted to a final concentration of 9 µM (or lower depending on the titration curve profile for the specific compound) and added to the deep 96-well plate (Fig. 2.5). 1:3 serial dilutions (or 1:2 depending on the titration curve profile for the specific compound) were made vertically up the deep 96-well plate, and then transferred to the 384-well plate from day 0 (Fig. 2.6).

As previously described, on day 5 the cells were stained, imaged and quantified using the CX7 CellInsight. % Viability for each test well was determined by dividing the number of live cells in each well by the number of live cells in solvent control wells and multiplying by 100. The EC_{50} values were determined using the PRISM software.

2.3.6 Combination Drug Titration Experiments

Combination drug titration experiments were performed to determine potential selective cytotoxic sensitivity and synergy of the top 4 compounds with hallmark chemotherapeutic reagents, doxorubicin (A3966, ApexBio) and paclitaxel (10461, Cayman Chemical) in the paired TNBC cell lines CREB3L1-deficient HCC1806 cells and CREB3L1 re-expressing HCC1806 +HACREB3L1 Cl3 cells. Novel multi-target combinatorial treatment plans could be implemented, especially following patient relapse and within the metastatic setting of TNBC in order to achieve a stronger therapeutic response with decreased dosing (and thus, toxic side effects) and overcome multi-drug resistance (Malyutina, Majumder, Wang, Pessia, Heckman & Tang, 2019).

A cost-effective and robust cross-design format was implemented as in Malyutina *et al.* (2019). The design combines a background drug with a foreground drug. The background drug is added at a fixed concentration, specifically, its EC_{50} value. The foreground drug is added at titrated doses. Each drug in the combination is tested as a both a background drug and a foreground drug (Fig. 2.7). As described in previous drug titration experiments, on day 0, HCC1806 and HCC1806 +HACREB3L1 cells were seeded at 500 cells/well and 600 cells/well, respectively, in a volume of 50 µL in a sterile 384-well black-walled optical bottom plate (6007558, PerkinElmer, Fig. 2.2).

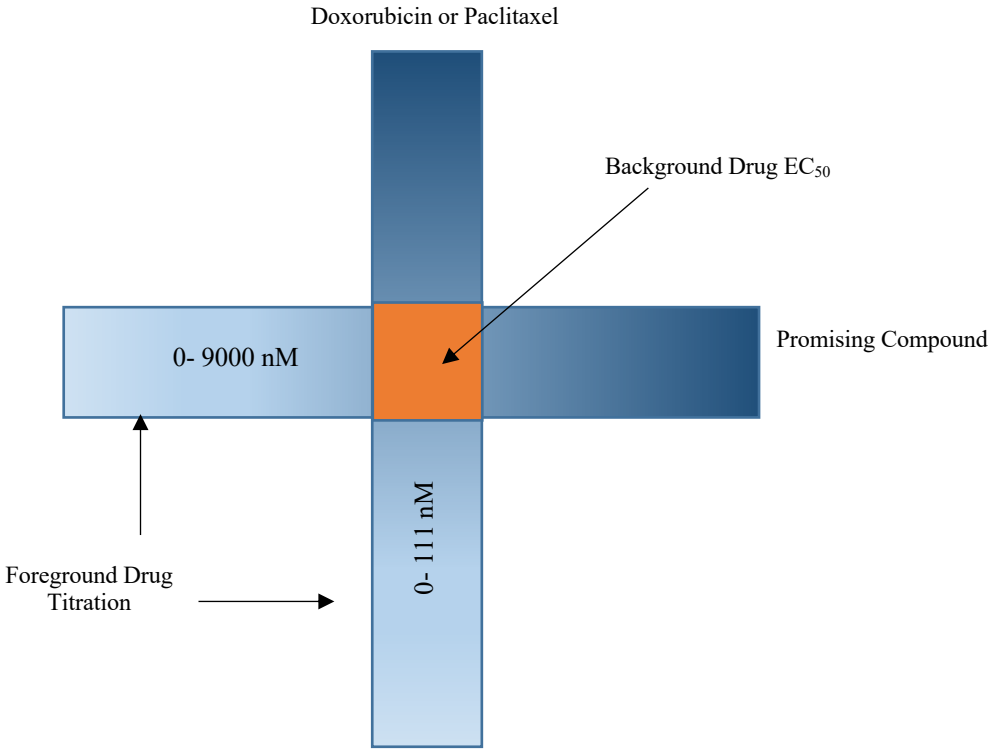

Figure 2.7: Cross Design Combination Drug Titration.

Doxorubicin or paclitaxel was diluted using media to a final concentration of 2x the highest concentration (111 nM) for its drug titration. The top 4 promising compounds were diluted using media to a final concentration of 2x the highest concentration (9 µM or lower depending of the titration curve profile of the drug) for its drug titration. As before, a number of serial dilutions were performed in a deep 96-well plate using the ASSIST PLUS pipetting robot and an 8-channel VOYAGER pipette (Grenier; 4723, INTEGRA Biosciences AGm, Fig. 2.8). Drugs were serially diluted 1:3 (or 1:2) so that when combined with the background drug (at 2x its EC_{50} value), the final concentrations were: 9000 nM, 3000 nM, 1000 nM, 333 nM, 111 nM, 37 nM, 12 nM, and 4 nM and such that each dilution was in a volume of 240 µL. Two drug combinations (foreground drug and background drug) were serially diluted in each 96 deep-well plate. Then, 240 µL of 2x the EC_{50} value of each background drug was added to the wells of the 96 deep-well plate containing serially diluted drug (Fig. 2.8), so that when combined with the foreground drug, each background drug's final concentration was 1x its EC_{50} value. The concentration at which isolanid was fixed was lower than its EC_{50} value. This was due to an error in calculation from the initial monotherapy analysis performed.

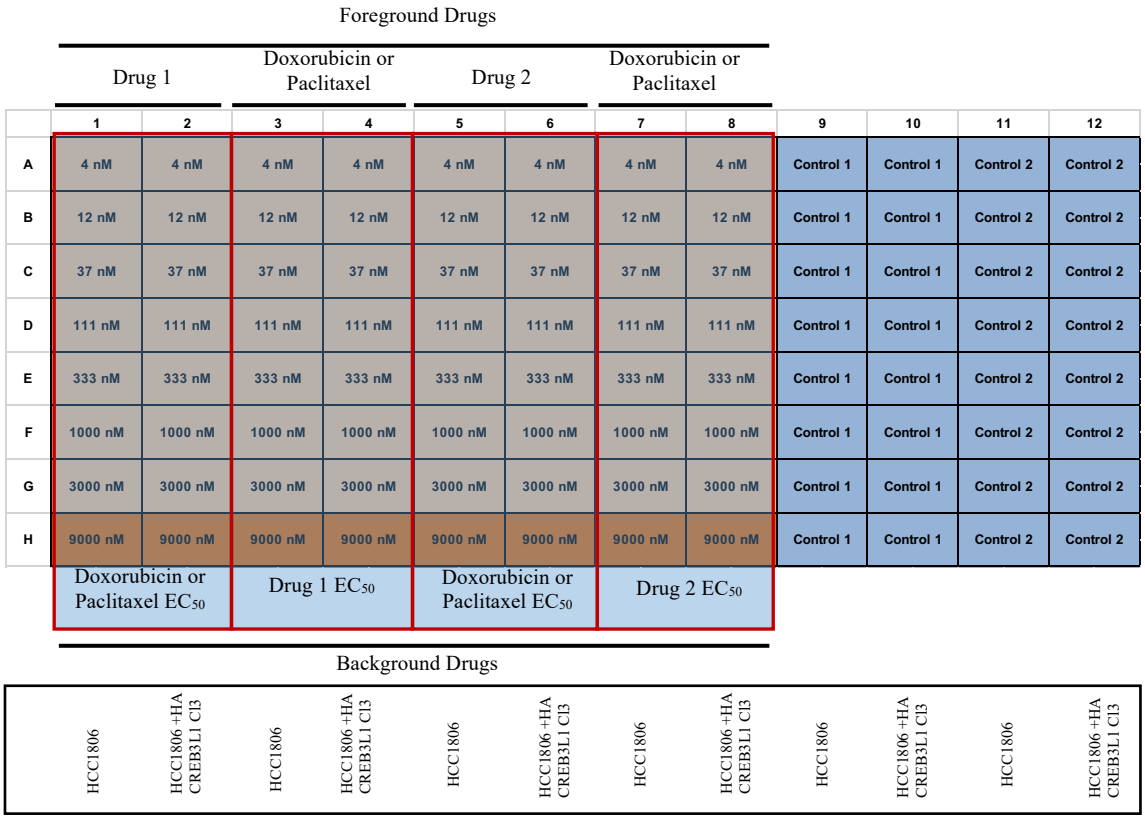

Figure 2.8: Drug Titration Experiment: Day 1, 96-well plate final foreground and background drug concentrations. 360 µL (or 480 µL for 1:2 serial dilutions) of foreground drugs were added, in duplicate, to row H of a deep 96-well plate. 240 µL of media was added to rows A-G and columns 1-8. 1:3 Foreground drug serial dilutions were made vertically up the plate. Then, 240 µL of background drug was added to wells of the deep 96-well plate containing serially diluted drug. 240 µL of 0.1% solvent controls were also added.

As in previous drug titration experiments, media was removed from the wells of the 384-well plate from day 0 using the ASSIST PLUS pipetting robot. The serial dilution of each drug was then transferred in triplicate, in a volume of 50µL per well, to the 384-well plate for each cell line using the ASSIST PLUS (Fig. 2.9). Solvent control wells containing media and DMSO, DMF or ETOH were also added to the plate (Fig. 2.9). Cells were incubated for 96 hours at 37°C with 5% CO_2.

Additional combination drug titration curves were carried out for two of the most promising drug combinations (palbociclib isethionate + doxorubicin; and cladribine + doxorubicin) so that a total of three biological replicates were performed for these drug pairs.

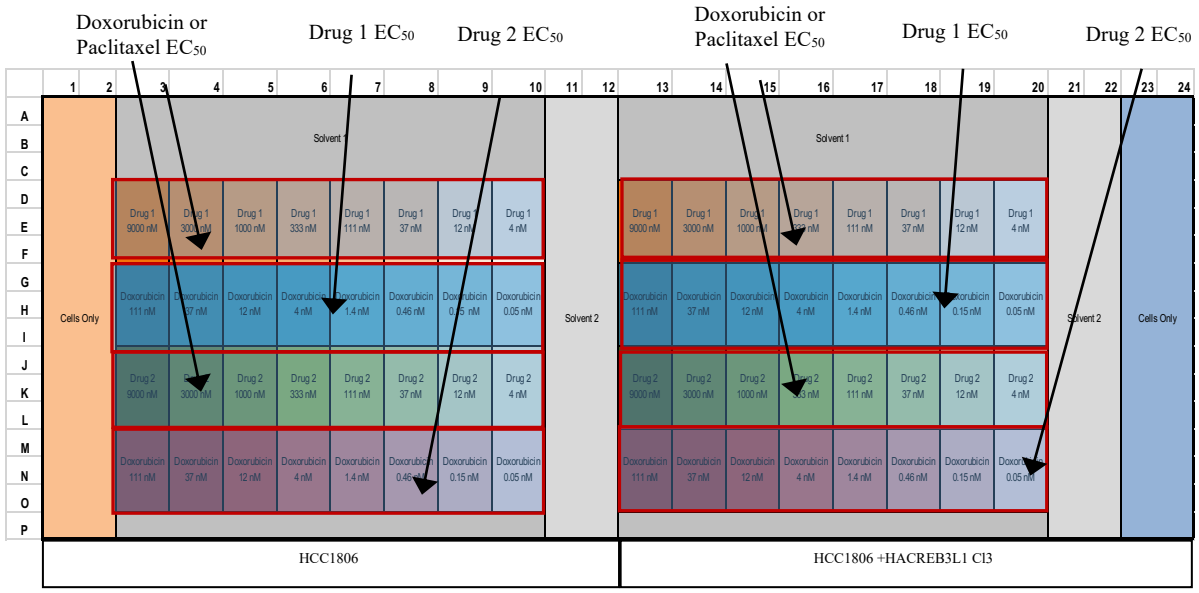

Figure 2.9: Combination Drug Titration Experiment: Day 1, 384-well plate. Drugs were added, in combination in a final volume of 50 µL. Foreground drugs were added in triplicate at final concentrations ranging from 0-9 µM for promising drugs (or lower depending on the titration curve profile of the drug) or 0-111 nM for doxorubicin and paclitaxel. Background drugs were added at the EC50 value of the drug. Solvent controls (<0.5%) were also added in a final volume of 50 µL in each well.

As previously described, on day 5 the cells were stained, imaged and quantified using the CX7 CellInsight. % Viability values were determined taking into account any dead cells on the plate, dead cells that had lifted off the plate and by adjusting to solvent control wells.

Unlike in previous experiments, the PRISM software was not used for analysis. Due to the complexity of possible additive, synergistic, or antagonistic effects, SynergyFinder (version 2.0.11) was used with default settings in R (version 3.6.1) to determine the interaction, if any, of the combined drugs. The SynergyFinder package can be flexibly applied to HCS experiments (He et al., 2018). The recently developed synergy model used in this project is called Zero Interaction Potency (ZIP). This scoring model improves upon previous scoring models including Highest simple agent (HSA), Lowe additivity and Bliss models (Yadav, Wennerberg, Aittokallio & Tang, 2015). The SynergyFinder package characterizes a synergy landscape of drug interaction by calculating ZIP defined delta scores for every input data point and interpolating untested data points in between (He et al., 2018). The ZIP defined delta score is the additional response (% Inhibition) observed beyond the expected effect (as determined by the ZIP model) for the given concentrations of two drugs (Yadav, Wennerberg, Aittokallio & Tang, 2015). For example, a ZIP defined delta score of 20 indicates that the response observed had a 20% higher inhibition than

would be expected if the combined drug effect was non-interactive or additive (Yadav, Wennerberg, Aittokallio & Tang, 2015).

The SynergyFinder package adjusted the % Viability (response) values input to % Inhibition values. There were no other adjustments made to the data. Both monotherapy and combination data were input into the program. There were multiple graphical and numerical outputs given by the SynergyFinder package. The program created an adjusted dose response matrix which characterized the response (% Inhibition) seen at different concentrations of the two combined drugs (Fig. 2.10A). Additionally, 2D and 3D figures were generated that represented the synergy landscape of each drug combination (Fig. 2.10B-C). The raw numerical data (delta score at every test point) was also made available.

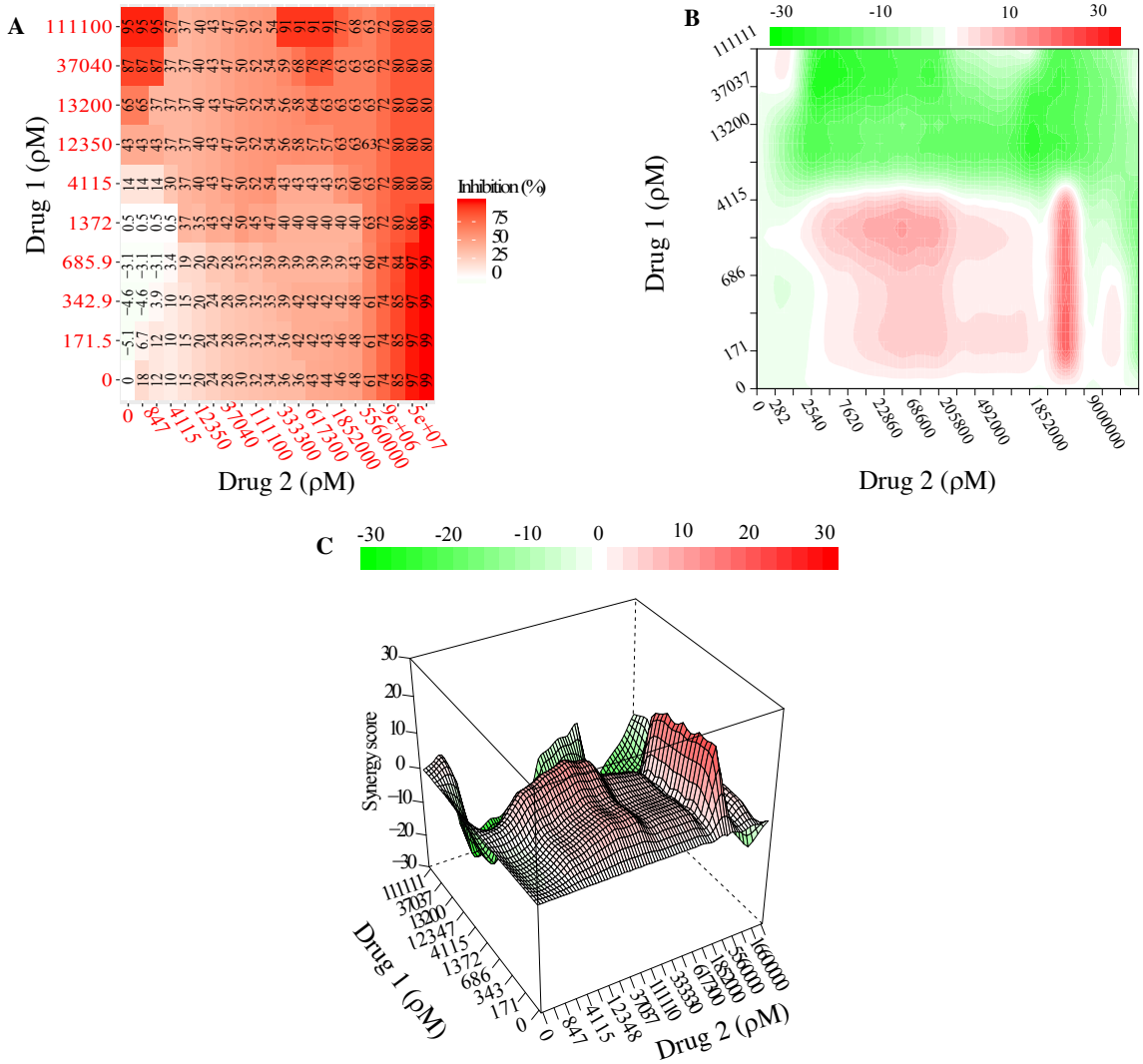

Figure: 2.10 (A) Dose-response matrix, (B) 2D and (C) 3D synergy landscapes for two drugs in combination.

The 2D and 3D landscapes represented the drug interactions (ZIP defined delta scores) observed over a range of combination drug concentrations. A delta score of 0 indicated both no interaction and the probability of additivity (white in the 2D synergy landscape and minor fluctuations in the 3D synergy landscape). A positive delta score indicated synergy (red in the 2D synergy landscape and positive fluctuations in the 3D synergy landscape). A negative delta score indicated antagonism (green in the 2D synergy landscape and negative fluctuations in the 3D synergy landscape).

Minor banding patterns in the landscape characterize interpolated portions of the landscape for which there were no observed values collected and these patterns are less important features in the synergy landscape than major transition areas (Fig. 2.11A-B). As well, in areas where the response (% Inhibition) nears its maximal effect, a stochastic effect may be observed, where noise is amplified in these portions of the landscape and fluctuations in the landscape are exaggerated (Fig. 2.11A-B).

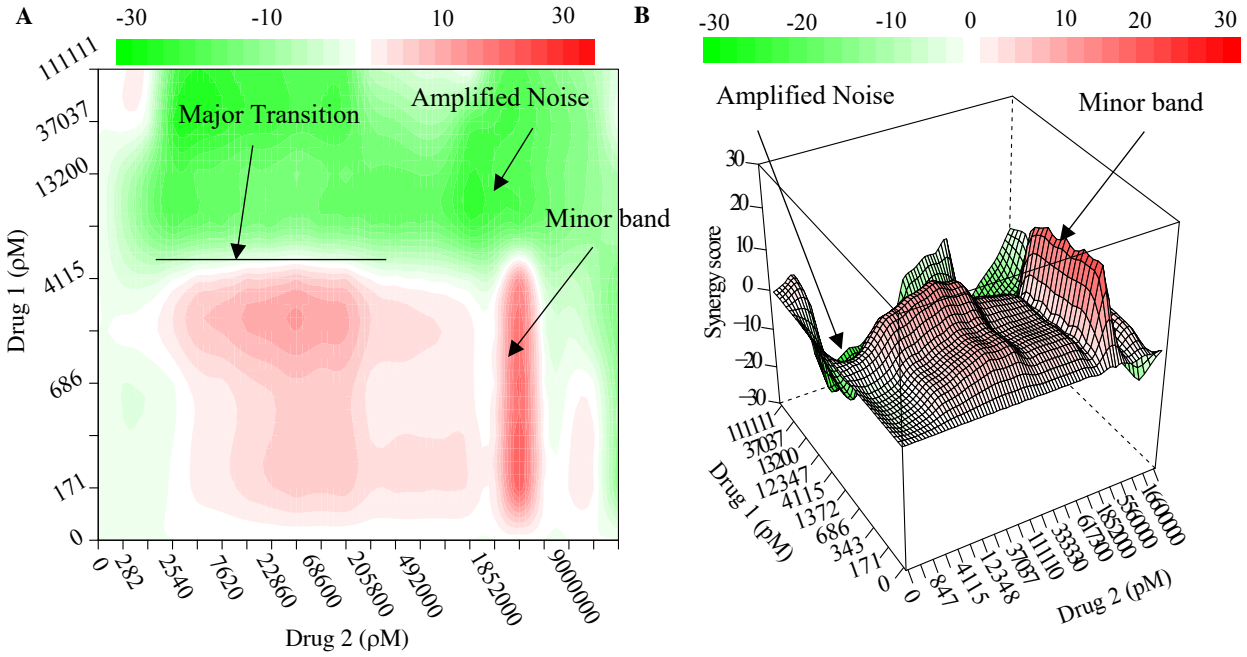

Figure 2.11: (A) 2D and **(B)** 3D synergy landscapes for two drugs in combination.

Although areas of synergy may appear promising, the maximal response that can be produced at synergistic concentrations must also be considered. Therefore, after identifying maximum synergy (the largest delta score) within a synergy landscape (Fig. 2.12) from the raw numerical data, the adjusted % Inhibition (local response) was also identified at the point of

maximum synergy to fully understand the potential of the drug combination.

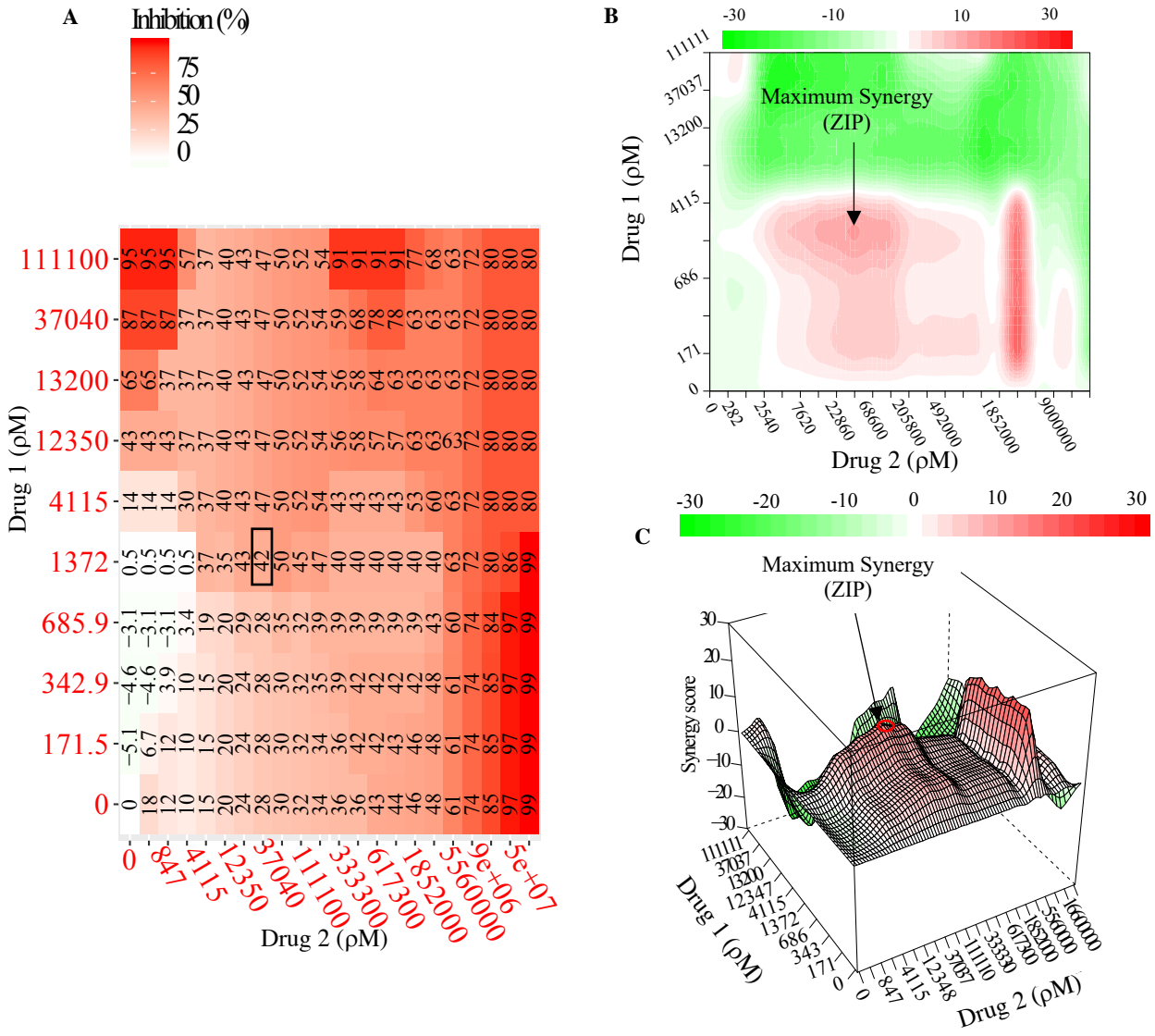

Figure. 2.12: (A) Dose-response matrix (B) 2D and (C) 3D synergy landscapes for two drugs in combination.

2.3.7 Spheroid Optimization Experiments

3D culture (spheroid) assays are thought to provide a better indication of drug effectiveness *in vivo* (Vinci et al., 2012). For the purposes of future validation work for the most promising drugs, HCC1806 and HCC1806 +HACREB3L1 spheroid formation was optimized.

The formation of HCC1806 and HCC1806 +HACREB3L1 spheroids was achieved in Costar® ultra-low attachment 96-well plates (CLS3474, Corning). Spheroids were plated so that on the 4th day they would be between 300 and 500 µm in diameter as recommended in Vinci *et al.*

($5x10^5$ cells/well and $8x10^3$ cells/well in a final volume of 200 μL for HCC1806 and HCC1806 +HACREB3L1 Cl3 cells, respectively) (Vinci et al., 2012). Since both the HCC1806 and HCC1806 + HACREB3L1 Cl3 cells migrate in this environment, different concentrations of Matrigel (354230, Corning) were used to plate the cells. Then, the plates were spun down for a total of 5 min at 2500 rpm in a VWR plate spinner (10144-214) to aid in spheroid formation.

Spheroids were imaged on day 4 (the day on which drug would be added) and day 8 (the day data would be acquired following a 4-day drug treatment) using the CX7 CellInsight. The spheroids were imaged and identified on a brightfield channel and then validated using shape and size characteristics within the Cellomics software.

3. RESULTS

Using a global drug discovery approach, drugs that selectively killed CREBL31-deficient highly metastatic cells were identified and validated *in vitro* for use in CREB3L1-deficient TNBC (Fig. 3.1).

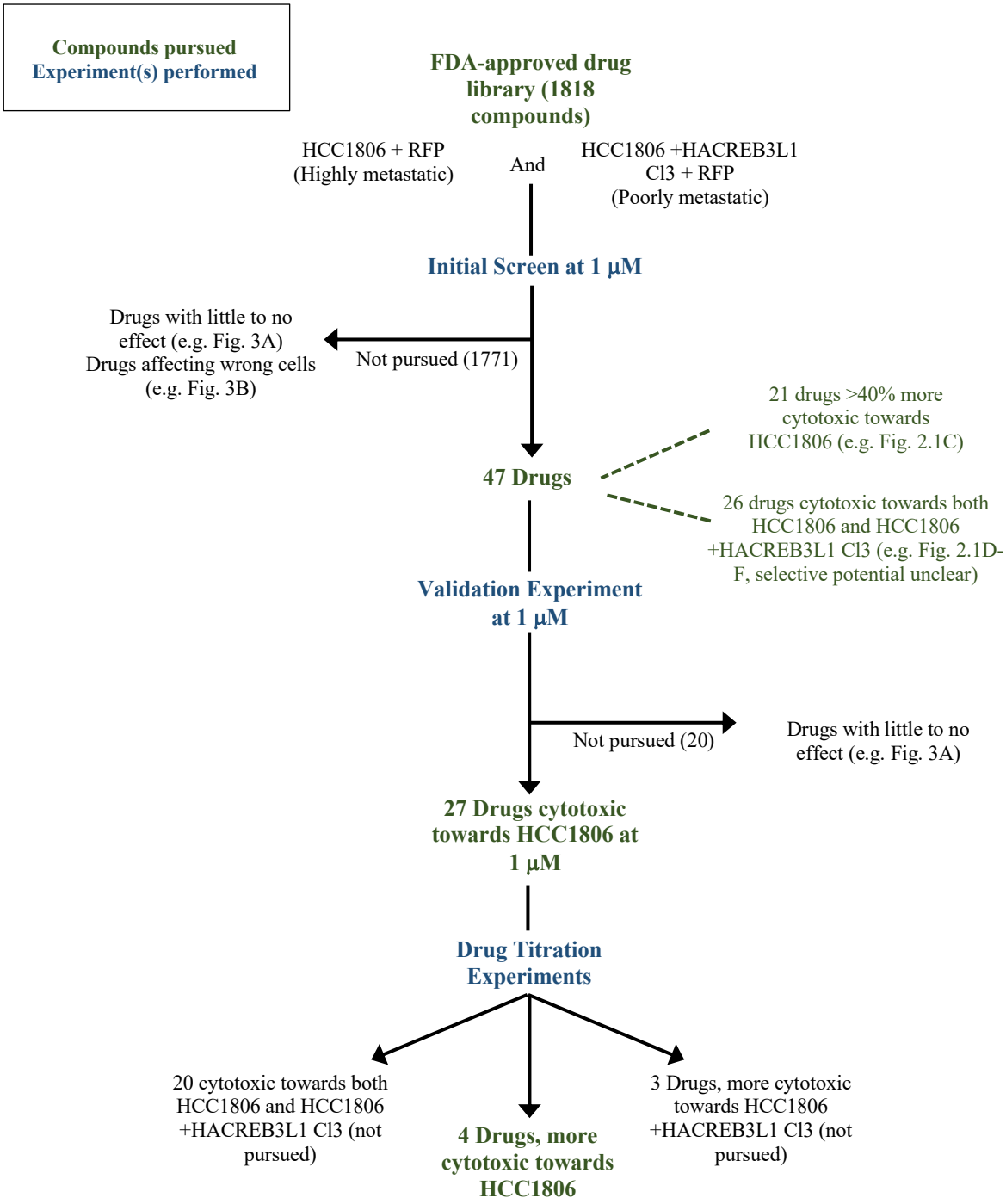

Figure 3.1: Overview of Research Plan. RFP = red fluorescent protein.

3.1 Drug Screen

A high-throughput drug screen was performed on an FDA-approved library of 1,818 compounds at a single test concentration of 1 μM (Fig. 3.1). Due to cost, the drug screen was performed on one cell line pair: CREB3L1-deficient TNBC cell line HCC1806 (+RFP) and that same cell line engineered to stably re-express CREB3L1 and RFP, HCC1806 +HACREB3L1 Cl3. Cells were plated in 384-well plates and allowed to recover and adhere overnight. The next day, 1,818 drugs/inhibitors were added to the 384-well plates. Cells were then imaged over a five-day period and quantified using automated imaging fluorescence microscope system, ImageXpress Micro XLS Widefield.

The top hits from the HCC1806 +/- CREB3L1 drug screen can be categorized based on the ability of the compound to inhibit cell survival of the CREB3L1-deficient TNBC, HCC1806 cell line alone, or in addition with the CREB3L1 re-expressing cell line, HCC1806 +HACREB3L1 Cl3. A total of 47 drugs were identified from the initial screen that warranted further analyses (Fig. 3.1). Of these drugs, 21 showed 40% or greater cytotoxicity to the HCC1806 TNBC cell line, than to the same cell line re-expressing CREB3L1, HCC1806 +HACREB3L1 Cl3 (Table 3.1). The remaining 26 drugs were similarly cytotoxic to both cell lines.

Interestingly, of the 21 drugs showing greater cytotoxicity towards the CREB3L1-deficient TNBC cell line HCC1806, several impacted the same target or pathway. These targets included: the 20S proteasome, the epidermal growth factor receptor, phosphodiesterases, and the retinoic acid receptor (Table 3.1). The remaining 26 drugs showed similar cytotoxicity towards both cell lines at the 1 μM concentration (Table 3.2). Most of these drugs were potent treatments for a number of conditions including congestive heart failure, anti-bacterial or anti-fungal agents, or chemotherapeutic reagents – some of which are used in breast cancer therapy and many of which are indicated for use in other cancers (Table 3.2). These 47 drugs were prioritized in follow-up validation experiments.

3.2 1 μM Validation Assay

A 1 μM validation assay was performed to validate the compounds identified in the initial 1 μM drug screen (Fig. 3.1). The 47 compounds identified from the drug library using the initial high-throughput drug screen were purchased from commercial sources.

Table 3.1: Drugs that are more effective at blocking cell growth and/or killing the CREB3L1-deficient TNBC HCC1806 cells, as compared to the HCC1806 + HACREB3L1 cells. HCC1806 and HCC1806+HACREB3L1 were separately transfected with a plasmid encoding red fluorescence protein (RFP) and selected in hygromycin to kill non-transfected cells. Each cell line was separately plated in six 384-well plates, allowed to attach and grow overnight. Cells were imaged and counted in each well using the ImageXpress Micro XLS widefield high content screening system. To each well for each cell line, one compound of an FDA-approved drug library of 1,818 compounds (L1000 from TargetMol) was added (to 1 μM final concentration). Control wells with no drug and DMSO alone (solvent for drugs) were included on each plate. Cells were imaged and counted daily for 5 days. DMSO (max 0.1%) had little or no effect on the cell growth/number. Cell viability (%) was calculated as (# cells in experimental well) / (# cells in DMSO control well)*100. The difference in cell viability is (HCC1806 % viability) – (HCC1806 + HACREB3L1 % viability).

	Drug Name	Drug Target or Class of Agent	HCC1806 % Viability	HCC1806 +HACREB3L1 Cl3 % Viability	Difference in %Viability
1	MLN9708	20S proteasome	10.7	74.1	-63.4
2	MLN2238	20S proteasome	28.4	72.8	-44.4
3	Erlotinib HCl	EGFR	21.4	63.5	-42.2
4	Icotinib HCl	EGFR	37.8	83.2	-45.4
5	Aminophylline	PDE	22.4	79.2	-56.8
6	Tadalafil	PDE	51.1	92.8	-41.7
7	Cobimetinib	MEK1 pathway	35.6	87.5	-51.9
8	Rabeprazole Na	ERK pathway	44.7	88.4	-43.7
9	Acitretin	Retinoic Acid Receptor	56.8	97.4	-40.6
10	Bexarotene	Retinoic Acid Receptor	76.1	124.5	-48.4
11	Climbazole	Anti-fungal	49.3	90	-40.7
12	Thioctamide	Anti-oxidant	58.1	102.3	-44.2
13	Moxifloxacin HCl	Antibiotic	70.8	119.8	-48.9
14	Quinacrine Dihydrochloride	Anti-malarial	73.9	115	-41.1
15	Moclobemide	Monoamine Oxidase A	66.2	141.6	-75.3
16	Tolazoline HCl	beta-adrenergic receptor	42.9	95	-52.1
17	Benorilate	Anti-inflammatory, analgesic	47.5	94.2	-46.7
18	Cisatracurium besylate	Neuromuscular blocking agent	48.3	96	-47.8
19	Felypressin	Vasoconstrictor	52.5	93.7	-41.2
20	Liothyronine	Thyroid hormone receptor	55.9	98.4	-42.5
21	Alfactadine	Histamine receptor	60.5	101.8	-41.3

Table 3.2: Drugs that are highly cytotoxic towards both the CREB3L1-deficient TNBC HCC1806 cells, and also the HCC1806 + HACREB3L1 cells at 1 μM. These results were obtained as described in Table 1.

	Drug Name	Drug Target or Class of Agent	HCC1806 % Viability	HCC1806 +HACREB3L1 Cl3 % Viability	Difference in % Viability
1	Sanguinarine Cl	STAT3, MMPs	5.1	3.7	1.4
2	Zinc Pyrithione	Anti-bacterial, Anti-fungal	1.1	2.7	-1.6
3	Digitoxin	Na+/K+ ATPase	2.8	6.5	-3.8
4	Doxorubicin HCl	Anthracycline - chemotherapy	18.7	35.3	-16.6
5	Digoxin	Na+/K+ ATPase	4.2	6.9	-2.7
6	Ouabain Octahydrate	Na+/K+ ATPase	4.5	6.3	-1.8
7	Bortezomib	20S proteasome	3.6	15.5	-11.9
8	Doxorubicin	Anthracycline - chemotherapy	9.6	36.6	-27
9	Nocodazole	Tubulin and microtubules	12.2	26	-13.8
10	Cladribine	Nucleoside Analog	13.4	27.7	-14.2
11	Cyclocytidine HCl	Nucleotide Analog	14	25.9	-11.9
12	Teniposide	Topoisomerase II	22.1	48.2	-26.1
13	Carfilzomib	Proteasome	2.4	3.8	-1.4
14	Isolanid	Na+/K+ ATPase	4	9.7	-5.6
15	Daunorubicin HCl	Anthracycline - chemotherapy	14	28.3	-14.3
16	Cephalomannine	Microtubules	15.2	26.3	-11.2
17	Panobinostat	HDACs	15.7	32.5	-16.8
18	Irinotecan	Topoisomerase I	17.8	31	-13.2
19	Verteporfin	light activated vascular occlusion	18.1	44	-25.9
20	Palbociclib Isethionate	CDK4/6	18.6	35.7	-17.1
21	Belinostat	HDACs	21.3	37.6	-16.3
22	Homoharringtonine	Inhibits protein translation	3.9	3.6	0.3
23	Hydroxy Campothecine	Topoisomerase I	6.5	11.2	-4.7
24	Romidepsin	HDACs	10.2	24.4	-14.2
25	Octenidine	Anti-infective	12.3	38.1	-25.8
26	Malathion	Acetylcholinesterase	21.3	54.7	-33.4

This initial validation experiment consisted of performing a cytotoxic assay with drugs at a test concentration of 1 μM in triplicate. Utilizing an Integra ASSIST PLUS liquid handling system, HCC1806 and HCC1806 + HACREB3L1 Cl3 cells were plated in 384-well black-walled

plates. The following day, each of the 47 compounds were added, in triplicate wells, to the cells in the 384-well black-walled plates to a final concentration of 1 μM. After 4 days, the cells were stained (nuclei and dead cells) and imaged using a ThermoFisher Scientific CX7 imager to quantify total and dead cells (Fig. 3.2).

Of the original 47 drugs, 20 of them were not considered validated (Table 3.3), as they did not impact the survival of either cell line by producing at least a 10% decrease in cell survival. These drugs were then also unlikely to produce a response in more robust *in vitro* and *in vivo* models at concentrations below 1 μM. Drugs that require concentrations above 1 μM *in vitro* to be effective will likely be intolerable at higher concentrations, so these drugs were not pursued further.

Promisingly, 27 drugs (Table 3.4) were validated as killing HCC1806 at a concentration of 1 μM. These drugs either killed both cell lines (HCC1806 and HCC1806 +HACREB3L1 Cl3) with similar efficacy or killed the HCC1806 cells more than the HCC1806 +HACREB3L1 cells (Table 3.4). By titrating the drugs out to lower concentrations with further follow-up experiments, it was possible that there would be a difference in killing efficiency between the two cell lines for some of the drugs. Therefore, these drugs were investigated further in drug titration assays at lower concentrations.

3.3 Drug Titration Experiments

Drug Titration experiments were carried out on the 27 drugs identified in the 1 μM validation assay to determine the EC_{50} values of each potential drug and compare the efficacy of each drug (Fig. 3.1). Utilizing an Integra ASSIST PLUS liquid handling system, HCC1806 and HCC1806 + HACREB3L1 Cl3 cells were plated in 384-well black-walled plates. The following day, 4 drugs were serially diluted, either 1:2 or 1:3 depending on the titration curve profile of the drug. Each drug, in a range of concentrations, was then added to each 384-well plate, in triplicate. After a 4-day drug treatment, the cells were stained, imaged, and viable cells were quantified using a ThermoFisher Scientific CX7 imager (Fig. 3.2).

The majority of drugs, like hallmark anthracycline chemotherapeutic reagent doxorubicin, were equally cytotoxic to both the CREB3L1-deficient HCC1806 cells or the CREB3L1 re-expressing HCC1806 +HACREB3L1 Cl3 (Fig. 3.3).

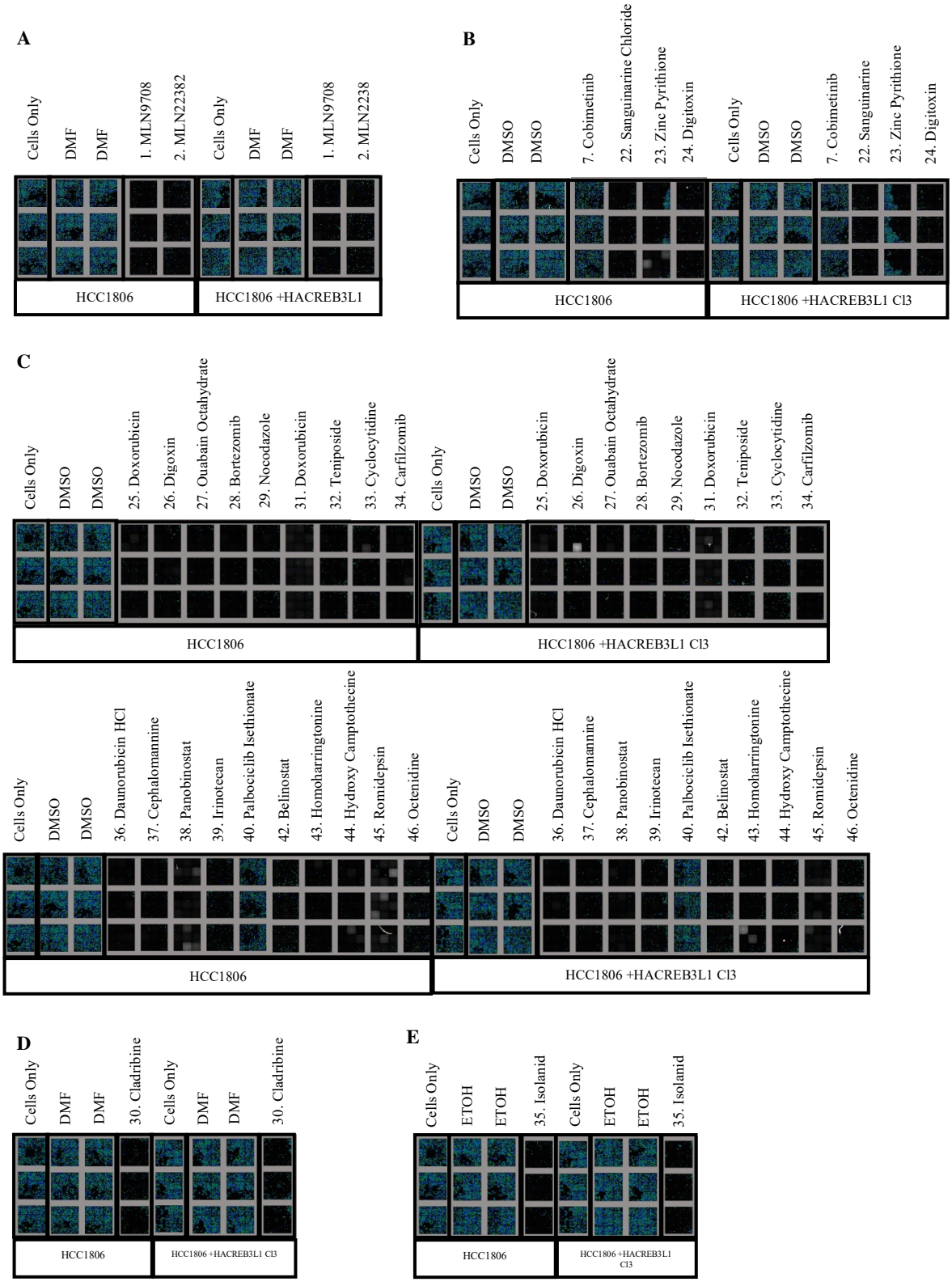

Figure 3.2: Drugs (27) that were validated as killing HCC1806 cells at a concentration of 1 μM. Cells were imaged and counted after a 4-day drug treatment using a Thermo Scientific™ CellInsight™ CX7 High Content Screening Platform. Images are labelled as Drug number (from Table 2.1). Drug name. (A) Plate 1, Drugs reconstituted with DMF. (B) Plate 1, Drugs reconstituted with DMSO. (C) Plate 2, Drugs reconstituted with DMSO. (D) Plate 2, Drugs reconstituted with DMF. (E) Plate 2, Drugs reconstituted with ETOH.

Table 3.3: Drugs (20) that were not validated at 1 μM. Each cell line was plated in two 384-well plates, allowed to attach and grow for 24 hrs. For each cell line, each compound was added in triplicate (to 1 μM final concentration). Control wells with no drug and DMSO, DMF or ETOH alone (solvent for drugs) were included on each plate. Solvents (max 0.1%) had little or no effect on the cell growth/number. Cells were imaged and counted after a 4-day drug treatment using a Thermo Scientific™ CellInsight™ CX7 High Content Screening Platform. Cell viability (%) was calculated as (# cells in experimental well) / (# cells in DMSO control well)*100. The difference in cell viability is (HCC1806 % viability) – (HCC1806 + HACREB3L1 % viability).

Drug #	Drug Name	HCC1806 Average % Viability	HCC1806 +HACREB3L1 Cl3 Average % Viability	Difference in % Viability
3	Erlotinib HCl	91.1	98.9	-7.8
4	Icotinib HCl	103.4	93.0	10.4
5	Aminophylline	122.3	105.0	17.2
6	Tadalafil	100.7	107.8	-7.1
8	Raberprazole Sodium	118.6	106.7	11.9
9	Acitretin	97.2	109.3	-12.2
10	Bexarotene	100.4	108.9	-8.6
11	Climbazole	114.1	111.1	3.1
12	Thioctamide	110.5	109.5	1.0
13	Moxifloxacin HCl	102.8	109.2	-6.4
14	Quinacrine dihydrochloride	98.9	106.7	-7.8
15	Moclobemide	111.5	101.8	9.7
16	Tolazoline HCl	116.3	99.3	17.0
17	Benorilate	113.8	104.5	9.4
18	Cisatracurium besylate	117.3	100.7	16.5
19	Felypressin	104.8	109.0	-4.2
20	Liothyronine	105.9	102.5	3.4
21	Alcaftadine	118.0	104.3	13.6
41	Verteporfin	100.1	114.7	-14.6
47	Malathion	108.8	116.8	-8.0

Table 3.4: Drugs (27) that were validated as killing HCC1806 cells at a concentration of 1 μM. Each cell line was plated in two 384-well plates, allowed to attach and grow for 48 hrs. For each cell line, one compound was added in triplicate (to 1 μM final concentration). Control wells with no drug and DMSO, DMF or ETOH alone (solvent for drugs) were included on each plate. Solvents (max 0.1%) had little or no effect on the cell growth/number. Cells were imaged and counted after a 4-day drug treatment using a Thermo Scientific™ CellInsight™ CX7 High Content Screening Platform. Cell viability (%) was calculated as (# cells in experimental well) / (# cells in DMSO control well)*100. The difference in cell viability is (HCC1806 % viability) – (HCC1806 + HACREB3L1 % viability).

Drug #	Drug Name	HCC1806 Average % Viability	HCC1806 +HACREB3L1 Cl3 Average % Viability	Difference in % Viability
1	MLN9708	0.8	1.0	-0.1
2	MLN2238 (Ixazomib)	3.3	3.0	0.3
7	Cobimetinib	62.1	70.5	-8.4
22	Sanguinarine Cl	2.1	1.8	0.3
23	Zinc pyrithione	7.3	32.7	-25.4
24	Digitoxin	1.0	2.1	-1.1
25	Doxorubicin HCl	0.7	1.2	-0.5
26	Digoxin	0.7	1.2	-0.6
27	Ouabain octahydrate	0.7	0.9	-0.2
28	Bortezomib (PS-341)	0.3	0.4	-0.2
29	Nocodazole	1.1	1.2	-0.1
30	Cladribine	1.7	2.5	-0.8
31	Doxorubicin	0.6	0.9	-0.3
32	Teniposide	0.7	1.4	-0.7
33	Cyclocytidine hydrochloride	0.6	2.1	-1.5
34	Carfilzomib (PR-171)	0.2	0.4	-0.2
35	Isolanid	1.3	2.3	-1.0
36	Daunorubicin hydrochloride	0.1	0.3	-0.2
37	Cephalomannine	0.6	0.5	0.2
38	Panobinostat (LBH589)	0.1	0.2	-0.1
39	Irinotecan	1.6	2.0	-0.4
40	Palbociclib (PD0332991) Isethionate	52.3	75.9	-23.6
42	Belinostat (PXD101)	4.0	3.8	0.2
43	Homoharringtonine	0.5	0.7	-0.2
44	Hydroxy Camptothecine	0.1	0.3	-0.1
45	Romidepsin	0.1	0.0	0.0
46	Octenidine	6.8	6.4	0.3

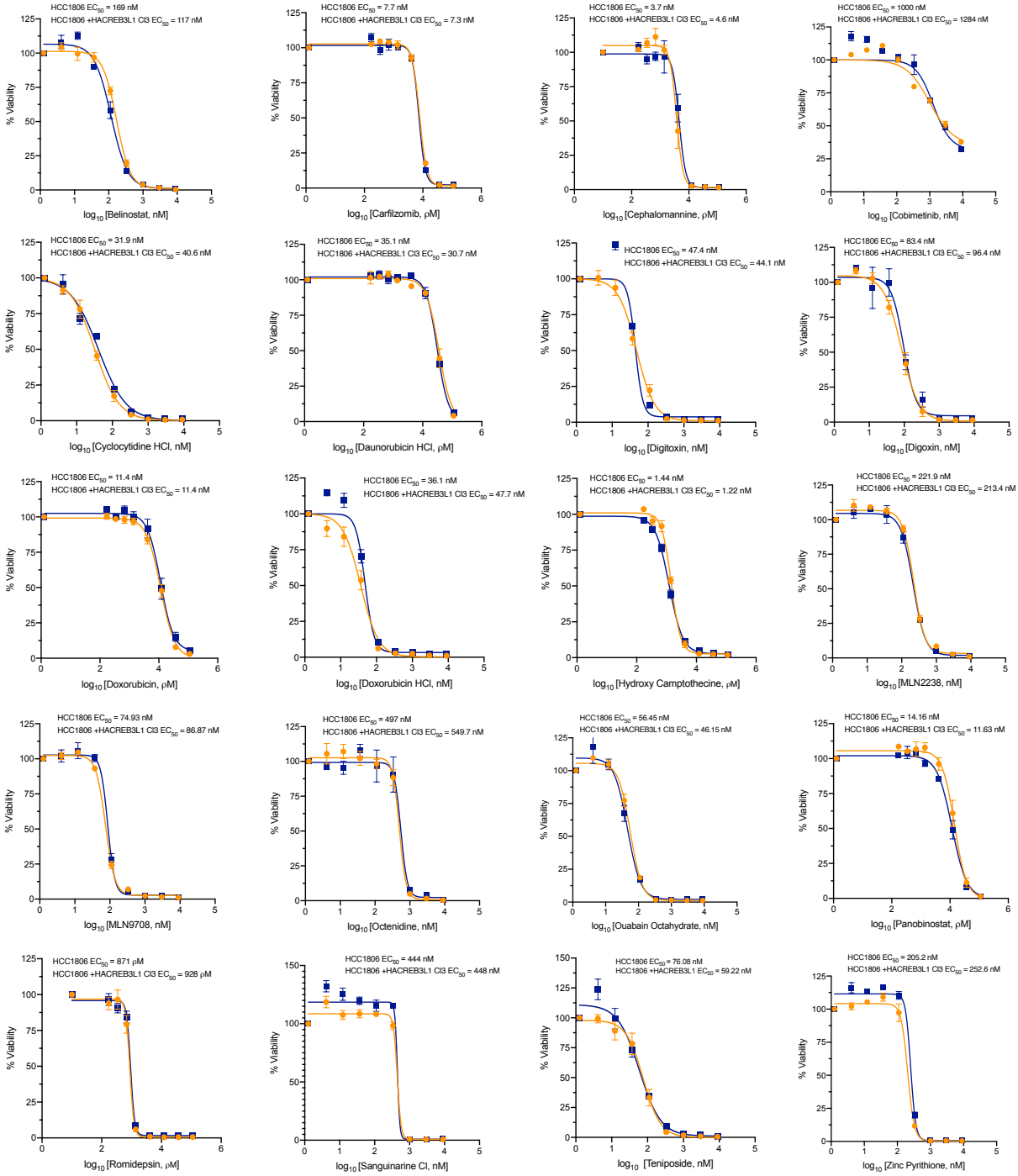

Figure 3.3: EC_{50} Determination for drugs that killed CREB3L1-deficient HCC1806 cells (Orange) and CREB3L1 re-expressing HCC1806 +HACREB3L1 cells (Blue) with similar efficacy at concentrations lower than 1 µM. Each cell line was plated in 384-well plates, allowed to attach and grow for 24 hrs. Control wells with DMSO, DMF or ETOH alone were included on each plate. Solvents (max 0.4%) had little or no effect on the cell growth/number. Cells were stained, imaged and counted after a 4-day drug treatment using a Thermo Scientific™ CellInsight™ CX7 High Content Screening Platform. Cell viability (%) was calculated as (# live cells in experimental well) / (# live cells in solvent control well)*100. % Viability values are reported with standard error of the mean of triplicate measurements (SE; n=1). 1:3 serial dilutions were made and added, in triplicate, to the plate.

Three drugs, like topoisomerase I inhibitor Irinotecan, selectively killed the CREB3L1 re-expressing cell line, HCC1806 +HACREB3L1 Cl3 at concentrations lower than 1 μM (Fig. 3.4).

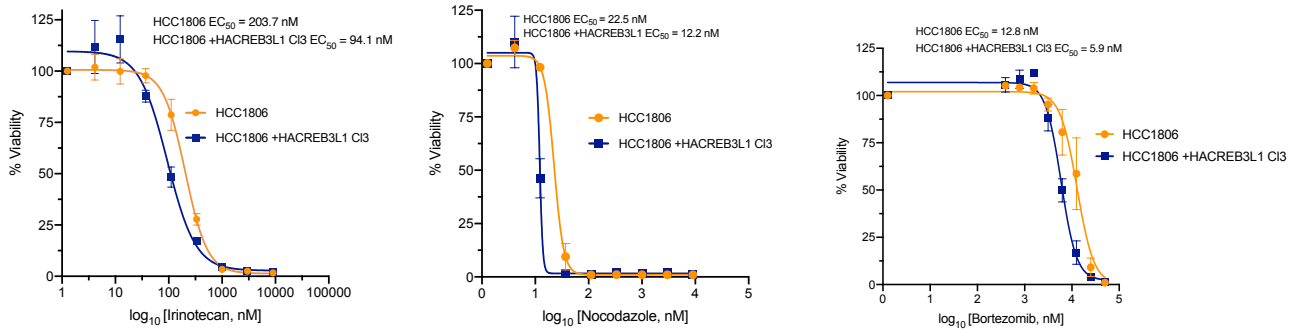

Figure 3.4: EC_{50} Determination for drugs that preferentially killed CREB3L1 re-expressing HCC1806 +HACREB3L1 cells at concentrations lower than 1 μM. Each cell line was plated in 384-well plates, allowed to attach and grow for 24 hrs. Control wells with DMSO, DMF or ETOH alone were included on each plate. Solvents (max 0.4%) had little or no effect on the cell growth/number. Cells were stained, imaged and counted after a 4-day drug treatment using a Thermo Scientific™ CellInsight™ CX7 High Content Screening Platform. Cell viability (%) was calculated as (# live cells in experimental well) / (# live cells in solvent control well)*100. % Viability values are reported with standard error of the mean of triplicate measurements (SE; n=1). 1:3 serial dilutions were made and added, in triplicate, to the plate.

There were 4 drugs that selectively killed the CREB3L1-deficient HCC1806 cells at concentrations lower than 1 μM (Fig. 3.5). The EC_{50} determinations for these drugs revealed that a smaller concentration of drug was required to achieve half of the maximal response (lowest % Viability) in the CREB3L1-deficient TNBC cells as compared to the CREB3L1-expressing TNBC cells. These drugs were then ranked in regard to their impact on HCC1806 CREB3L1-deficient breast cancer cells. Rankings were achieved according to differences in EC_{50} values, the differences in % Viability between the CREB3L1-deficient and CREB3L1-expressing cells, and mechanism of action of the drugs. The difference in EC_{50} values between the drugs was a valuable indicator of potency towards the cancer cells. Selective killing of the CREB3L1-deficient cells was another important consideration because it reflected the major goal of this project which is to identify targeted therapies for CREB3L1-deficient breast cancer. Finally, the mechanism of action of the drug, especially within the context of TNBC, was important to consider because identifying a rationale for the use of a promising drug (and possibly drug class) is important. The ranking is as follows (From the most to least efficacious): 1. palbociclib isethionate, 2. cladribine, 3. isolanid, 4. homoharringtonine.

Cladribine, a purine analog caused the largest decrease in % Viability in the HCC1806 cell line as compared to the HCC1806 +HACREB3L1 Cl3 cell line and had a fairly low EC_{50} value of

79 nM (Fig. 3.5). However, this drug is ranked 2nd to palbociclib isethionate due to its large number of possible serious side effects and its cytotoxic mechanism of action, discussed later (Voelker, 2019).

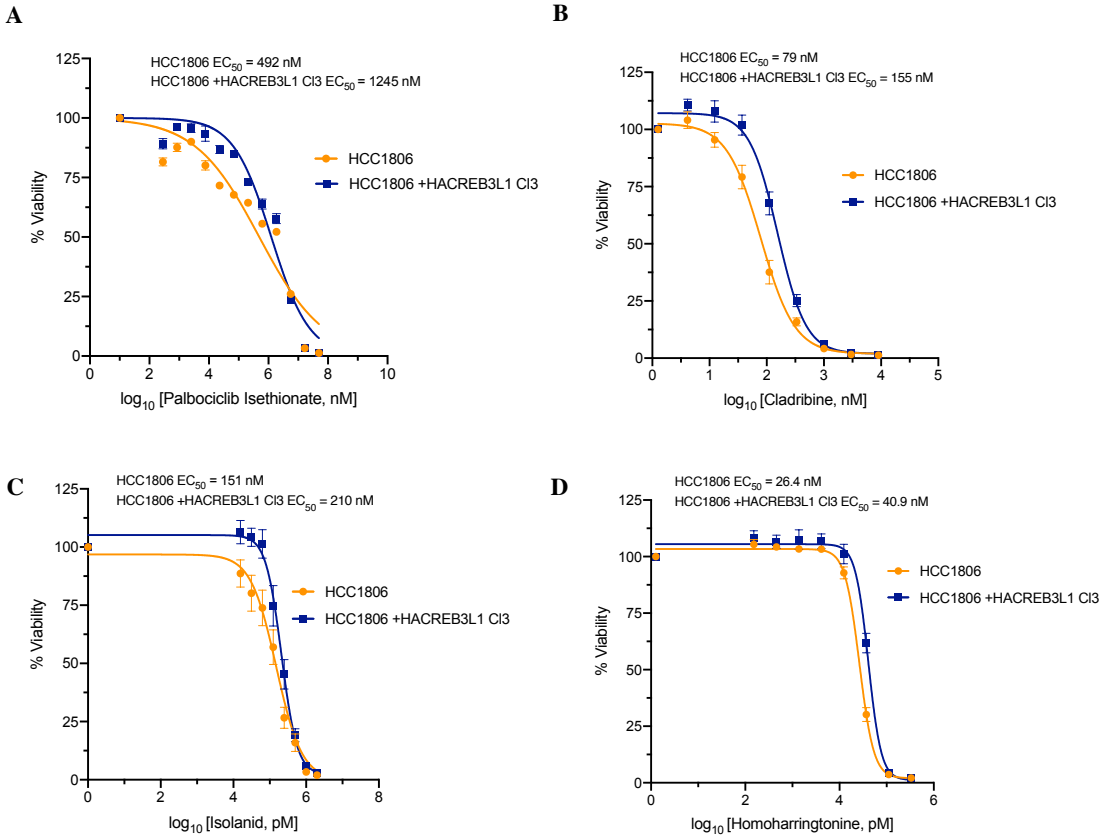

Figure 3.5: EC_{50} Determination for drugs that preferentially killed CREB3L1-deficient HCC1806 cells at concentrations lower than 1 µM. Experiments performed as in Figure 3.5. % Viability values are reported with standard error of the mean (SE; n=3). (A) Palbociclib Isethionate, *p<0.0001 (two-way ANOVA). 1:3 serial dilutions were made ranging from concentrations 0-50 µM and added, in triplicate, to the plate. (B) Cladribine, *p<0.0001 (two-way ANOVA). 1:3 serial dilutions were made ranging from concentrations 0-9 µM and added, in triplicate, to the plate. (C) Isolanid, *p<0.0001 (two-way ANOVA). 1:2 serial dilutions were made ranging from concentrations 0-2 µM and added, in triplicate, to the plate. (D) Homoharrintonine, **p<0.0011 (two-way ANOVA). 1:3 serial dilutions were made ranging from concentrations 0-333.33 nM and added, in triplicate, to the plate.

Palbociclib isethionate, a CDK4/6 inhibitor, was ranked as the most promising drug towards the CREB3L1-deficient HCC1806 TNBC cells because it caused a significantly larger decrease in % Viability in the CREB3L1-deficient HCC1806 cells as compared to the HCC1806 +HACREB3L1 Cl3 cells (Fig. 3.5). Although the difference in % Viability created by this drug was not as large as the 2nd ranked drug, cladribine, palbociclib isethionate's mechanism of action renders is more promising in the context of TNBC therapy due to current investigations of this drug class within the specific subtype. CDK4/6-inhibitors are emerging as potentially more

selective drugs than traditional chemotherapeutic reagents for TNBC (Matutino, Amaro & Verma, 2018).

From two-way ANOVA analysis, isolanid, a cardiac glycoside, had a larger difference of EC_{50} values between the HCC1806 and HCC1806 +HACREB3L1 Cl3 % Viability than the lowest ranked drug, homoharringtonine (Fig. 3.5). These two drugs did not show nearly as large a difference in selective killing between the HCC1806 cells and HCC1806 +HACREB3L1 Cl3 cells as compared to the top two drugs, cladribine and palbociclib isethionate (Fig. 3.5), though they are still very effective against both test cancer cell lines.

3.4 Adherent Nontumorigenic Control Drug Titration Experiments

Drug titration experiments were carried out in the CREB3L1-deficient TNBC cell line HCC1806 and control nontumorigenic breast cell line MCF10A for the top 4 promising compounds that selectively killed the HCC1806 cells. This was to determine if the compounds might have selective cytotoxicity within the CREB3L1-deficient cancer cells as compared to normal breast tissue.

As in other drug titration experiments, using an Integra ASSIST PLUS liquid handling system, HCC1806 and HCC1806 + HACREB3L1 Cl3 cells were plated in 384-well black-walled plates. The following day, 4 drugs were serially diluted, either 1:2 or 1:3 depending on the titration curve profile of the drug. Each drug, in a range of concentrations, was then added to each 384-well plate, in triplicate. After a 4-day interval of incubation with drug, the plates were imaged, and viable cells were quantified using a ThermoFisher Scientific CX7 imager.

Each of the top 4 promising drugs were cytotoxic to both the HCC806 and MCF10A cells with the exception of nucleoside analog cladribine (Fig. 3.6). However, palbociclib isethionate and homoharringtonine are chemotherapeutic drugs currently being used. Therefore, although they may be cytotoxic to the non-tumorigenic control cell line, this does not necessarily mean that they would not be useful therapeutically.

3.5 Drug Titration Experiments in Additional CREB3L1-deficient TNBC Cell Lines

To ensure that the effects of the most promising drugs were not just cell line specific to the CREB3L1-deficient HCC1806 cell line, the top 4 promising compounds were further tested in additional CREB3L1-deficient TNBC cell lines, HCC38 and BT549.

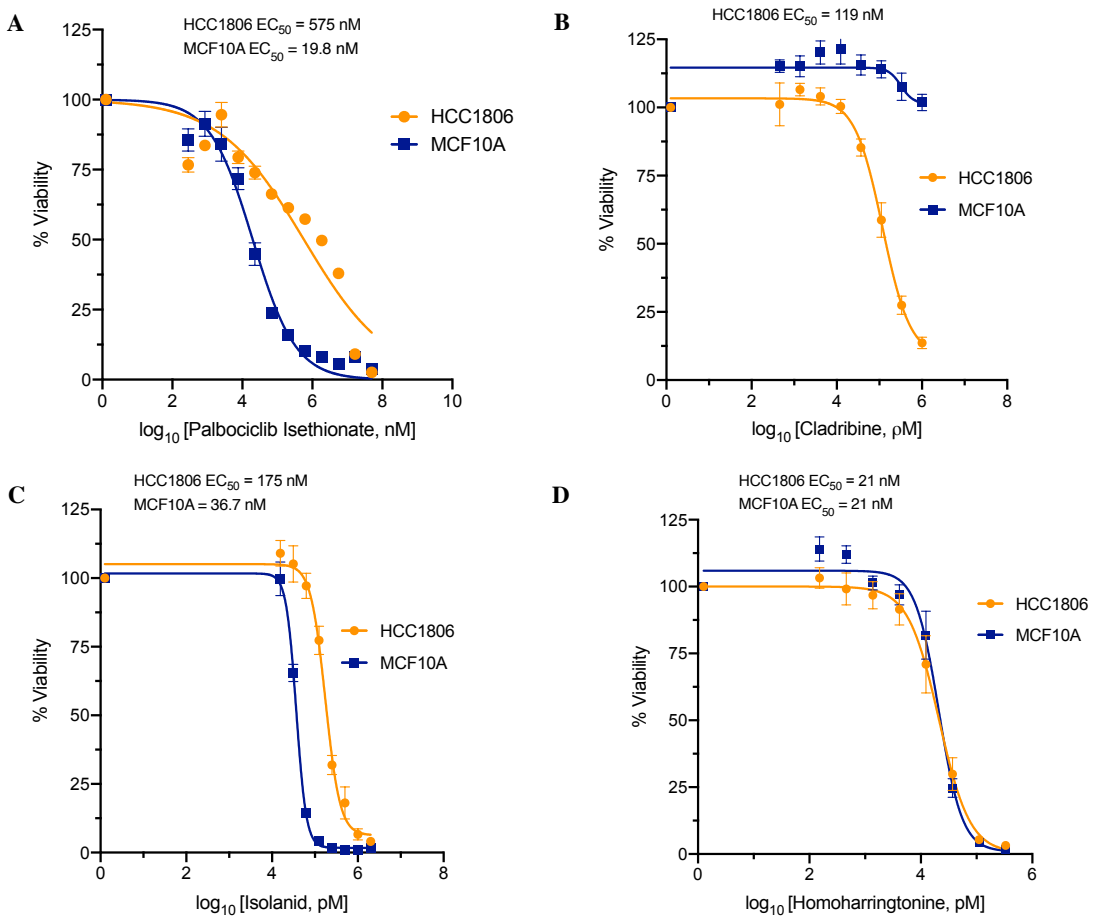

Figure 3.6: Drug Titrations for TNBC cell line HCC1806 and Control Non-Tumorigenic Breast cell line MCF10A. Each cell line was plated in 384-well plates, allowed to attach and grow for 24 hrs. Control wells with DMSO, DMF or ETOH alone were included on each plate. Solvents (max 0.4%) had little or no effect on the cell growth/number. Cells were imaged and counted after 4 days using a Thermo Scientific™ CellInsight™ CX7 High Content Screening Platform. Cell viability (%) was calculated as (# live cells in experimental well) / (# live cells in solvent control well)*100. Viability values are reported with standard error of the mean (SE; n=3). (A) Palbociclib isethionate, *p<0.0001 (two-way ANOVA). 1:3 serial dilutions were made ranging from concentrations 0-50 µM and added, in triplicate, to the plate. (B) Cladribine, *p<0.0001 (two-way ANOVA). 1:3 serial dilutions were made ranging from concentrations 0-9 µM and added, in triplicate, to the plate. (C) Isolanid, *p<0.0001 (two-way ANOVA). 1:2 serial dilutions were made ranging from concentrations 0-2 µM and added, in triplicate, to the plate. (D) Homoharringtonine, p = 0.0792, non-significant (two-way ANOVA). 1:3 serial dilutions were made ranging from concentrations 0-333.33 nM and added, in triplicate, to the plate.

As in all previous drug titration experiments, cells were plated on Day 0 using the ASSIST PLUS liquid handling system in 384 black-walled plates. The top 4 promising compounds (and doxorubicin, to determine the general sensitivity of the cells to drug) were added to the cells the next day (varying in concentration range and dilution factor depending on the optimal titration curve determined for each drug). After a 4-day drug treatment, the cells are stained, imaged and quantified, using the CX7 Cell Insight. Each experiment was repeated 3 times, with triplicate measurements for each additional cell line.

In the HCC38 cell line, all four promising drugs killed these CREB3L1-deficient cells (Fig. 3.7). Generally, the HCC38 cells were slightly less sensitive to each drug than the HCC1806 cells, (EC_{50} values; cladribine: 111 nM compared to 79 nM; isolanid: 240 nM compared to 151 nM; homoharringtonine: 50.1 nM compared to 26.4 nM), with the exception of palbociclib iseothionate (EC_{50} value 216 nM as compared to 492 nM) (Figs. 3.5 and 3.7). Of note, HCC38 cells were also less sensitive to standard of care chemotherapeutic reagent doxorubicin, suggesting they may be less sensitive to cytotoxic agents in general as compared to HCC1806 cells.

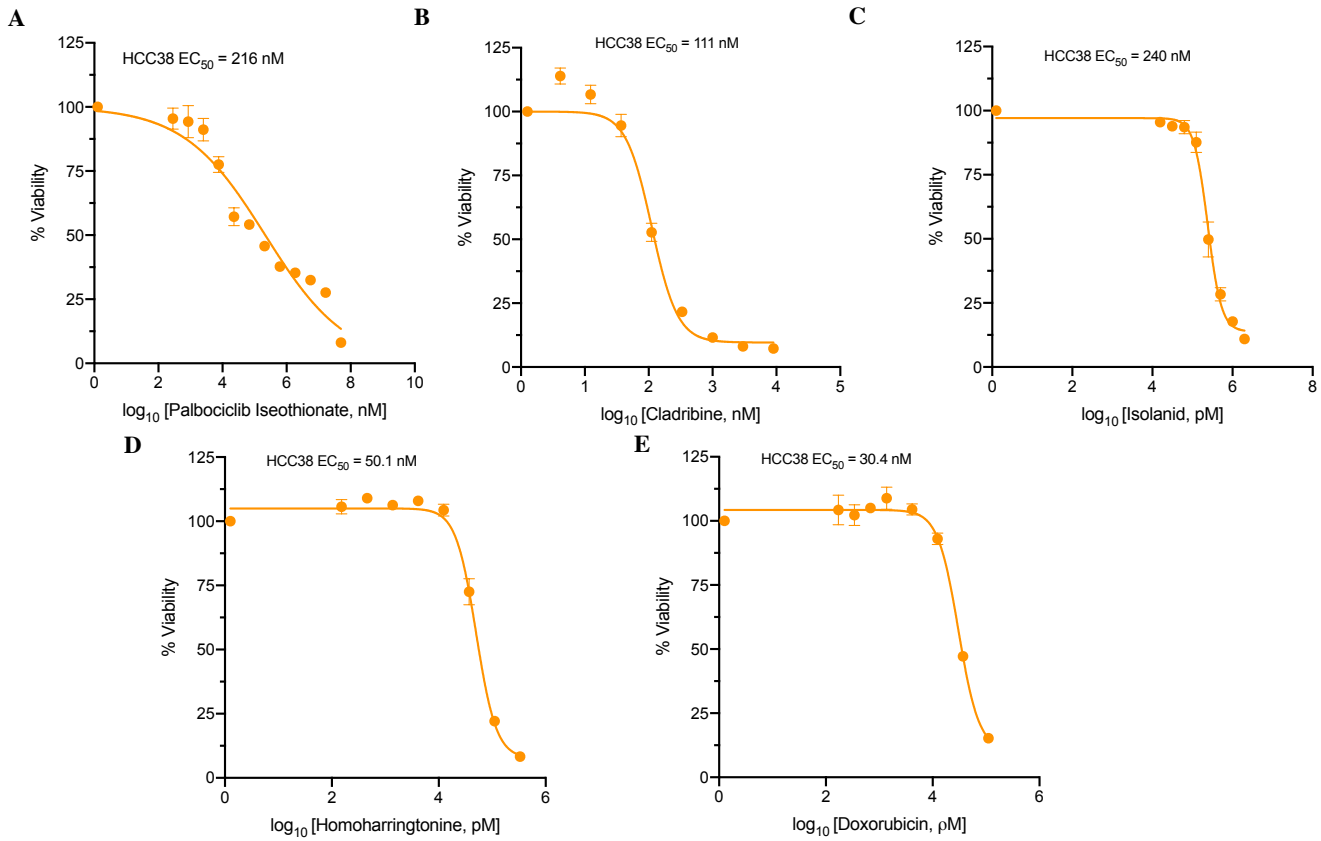

Figure 3.7: Drug Titration for TNBC cell line HCC38. Each cell line was plated in 384-well plates, allowed to attach and grow for 24 hrs. Control wells with DMSO, DMF or ETOH alone were included on each plate. Solvents (max 0.4%) had little or no effect on the cell growth/number. Cells were imaged and counted after a 4-day drug treatment using a Thermo Scientific™ CellInsight™ CX7 High Content Screening Platform. Cell viability (%) was calculated as (# live cells in experimental well) / (# live cells in solvent control well)*100. Viability values are reported with standard error of the mean (SE; n=3). **(A)** Palbociclib Isethionate, 1:3 serial dilutions were made ranging from concentrations 0-50 µM and added, in triplicate, to the plate. **(B)** Cladribine, 1:3 serial dilutions were made ranging from concentrations 0-9 µM and added, in triplicate, to the plate. **(C)** Isolanid, 1:2 serial dilutions were made ranging from concentrations 0-2 µM and added, in triplicate, to the plate. **(D)** Homoharringtonine, 1:3 serial dilutions were made ranging from concentrations 0-333.33 nM and added, in triplicate, to the plate. **(E)** Doxorubicin, 1:3 serial dilutions were made ranging from concentrations 0-111.11 nM and added, in triplicate, to the plate.

In the BT549 cell line, three of the four promising drugs killed these CREB3L1-deficient

cells with EC_{50} values in the nM range (EC_{50} values; cladribine: 216 nM; isolanid: 386 nM; homoharringtonine: 74.4 nM) (Fig. 3.8). Concentrations greater than 1 µM of palbociclib iseothionate were required to kill the BT549 cells since its EC_{50} value was 18 µM. Notably, BT549 cells were less sensitive to isolanid than HCC1806 or HCC38 cells, with an EC_{50} value of 386 nM compared to 151 nM and 240 nM, respectively. BT549 cells were also sensitive to doxorubicin treatment.

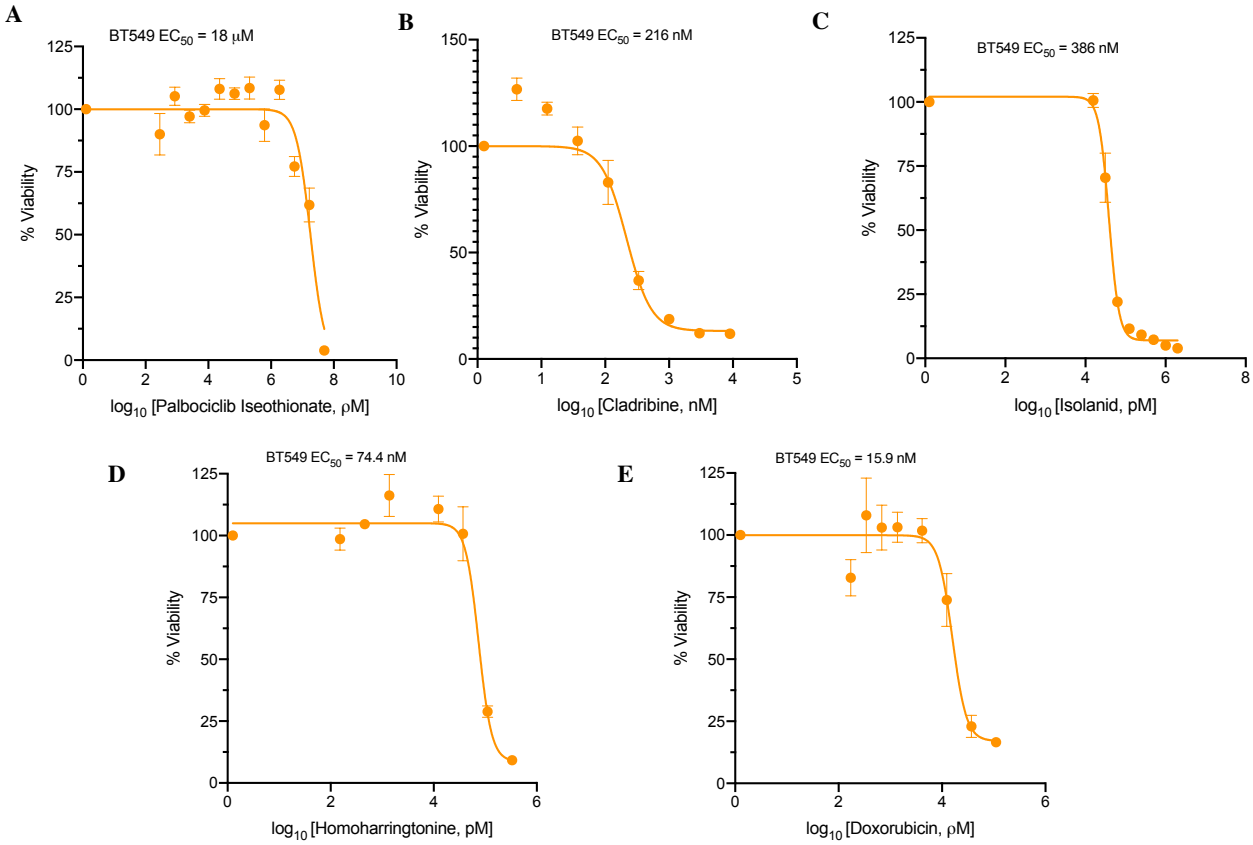

Figure 3.8: Drug Titration for TNBC cell line BT549. Each cell line was plated in 384-well plates, allowed to attach and grow for 24 hrs. Control wells with DMSO, DMF or ETOH alone were included on each plate. Solvents (max 0.4%) had little or no effect on the cell growth/number. Cells were imaged and counted after a 4-day drug treatment using a Thermo Scientific™ CellInsight™ CX7 High Content Screening Platform. Cell viability (%) was calculated as (# live cells in experimental well) / (# live cells in solvent control well)*100. Viability values are reported with standard error of the mean (SE; n=3). **(A)** Palbociclib isethionate, 1:3 serial dilutions were made ranging from concentrations 0-50 µM and added, in triplicate, to the plate. **(B)** Cladribine, 1:3 serial dilutions were made ranging from concentrations 0-9 µM and added, in triplicate, to the plate. **(C)** Isolanid, 1:2 serial dilutions were made ranging from concentrations 0-2 µM and added, in triplicate, to the plate. **(D)** Homoharringtonine, 1:3 serial dilutions were made ranging from concentrations 0-333.33 nM and added, in triplicate, to the plate. **(E)** Doxorubicin, 1:3 serial dilutions were made ranging from concentrations 0-111.11 nM and added, in triplicate, to the plate.

3.6 Standard of Care Combination Drug Titration Experiments

Currently, the standard of care treatment for TNBC patients in Saskatchewan is to give doxorubicin + cyclophosphamide and then paclitaxel, all hallmark, cytotoxic chemotherapeutic reagents. Due to obvious ethical considerations of implementing new promising therapies within the TNBC context, any new treatment would be most likely be offered in conjunction with existing therapies in a clinical trial setting. Therefore, to determine if any of the top promising compounds have a synergistic effect with standard of care chemotherapy treatments, combination drug titration experiments were carried out.

Cyclophosphamide is a nitrogen mustard alkylating agent and is metabolized to its active form by cytochrome P450 enzymes in the liver (Huttunen, Raunio & Rautio, 2011). Modifications to the cancer cells or very high concentrations of the parent compound is required for *in vitro* use in breast cancer cells to evaluate the effects of this compound *in vitro* (Chen, Waxman, Chen & Kufe, 1996; Kern & Schroeder, 2014). Additionally, how the metabolites of the prodrug exert their therapeutic effects is still not entirely understood (de Jonge, Huitema, Rodenhuis & Beijnen, 2005). Therefore, it is difficult to draw conclusions about the possible clinical applications of this chemotherapeutic reagent *in vitro*. For this reason, *in vitro* experiments were not carried out using cyclophosphamide. Promising drugs that advance to testing using *in vivo* mouse models of breast cancer could evaluate drug combinations and possible synergy that include cyclophosphamide.

The anthracycline doxorubicin and the microtubule stabilizing drug paclitaxel were the standard of care reagents used in these combination drug titration experiments. The EC_{50} values for these individual drugs were determined as previously described in drug titration experiments in order to be employed in the cross-design combination experiment were a pair of drugs were reciprocally titrated out as the second drug was used at their EC_{50} value (Fig. 3.9).

As in other drug titration experiments, on day 0, HCC1806 and HCC1806 +HACREB3L1 Cl3 cells (500 cells/well and 600 cells/well, respectively) were plated in a black-walled 384-well plate. The next day, foreground (titrated) and background (fixed EC_{50}) drugs were added to the plate in a cross-design format. After a four-day drug treatment, the cells were stained with Hoechst and Image IT Dead Green dye, imaged using the CX7, and % Viability was determined. The most promising combinations were analyzed in three separate experiments for 3 biological replicates.

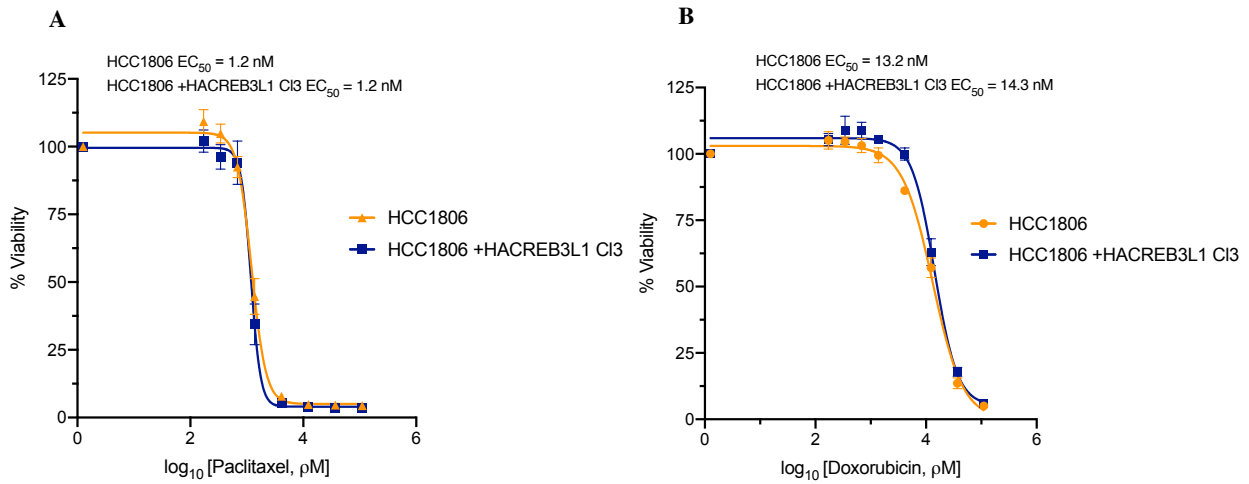

Figure 3.9: EC_{50} determination for current standard of care drugs for TNBC patients. 1:3 serial dilutions were made ranging from concentrations 0-111.11 nM and added, in triplicate, to the plate. Both paclitaxel (A) and doxorubicin (B) have similar EC_{50} values for the HCC1806 and HCC1806 +HACREB3L1 Cl3 cells.

SynergyFinder (version 2.0.11) was used with default settings in R (version 3.6.1) to determine the classification and degree of interaction between the most promising drugs and standard of care chemotherapeutic reagents doxorubicin and paclitaxel (He et al., 2018; R Core Team, 2019). The SyngergyFinder R-package converted the input % Viability values to % Inhibition (He et al., 2018). No other adjustments were made to the data. Data for both monotherapy and combination experiments were input. For every data point (% Inhibition at the intersection of a particular concentration of foreground drug and concentration of background drug), a delta score was assigned. The ZIP defined delta score is a quantification of the deviation of the observed response (% Inhibition) from the predicted response expected when the two drugs are combined and acting independently of each other (He et al., 2018; Yadav, Wennerberg, Aittokallio & Tang, 2015).

Positive delta scores are indicative of synergy (red in the synergy landscape) and negative delta scores are indicative of antagonism (green in the synergy landscape). The drugs could also have been non-interactive or additive (both shown in white in the synergy landscape). In order to display a continuous synergy landscape, the program interpolated data for which there was no measured response (He et al., 2018). As a result, minor banding patterns appear in some landscapes, and these patterns are less important predictors of synergy than major transitions within the landscape. Additionally, there are consistent areas of "antagonism" within each synergy landscape where drug concentrations are higher. However, this is more likely to be a stochastic

effect rather than true antagonism, as the response becomes saturated (there is maximal cytotoxicity) at these high concentrations and any noise becomes amplified there (He et al., 2018).

The maximum synergy (largest delta score [ZIP] that was not located in an extraneous band) of each combination in each cell line and the local response observed within the area of maximum synergy were used to evaluate the drug combination interactions (Table 3.5, Table 3.6).

The combinations involving the standard of care reagent paclitaxel were generally non-interactive in the CREB3L1-deficient cell line, HCC1806, with the exception of cladribine and paclitaxel (Fig. 3.10). However, in the case of cladribine, the synergy observed in the CREB3L1 re-expressing cell line, HCC1806 +HACREB3L1, was greater than that observed in the CREB3L1-deficient cell line (Table 3.5). Furthermore, the areas of synergy observed were not very large and did not occur at concentrations for which there is a significant local response (Fig. 3.10, Table 3.5). Overall, it is unlikely that combining any of the top four most promising drugs with paclitaxel would be beneficial for CREB3L1-deficient TNBC.

When combined with doxorubicin, isolanid did not show any synergistic interactions and the synergy landscape for this combination was mostly non-interactive (Fig. 3.11, Table 3.6). Thus, it is unlikely that combining this drug with doxorubicin would provide much benefit.

Combining doxorubicin with cladribine, homoharringtonine or palbociclib isethionate resulted in synergistic cytotoxicity (Fig. 3.11, Table 3.6). Ideally, the synergistic interactions observed in these drug combinations occurred at low drug concentrations (Table 3.6). When combined with doxorubicin, homoharringtonine produced the largest synergy delta score of any drug combination in areas of the landscape where the observed local response was approximately 30% (Table 3.6). Combining cladribine with doxorubicin produced synergy in areas of the landscape where the observed local response was approximately 20-40% (Table 3.6). The combination of palbociclib isethionate with doxorubicin produced synergy in areas of the landscape where the observed local response was the largest of the promising drug combinations, ~40-50% (Table 3.6). Higher maximum synergy was observed in the CREB3L1-deficient HCC1806 cell line than in the CREB3L1 re-expressing cell line when palbociclib isethionate or homoharringtonine was combined with doxorubicin (Table 3.6). The maximum synergy observed for cladribine, when tested in combination with doxorubicin, in each cell line was similar (Table 3.6). Although, a larger local response was observed in the CREB3L1-deficient cell line than in the CREB3L1 re-expressing cell line in areas of the landscape where maximum

synergy was achieved (Table 3.6). It is likely that combining cladribine, homoharringtonine or palbociclib isethionate with doxorubicin would be beneficial in CREB3L1-deficient TNBC.

Table 3.5: Synergy Scores for local maximums of the top 4 promising drugs combined with standard of care chemotherapeutic agent paclitaxel. (monotherapy EC_{50} = 1.2 nM for both HCC1806 ±HACREB3L1).

Cell line	Promising Drug (EC_{50} for monotherapy)	Maximum Synergy (ZIP)[1]	Local Response[2]	Paclitaxel Concentration (nM)[3]	Promising Drug Concentration (nM)[4]
HCC1806	Palbociclib Isethionate (492 nM)	5.6	~35% Inhibition	0.34	69
HCC1806 +HACREB3L1 Cl3	Palbociclib Isethionate (1245 nM)	10.1	~35% Inhibition	0.69	69
HCC1806	Cladribine (79 nM)	13.9	~25% Inhibition	0.69	12
HCC1806 +HACREB3L1 Cl3	Cladribine (155 nM)	22.9	~30% Inhibition	0.69	37
HCC1806	Isolanid (151 nM)	10.6	~70% Inhibition	1.4	16
HCC1806 +HACREB3L1 Cl3	Isolanid (210 nM)	11.0	~10% Inhibition	0.69	16
HCC1806	Homoharringtonine (26.4 nM)	6.4	~15% Inhibition	0.69	12
HCC1806 +HACREB3L1 Cl3	Homoharringtonine (40.9 nM)	22.7	~20% Inhibition	0.69	12

[1] Maximum Synergy (ZIP) = The largest delta score for a particular drug combination in a particular cell line that is not extraneous (e.g. minor banding).
[2] Local Response = The approximate % Inhibition at a given area of maximum synergy.
[3] Paclitaxel Concentration = The concentration of paclitaxel at a given area of maximum synergy.
[4] Promising Drug Concentration = The concentration of a promising drug at a given area of maximum synergy.

Table 3.6: Synergy Scores for local maximums of the top 4 promising drugs combined with standard of care chemotherapeutic agent doxorubicin. (monotherapy EC_{50} = 13.2 nM and 14.3 nM for HCC1806 ±HACREB3L1).

Cell line	Drug (EC_{50} for monotherapy)	Maximum Synergy (ZIP)[1]	Local Response[2]	Doxorubicin Concentration (nM)[3]	Promising Drug Concentration (nM)[4]
HCC1806	Palbociclib Isethionate (492 nM)	12.1	~40-50% Inhibition	1.4	37
HCC1806 +HACREB3L1 Cl3	Palbociclib Isethionate (1245 nM)	5.6	~20% Inhibition	1.4	37
HCC1806	Cladribine (79 nM)	15.7	~20-40% Inhibition	1.4	12.5
HCC1806 +HACREB3L1 Cl3	Cladribine (155 nM)	18.7	~25% Inhibition	4.1	37
HCC1806	Isolanid (151 nM)	4.5	~90% Inhibition	0.69	500
HCC1806 +HACREB3L1 Cl3	Isolanid (210 nM)	11.9	~10% Inhibition	4.1	63
HCC1806	Homoharringtonine (26.4 nM)	25.3	~30% Inhibition	4.1	12.3
HCC1806 +HACREB3L1 Cl3	Homoharringtonine (40.9 nM)	18.0	~10% Inhibition	1.4	4.1

[1] Maximum Synergy (ZIP) = The largest delta score for a particular drug combination in a particular cell line that is not extraneous (e.g. minor banding).
[2] Local Response = The approximate adjusted % Inhibition at a given area of maximum synergy.
[3] Doxorubicin Concentration = The concentration of doxorubicin at a given area of maximum synergy.
[4] Promising Drug Concentration = The concentration of a promising drug at a given area of maximum synergy.

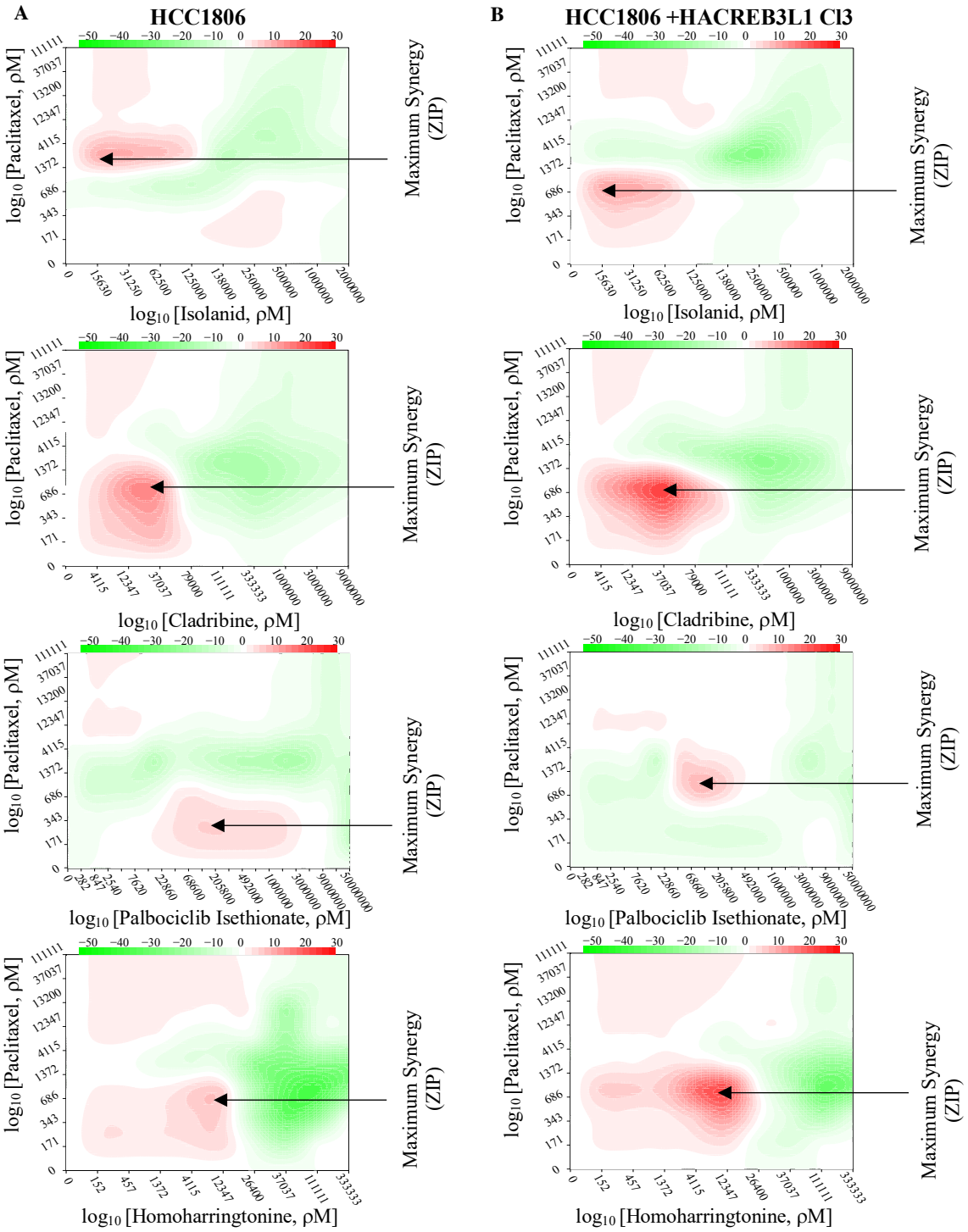

Figure 3.10: Synergy landscapes of the 4 most promising drugs combined with paclitaxel. Each cell line was plated in 384-well plates, allowed to attach and grow for 24 hrs. Promising drugs were fixed at their EC_{50} values and paclitaxel was titrated 1:3 (0-111.11 nM) and added to the plate. Control wells with DMSO, DMF or ETOH alone were included on each plate. Solvents (max 0.4%) had little or no effect on the cell growth/number. Cells were imaged and counted after 4 days using a Thermo Scientific™ CellInsight™ CX7 High Content Screening Platform. A delta score (ZIP) was calculated by the SynergyFinder R-package for at each data point as a measurement of drug interaction. ZIP scores are reported as an average of triplicate measurements (n=1). **(A)** HCC1806 **(B)** HCC1806 +HACREB3L1 Cl3

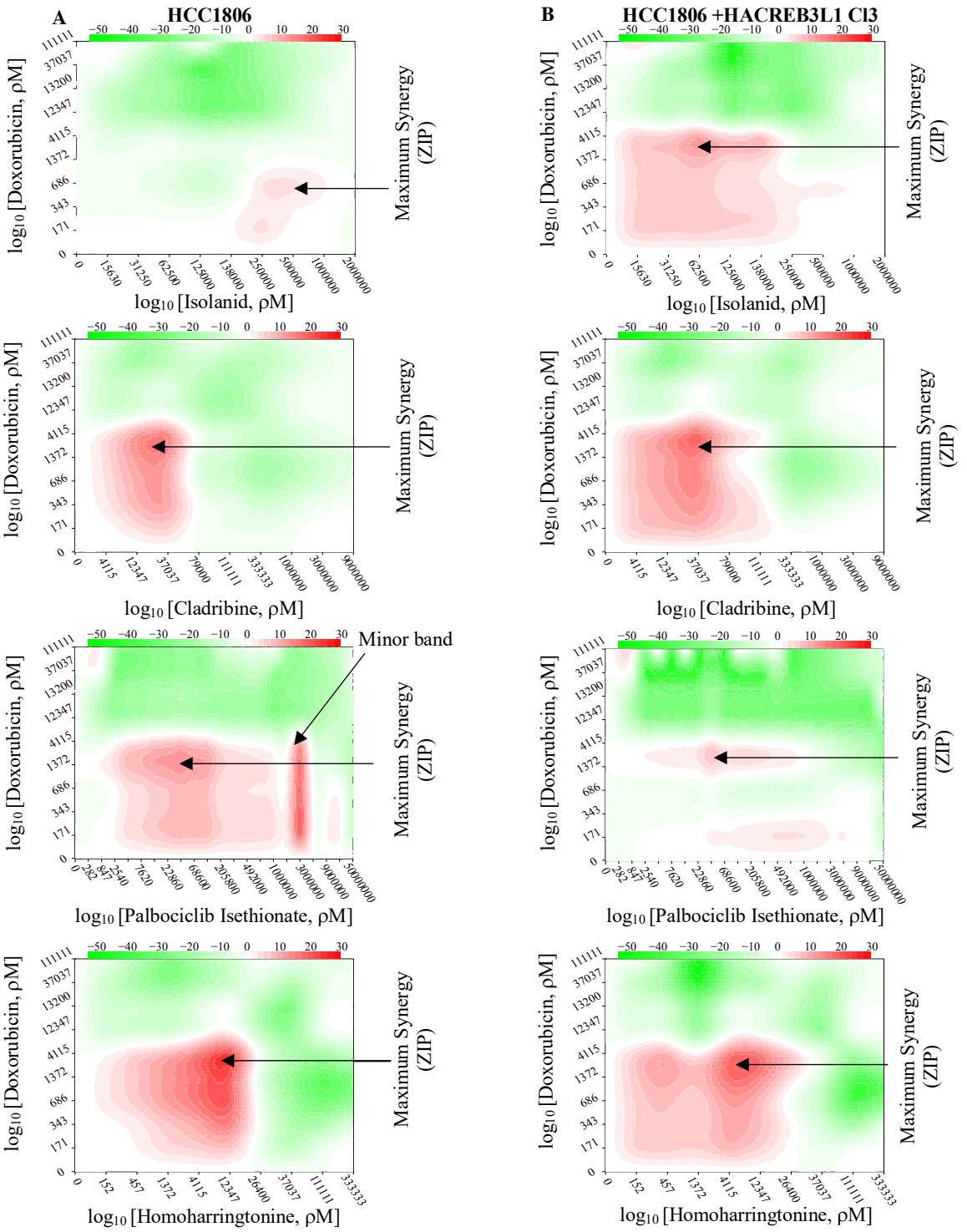

Figure 3.11: Synergy landscapes for the four most promising drugs combined with doxorubicin. Experiment was performed as described in Fig. 21. Isolanid (n=1) EC_{50} value = 151 nM; 1:2 serial dilutions (0-2 µM). Cladribine (n=3) EC_{50} value =79 nM; 1:3 serial dilutions (0-9 µM). Palbociclib Isethionate (n=3) EC_{50} value = 492 nM; 1:3 serial dilutions (0-9 µM). Homoharringtonine (n=1) EC_{50} value = 26.4 nM; 1:3 serial dilutions (0-333.33 nM). Doxorubicin EC_{50} value = 13.2 nM; 1:3 serial dilutions (0-111.11 nM). Maximum Synergy (ZIP) is reported as an average of triplicate measurements (n=1) or 3 biological replicates (n=3). (A) HCC1806 (B) HCC1806 +HACREB3L1 Cl3.

3.7 Spheroid Generation for Future Validation Assays

3D culture (spheroid) assays are thought to provide a better indication of drug effectiveness *in vivo* (Vinci et al., 2012). This 3D format can also model some characteristics of the tumor microenvironment including nutrient and oxygen gradients, cell-cell interactions, matrix deposition and gene expression profiles (De Witt Hamer et al., 2008; Ernst et al., 2009; Fischbach et al., 2007; Friedrich, Ebner & Kunz-Schughart, 2007; Ghosh et al., 2005; Weaver et al., 1997). Therefore, in order for the most promising drugs to be further evaluated as effective drugs for CREB3L1-deficient breast cancer, spheroid formation of the HCC1806 and HCC1806 +HACREB3L1 Cl3 cells was optimized.

Matrigel (1.5%) was determined to be the optimal concentration to plate the HCC1806 cells (at $5x10^3$ cells/well) and HCC1806 +HACREB3L1 Cl3 cells (at $8x10^3$ cells/well) in a final volume of 200 μL (Fig. 3.12). Matrigel concentrations above 1.5% impaired spheroid formation and concentrations below did not prevent cells from migrating. The continued optimization of this model will provide a better measure of the capability of drugs to exhibit robust activity *in vivo*.

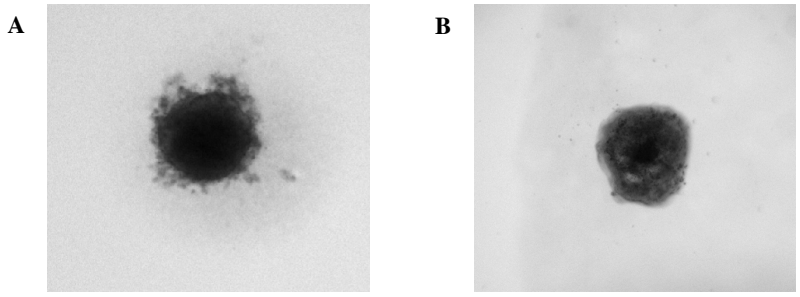

Figure. 3.12: HCC1806 spheroids with and without Matrigel 4 days after plating at $5x10^3$ cells/well. (A) HCC1806 spheroid plated without Matrigel. (B) HCC1806 spheroid plated with 1.5% Matrigel.

4. DISCUSSION

Breast cancer is the most common type of cancer affecting approximately 1 in 8 women in Canada (Canadian Cancer Society, 2015). The four major clinical subtypes of breast cancer are luminal A, luminal B, HER2+ and TNBC, which lacks expression of the receptors that define the other three subtypes: ER, PR, and HER2 (Eroles, Bosch, Pérez-Fidalgo & Lluch, 2012). Luminal A, luminal B and HER2+ breast cancers are treated with selective therapies that target the ER and/or HER2 receptors (Eroles, Bosch, Pérez-Fidalgo & Lluch, 2012). Unfortunately, despite the initial success of these treatments patients often relapse. Reoccurring metastatic breast cancer and TNBC are currently treated mainly with chemotherapy (Eroles, Bosch, Pérez-Fidalgo & Lluch, 2012). However, there are new more targeted treatments emerging that show promise in certain molecular contexts (Pernas & Tolaney, 2019; Robson, Goessl & Domchek, 2017; Turner, Neven, Loibl & Andre, 2017).

Recently, the genetic landscapes of clinical breast cancer subtypes have become better defined. For example, TNBC can now been divided into seven different molecular subtypes (Lehmann et al., 2011). There has been a shift in breast cancer drug development from focusing on single oncogenes towards understanding the heterogenous disease by its complex web of molecular interactions (Gibbs, 2000). The use of novel molecular signatures will help identify more targeted therapies that address the shortcomings of current treatments like drug resistance and the plethora of harmful off-target effects of chemotherapy.

CREB3L1-decifiency can be used as a novel molecular signature in the context of reoccurring metastatic breast cancer and TNBC. This transcription factor was discovered by our lab to be a key protein that was expressed in non- or poorly metastatic cells, but its expression was downregulated or lost in metastatic human and rat breast cancer cells. CREB3L1 acts as a metastasis suppressor in breast cancer and it represses the expression of genes involved in angiogenesis, metastasis and tumorigenesis (Mellor, Deibert, Calvert, Bonham, Carlsen & Anderson, 2013; Ward et al., 2016).

CREB3L1-expression is frequently downregulated or completely lost in approximately 30% of breast cancers, 90% of which are TNBCs, and loss of CREB3L1 expression is a predictor of poor prognosis (Ward et al., 2016). CREB3L1 can be downregulated in breast and bladder cancer by epigenetic silencing (Rose et al., 2014; Ward et al., 2016). In prostate cancer, there are frequent alterations to the regulatory region of the CREB3L1 gene which are thought to contribute

to tumorigenesis (Dhingra et al., 2017). In these contexts, CREB3L1 has a protective role as a tumor suppressor and its loss is associated with progression of the disease. Identifying new therapies for CREB3L1-deficient breast cancers is an unmet clinical need due to the poor prognosis these patients typically face and the lack of targeted therapies available.

The results in this thesis identify a number of drugs that selectively target CREB3L1-deficient human breast cancer cells. The identification of these drugs, and the possible connections that can be made from their anticancer mechanisms of action will provide a rationale for selection of the best therapies for CREB3L1-deficient TNBC and shape further development of new drugs for CREB3L1-deficient TNBC.

The new compounds for CREB3L1-deficient breast cancers identified in this project were selected and validated using a global drug discovery approach. Newly emerged HCS technologies were used to support the goal of understanding and implementing new CREB3L1-deficient therapies within the complex heterogeneity of the disease, by testing a large number of compounds with a variety of indicated uses and mechanisms of action. The FDA-approved library (1,818 compounds) was screened in a TNBC cell line ±CREB3L1. From the screen, 27 drugs were identified and then validated as killing CREB3L1-deficient cells. These 27 drugs were then tested over a wider range of concentrations. From these follow-up drug titration experiments, a total of four compounds were identified that preferentially killed CREB3L1-deficient cells. Furthermore, these drugs were effective across multiple CREB3L1-deficient TNBC cell lines and one drug was not cytotoxic towards a non-tumorigenic control breast cell line.

Palbociclib isethionate, a CDK4/6 inhibitor, cladribine, a purine analog, isolanid, a cardiac glycoside and homoharringtonine, a protein synthesis inhibitor were the four drugs identified that specifically killed the CREB3L1-deficient line (HCC1806) significantly more than the cell line re-expressing CREB3L1 (HCC1806 +HACREB3L1 Cl3). Additionally, all four of these drugs were further evaluated across three TNBC cell lines (HCC1806, HCC38 and BT549). Palbociclib isethionate was only effective in two TNBC cell lines (HCC1806 and HCC38). The other three drugs were generally effective against the three CREB3L1-deficient TNBC cell lines tested, suggesting that they are the most promising.

The non-tumorigenic control breast cell line, MCF10A was sensitive to all of the most promising drugs, with the exception of cladribine which was not cytotoxic towards this cell line. Since cladribine was selectively toxic towards the cancerous cells and not the noncancerous normal

breast cells, this suggests that this drug will have limited off-target cytotoxicity. However, even though the other promising drugs were cytotoxic towards the MCF10A cells, this does not mean that these treatments will not be effective in treating CREB3L1-deficient breast cancers. Furthermore, there is the possibility that these promising compounds could be given in combination with current chemotherapeutic reagent, doxorubicin at lower doses to reduce cytotoxic effects in normal cells.

Currently, in Saskatchewan, the standard of care chemotherapy treatment is to give doxorubicin with cyclophosphamide once every 2 weeks for four cycles, followed by paclitaxel once per week for 12 cycles. Addition of any of the four promising drugs with paclitaxel did not show synergy in the CREB3L1-deficient HCC1806 cells, therefore, there is likely no benefit in combining them for TNBC. The combination of isolanid with doxorubicin also did not appear to provide synergic treatment benefits. Three drugs, homoharringtonine, cladribine and palbociclib isethionate, each showed synergy when tested in combination with doxorubicin, and provided more inhibition/cytotoxicity towards the HCC1806 TNBC cells at lower drug concentrations than when each drug was used separately.

In this project, drug synergy occurred when the drugs that were combined (homoharringtonine, cladribine or palbociclib isethionate and doxorubicin) targeted the same cellular process. Cladribine is a nucleoside analog and directly halts DNA replication (Piro, Carrera, Carson & Beutler, 1990). Palbociclib isethionate creates a G_1 block and prevents the entry of the cells into the DNA replication (S) phase of the cell cycle (Toogood et al., 2005). Doxorubicin is a topoisomerase II inhibitor whose activity leads to further DNA damage, and disruption of DNA replication (Pommier, Leo, Zhang & Marchand, 2010). Therefore, all three of these drugs interfere with DNA replication. Homoharringtonine is a direct inhibitor of protein synthesis whose pharmacological activity may be augmented by the additional destruction of proteins by reactive oxygen species (ROS) produced by doxorubicin (Thorn et al., 2011). The synergistic potential between homoharringtonine, cladribine or palbociclib isethionate and doxorubicin, suggests that combining one of these therapies with doxorubicin might improve the success of the therapy and reduce the dose necessary, which would in turn reduce the intensity of harmful off-target side effects experienced by currently prescribed cytotoxic doses. It would also be interesting in the future to test if there is synergistic potential between any of the promising drugs (homoharringtonine, cladribine, palbociclib isethionate and isolanid).

Interestingly, all of these drugs have very different mechanisms of action and are indicated in a wide variety of cancers, and conditions (e.g. heart failure for isolanid). As we have just identified these drugs as potential drugs that could target CREB3L1-deficient breast cancers, we do not currently know their mechanism of action in this context. However, from our knowledge of CREB3L1 and the current literature on these drugs it is possible to speculate on potential modes of action, which can be assessed in future studies. Since CREB3L1 is a transcription factor that represses genes promoting metastasis, angiogenesis and tumorigenesis, it is possible that genes dysregulated in the absence of CREB3L1 could make direct or indirect targets for one, or many of the most promising drugs.

Palbociclib isethionate is a highly specific cyclin-dependent kinase 4 (CDK4) and CDK6 inhibitor and is currently under investigation in a phase I/II nonrandomized, open-label, single-arm trial in combination with bicalutamide (a non-steroidal androgen receptor inhibitor) for safety and efficacy in TNBC (Fry et al., 2004; Matutino, Amaro & Verma, 2018). Currently, combining CDK4/6 inhibitors with hormonal treatments is indicated for hormone receptor positive, HER2 negative breast cancer. The retinoblastoma (Rb1) pathway is frequently dysregulated in breast cancer, often as a result of the amplification and/or overexpression of cyclin D1 (Cancer Genome Atlas, 2012; Sherr & McCormick, 2002). CDK4/6 inhibitors show promise as potential biomarkers because these targets are frequently amplified in breast cancer and specifically inhibiting these targets might produce selective antiproliferative activity in TNBC cells (Cancer Genome Atlas, 2012; Fry et al., 2004). Palbociclib is highly selective and is thought to rely on the Rb1 pathway to provide a G1 block, inhibiting cells from entering S phase, thereby preventing cell growth and DNA replication (Toogood et al., 2005). This inhibitor prevents the phosphorylation of Rb by CDK4 and CDK6, which normally promotes DNA replication and therefore cell division (Sherr & McCormick, 2002). Many CDK inhibitors actually favor CDK1 and CDK2 inhibition even though CDK4 and CDK6 have been identified as the most important CDKs for regulating cell proliferation (Fry et al., 2004; Toogood et al., 2005). Palbociclib is especially effective in Rb+ breast cancers, including advanced hormone receptor positive, Rb+ breast cancers (DeMichele et al., 2015).

Since palbociclib isethionate was not cytotoxic towards BT549 cells, and the BT549 cell line is completely devoid of Rb expression, it is possible that this pathway component was necessary for the CDK4/6 inhibitor to exert its effects (Robinson et al., 2013). HCC38 cells and

HCC1806 cells contain the Rb protein, so this may explain their sensitivity to the drug (Raspé et al., 2017).

Rb expression is lost in approximately 30% of TNBCs (Witkiewicz & Knudsen, 2014). However, while the presence of Rb expression in TNBC has been shown in some cases to predict response to CDK4/6 inhibitors like palbociclib isethionate (Witkiewicz et al., 2018), there are a number of other possible targets linked to CDK4/6 that sensitize TNBC cells to CDK4/6 inhibitors beyond Rb like Forkhead Box M1, p16, VEGFA, Death Effector Domain-containing DNA-binding protein and epidermal growth factor receptor (Anders et al., 2011; Foidart et al., 2019; Kollmann et al., 2013). Furthermore, one study demonstrated that Rb expression did not influence sensitivity of TNBC cells to palbociclib (Robinson et al., 2013).

Interestingly, the activin-SMAD pathway, a downstream target of CDK4/6 (independent of Rb) was shown to be a good target for palbocilcib in CREB3L1-deficient T47D luminal A breast cancer cells (Harada et al., 2019). Therefore, it is possible that in CREB3L1-deficient TNBC there are mediators of cytostasis (independent of Rb), downstream of CDK4/6, like the activin-SMAD pathway. Inhibition of CDK4/6 by palbociclib worked together with SMAD signaling in T47D cells to prevent cell division (Harada et al., 2019). The SMAD pathway promotes cytostasis, enhanced by palabociclib in ER+ T47D cells, but in aggressive CREB3L1-deficient (Hs578T) cells this pathway possibly promotes tumorigenesis, and the way in which the activin-SMAD pathway interacts with CDKs in this context is unknown (Harada et al., 2019).

Homoharringtonine inhibits protein synthesis and induces the rapid loss of proteins with short half-lives, regulating cell proliferation and cell survival in chronic myeloid leukemia (Lü & Wang, 2014). In CREB3L1-deficient TNBC cell lines, (MDA-MB-157, MDA-MB-468 and MDA-MB-231) homoharringtonine was shown to rapidly reduce protein expression of anti-apoptotic proteins, in particular Mcl-1, in a cell line, dose and time dependent manner, inhibiting cell survival (Yakhni et al., 2019). It is possible that CREB3L1 normally has a role to play in regulating anti-apoptotic proteins and that homoharringtonine restored the apoptotic process that killed the breast cancer cells lacking CREB3L1. One study has also implicated CREB3L1 as having a role in mitochondrial-mediated apoptosis (discussed later) (Zou et al., 2016).

Isolanid is a cardiac glycoside and inhibits the alpha subunit of the Na^+/K^+-ATPase and has recently been shown to induce apoptosis selectively in breast, lung and liver cancer cells (Reddy, Kumavath, Ghosh & Barh, 2019). Cardiac glycosides are indicated in the treatment of

cardiovascular disease and increase cardiac output by indirectly increasing intracellular calcium of cardiomyocytes through the inhibition of the Na+/K+-ATPase. It would be interesting, in the future, to identify the specific mechanism through which isolanid exhibits its CREB3L1-deficient selective toxicity. In lung, liver and CREB3L1-deficient luminal A breast cancer cells (MCF7), Isolanid was shown to selectively kill cancerous cells by arresting the cells in G2 and M phase and it is likely that a number of pathways are involved, including Janus kinase/signal transducers and activators of transcription (JAK/STAT) signalling and the phosphatase and tensin homolog (PTEN)/p53 pathways (Reddy, Kumavath, Ghosh & Barh, 2019). Whereas CREB3L1 has currently not been shown to be connected to JAK/STAT or PTEN/p53 pathways, it would be interesting to investigate the possible connection of CREB3L1 to these pathways in future experiments. In hepatocarcinoma, isolanid was found to act through protein kinase C (PKCδ) to induce apoptosis (Chao et al., 2017). Again, the role of CREB3L1 in regulating apoptosis should be further evaluated in the future (discussed later).

Cladribine is a cytotoxic purine analog and it has previously been demonstrated to be highly cell specific, producing less toxic side effects as a result (Piro, Carrera, Carson & Beutler, 1990). Cladribine specifically targets lymphocytes and produces a remarkably strong clinical response in hairy-cell leukemia, chronic lymphocytic leukemia, and non-hodgkin's lymphoma (Piro, Carrera, Carson & Beutler, 1990; Sigal, Miller, Schram & Saven, 2010). Lymphocytes are unique in that they express high levels of deoxycytidine kinase (DCK). Cladribine is a prodrug and requires phosphorylation by DCK to generate its active form, 2-chlorodeoxyadenosine triphosphate (Sigal, Miller, Schram & Saven, 2010), and this requirement fulfilled by the high levels of DCK in lymphocytes is the likely attribute of its high cellular specificity. Once active, cladribine competes with dATP for incorporation into DNA and also potently inhibits ribonucleotide reductase (RNR), interfering with nucleotide metabolism (Sigal, Miller, Schram & Saven, 2010; Tsesmetzis, Paulin, Rudd & Herold, 2018).

DCK is also overexpressed in poor outcome breast cancers, including the metastatic CREB3L1-deficient breast cancer cell lines (HCC1954, BT474, SK-BR-3, MDA-MB-231, MCF7, and T47D) and has low expression in the non-tumorigenic breast cell line MCF10A (Geutjes, Tian, Roepman & Bernards, 2012; Ward et al., 2016). This may explain the specific cytotoxic effects of cladribine in the CREB3L1-deficient TNBC cell line HCC1806 and not in the same cell line expressing CREB3L1 or the MCF10A cells. Future experiments that test the effectiveness of

cladribine against the cell lines listed above that overexpress DCK might identify upregulated DCK as a possible explanation for their selective sensitivity. Reciprocally, downregulation of DCK is likely the major contributor to cladribine resistance (Lotfi, Juliusson & Albertioni, 2003) and downregulation of DCK in breast cancer cells also likely confers resistance to another nucleoside analog, gemcitabine (Wu, Zhao, Tan, Wang & Shen, 2019). It would be good to determine if there is a direct relationship between CREB3L1 and DCK.

One common mode of action of all of the promising drugs identified in this study is the alteration of the mitochondrial membrane potential of cancer cells, which eventually leads to apoptosis. Semisynthetic homoharringtonine decreased the mitochondrial membrane potential and caused the release of cytochrome c in myeloid leukemia cells to induce apoptosis (Tang et al., 2006). Cladribine decreased the mitochondrial membrane potential in human leukemia cells leading to caspase-dependent and independent apoptosis (Marzo, Pérez-Galán, Giraldo, Rubio-Félix, Anel & Naval, 2001). In hepatocellular carcinoma cells, isolanid, through the inhibition of PKCδ, caused a decrease in mitochondrial membrane potential to induce apoptosis (Chao et al., 2017). Palbociclib isethionate has been shown to induce reactive oxygen species (ROS) which is known to trigger the mitochondrial-mediated pathway of apoptosis, although the molecular mechanism remains unclear (Vijayaraghavan et al., 2017).

Mitochondria are emerging as having an important role to play in cancer progression, including in metastasis. In addition to fulfilling their long known role of providing cells with energy, mitochondria are also home to signaling cascades that regulate apoptosis, adaptive responses and innate immunity (Altieri, 2019; Melber & Haynes, 2018).

Recently, the role of mitochondria in metastasis has emerged as a significant component of cancer progression. There are a number of ways in which mitochondria may contribute to this phenomenon: (Porporato, Filigheddu, Pedro, Kroemer & Galluzzi, 2018). Onco-promoting events such as DNA damage and the ability to sustain cell stress responses have also been identified within mitochondria. Mutations within mitochondrial DNA involving most notably the electron transport chain and ROS have been reported within tumors, and mitochondria have their own unfolded protein response (Beadnell, Scheid, Vivian & Welch, 2018; Melber & Haynes, 2018).

One study has connected CREB3L1 with the mitochondrial apoptotic pathway in human bronchial epithelial BEAS-2B cells that have been exposed to silica nanoparticles (Zou et al., 2016). In this context, CREB3L1 and B-cell lymphoma-2 (BCL-2) genes were hypermethylated,

and this led to their downregulation which was shown to be associated with the mitochondrial-mediated apoptosis via the PI3K/Akt signalling pathway (Zou et al., 2016). CREB3L1 has been silenced through methylation in breast and bladder cancer (Rose et al., 2014; Ward et al., 2016), although the possible role of CREB3L1 inducing mitochondrial-mediated apoptosis has not been studied in cancer. It is possible that genes regulated by CREB3L1 are involved in mitochondrial-mediated apoptosis, and in the absence of CREB3L1 they become dysregulated. It is also possible that the promising drugs in this study were able to restore aspects of mitochondrial-mediated apoptosis, dysregulated in the absence of CREB3L1 as part of their selective mechanism of action.

Further work needs to be done to understand the detailed mechanisms of action for these promising drugs, palbociclib isethionate, cladribine, isolanid, and homoharringtonine in selectively killing CREB3L1-deficient TNBC cells. This includes determining the possible role of CREB3L1 in mitochondrial-mediated apoptosis, the possible upregulation of DCK in CREB3L1-deficient cells, and the possible interaction of CREB3L1 with the SMAD pathway, evaluated in future experiments.

Furthermore, drugs of the same class as the promising CREB3L1-deficient therapies identified (i.e. additional CDK4/6 inhibitors, nucleoside analogs, protein synthesis inhibitors and cardiac glycosides) should be tested in CREB3L1-deficient cell lines to evaluate the potential of novel classes of drugs to treat CREB3L1-deficient breast cancer. The promising drugs identified and validated in this study should be tested in CREB3L1-deficient breast cancer subtypes beyond TNBC, especially luminal A breast cancers, for which CREB3L1-deficiency is also a predictor of poor prognosis (Ward et al., 2016). Finally, evaluation of these drugs in spheroid models that mimic an *in vivo* tumor environment and then further *in vivo* evaluations of these drugs in mouse xenograft and patient-derived xenograft models should be carried out as essential pre-clinical evaluations of drug efficacy.

The four compounds identified in this project show promise as novel, more selective drugs for CREB3L1-deficient breast cancer, especially TNBC. Additionally, a clearer understanding of the selective mechanisms used by these compounds in CREB3L1-deficient breast cancer can guide the development and optimization of additional novel drugs. The use of more targeted therapies like the treatments identified in this study will address the current shortcomings of "unselected" therapies for TNBC like chemotherapy that is not completely effective, possibly due to chemoresistance, and will help to address the treatment of breast cancers of other subtypes

particularly luminal A breast cancer that progresses after initial treatment failure (Martin, Smith & Tomlinson, 2014). The *in vitro* data collected in this project will lay the foundation for the collection of future *in vivo* data, and success in these experiments would warrant pursuit of clinical trials to swiftly implement the use of these drugs to benefit the ~30% of breast cancer patients and ~90% of TNBC patients whose cancers are CREB3L1-deficient.

5. CONCLUSION

In conclusion, we have identified multiple compounds that show promise as novel selective treatments for CREB3L1-deficient breast cancer, especially for CREB3L1-deficient TNBC. Our results show a selective effectiveness of palbociclib isethionate, a CDK4/6 inhibitor, cladribine, a nucleoside analog, isolanid, a cardiac glycoside, and homoharringtonine, a protein synthesis inhibitor, in multiple CREB3L1-deficient TNBC cell lines. Additionally, cladribine showed selective cytotoxicity to metastatic TNBC cells and not non-tumorigenic breast MCF10A cells. Finally, we have demonstrated that combining doxorubicin with cladribine, homoharringtonine, or palbociclib isethionate may improve the effectiveness and decrease the off-target toxicity of current treatment regimens in the clinic as these drugs produced synergistic effects *in vitro*. The future investigation and eventual implementation of these therapies and possibly other compounds from the same drugs classes could improve upon current "unselected" therapies for patients with metastatic reoccurring breast cancers and TNBCs with CREB3L1-deficiency, through a more selective mechanism of action.

REFERENCES

Aherne GW, McDonald E, & Workman P (2002). Finding the needle in the haystack: why high-throughput screening is good for your health. Breast Cancer Research 4**:** 148.

Altieri DC (2019). Mitochondrial dynamics and metastasis. Cellular and Molecular Life Sciences 76**:** 827-835.

Chemotherapy For Breast Cancer. [Online] Available from https://www.cancer.org/cancer/breast-cancer/treatment/chemotherapy-for-breast-cancer.html#written_by. [Accessed: February 18 2020].

ATCC Breast Cancer Panel. [Online] Available from http://www.atcc.org/. [Accessed: 15 August 2019].

Anders L, Ke N, Hydbring P, Choi Yoon J, Widlund Hans R, Chick Joel M*, et al.* (2011). A Systematic Screen for CDK4/6 Substrates Links FOXM1 Phosphorylation to Senescence Suppression in Cancer Cells. Cancer Cell 20**:** 620-634.

André F, & Zielinski CC (2012). Optimal strategies for the treatment of metastatic triple-negative breast cancer with currently approved agents. Annals of Oncology 23**:** vi46-vi51.

Angus L, Beije N, Jager A, Martens JWM, & Sleijfer S (2017). ESR1 mutations: Moving towards guiding treatment decision-making in metastatic breast cancer patients. Cancer Treatment Reviews 52**:** 33-40.

Bardia A, Aftimos P, Bihani T, Anderson-Villaluz AT, Jung J, Conlan MG*, et al.* (2019). EMERALD: Phase III trial of elacestrant (RAD1901) vs endocrine therapy for previously treated ER+ advanced breast cancer. Future Oncol 15**:** 3209-3218.

Beadnell TC, Scheid AD, Vivian CJ, & Welch DR (2018). Roles of the mitochondrial genetics in cancer metastasis: not to be ignored any longer. Cancer metastasis reviews 37**:** 615-632.

Bergin ART, & Loi S (2019). Triple-negative breast cancer: recent treatment advances. F1000Res 8**:** F1000 Faculty Rev-1342.

Cameron D, Piccart-Gebhart MJ, Gelber RD, Procter M, Goldhirsch A, de Azambuja E*, et al.* (2017). 11 years' follow-up of trastuzumab after adjuvant chemotherapy in HER2-positive early breast cancer: final analysis of the HERceptin Adjuvant (HERA) trial. Lancet (London, England) 389**:** 1195-1205.

Canadian Cancer Statistics publication. [Online] Available from http://www.cancer.ca/en/cancer-information/cancer-101/canadian-cancer-statistics-publication/?region=sk&gclid=CjwKEAjwp56wBRDThOSZ3vqGzmESJABjNaj9XD4dMUy6q4FHyAE3LQYJaQO5Tz7j0cFxZBBQtgk0bxoCCOXw_wcB. [Accessed: November 18th 2019].

Survival Statistics for Breast Cancer. [Online] Available from http://www.cancer.ca/en/cancer-information/cancer-type/breast/prognosis-and-survival/survival-statistics/?region=bc. [Accessed: November 18th 2019].

Cancer Genome Atlas N (2012). Comprehensive molecular portraits of human breast tumours. Nature 490**:** 61-70.

Cardoso F, Senkus E, Costa A, Papadopoulos E, Aapro M, Andre F*, et al.* (2018). 4th ESO-ESMO International Consensus Guidelines for Advanced Breast Cancer (ABC 4). Ann Oncol 29**:** 1634-1657.

Carey LA, Dees EC, Sawyer L, Gatti L, Moore DT, Collichio F*, et al.* (2007). The triple negative paradox: primary tumor chemosensitivity of breast cancer subtypes. Clin Cancer Res 13**:** 2329-2334.

Chaney SG, & Sancar A (1996). DNA Repair: Enzymatic Mechanisms and Relevance to Drug Response. JNCI: Journal of the National Cancer Institute 88**:** 1346-1360.

Chao M-W, Chen T-H, Huang H-L, Chang Y-W, HuangFu W-C, Lee Y-C*, et al.* (2017). Lanatoside C, a cardiac glycoside, acts through protein kinase Cδ to cause apoptosis of human hepatocellular carcinoma cells. Scientific reports 7**:** 46134-46134.

Chen L, Waxman DJ, Chen D, & Kufe DW (1996). Sensitization of human breast cancer cells to cyclophosphamide and ifosfamide by transfer of a liver cytochrome P450 gene. Cancer research 56**:** 1331-1340.

Chen Q, Denard B, Lee C-E, Han S, Ye JS, & Ye J (2016). Inverting the Topology of a Transmembrane Protein by Regulating the Translocation of the First Transmembrane Helix. Molecular cell 63**:** 567-578.

Citron ML (2008). Dose-Dense Chemotherapy: Principles, Clinical Results and Future Perspectives. Breast Care (Basel) 3**:** 251-255.

Clark MA, Finkel R, Rey JA, & Whalen K (2012) *Pharmacology*. 5th Edition edn. Wolters Kluwer Health/Lippincott Williams & Wilkins: Baltimore, MD.

Coates AS, Winer EP, Goldhirsch A, Gelber RD, Gnant M, Piccart-Gebhart M*, et al.* (2015). Tailoring therapies--improving the management of early breast cancer: St Gallen International Expert Consensus on the Primary Therapy of Early Breast Cancer 2015. Annals of oncology : official journal of the European Society for Medical Oncology 26**:** 1533-1546.

de Jonge ME, Huitema ADR, Rodenhuis S, & Beijnen JH (2005). Clinical Pharmacokinetics of Cyclophosphamide. Clinical Pharmacokinetics 44**:** 1135-1164.

De Laurentiis M, Cianniello D, Caputo R, Stanzione B, Arpino G, Cinieri S*, et al.* (2010). Treatment of triple negative breast cancer (TNBC): current options and future perspectives. Cancer Treat Rev 36 Suppl 3**:** S80-86.

De Witt Hamer PC, Van Tilborg AA, Eijk PP, Sminia P, Troost D, Van Noorden CJ*, et al.* (2008). The genomic profile of human malignant glioma is altered early in primary cell culture and preserved in spheroids. Oncogene 27**:** 2091-2096.

DeMichele A, Clark AS, Tan KS, Heitjan DF, Gramlich K, Gallagher M*, et al.* (2015). CDK 4/6 Inhibitor Palbociclib (PD0332991) in Rb+ Advanced Breast Cancer: Phase II Activity, Safety, and Predictive Biomarker Assessment. Clinical Cancer Research 21**:** 995-1001.

Denard B, Lee C, & Ye J (2012). Doxorubicin blocks proliferation of cancer cells through proteolytic activation of CREB3L1. Elife 1**:** e00090.

Denard B, Pavia-Jimenez A, Chen W, Williams NS, Naina H, Collins R*, et al.* (2015). Identification of CREB3L1 as a Biomarker Predicting Doxorubicin Treatment Outcome. PLoS One 10**:** e0129233.

Dhingra P, Martinez-Fundichely A, Berger A, Huang FW, Forbes AN, Liu EM*, et al.* (2017). Identification of novel prostate cancer drivers using RegNetDriver: a framework for integration of genetic and epigenetic alterations with tissue-specific regulatory network. Genome Biology 18**:** 141.

Di Leo A, Curigliano G, Diéras V, Malorni L, Sotiriou C, Swanton C*, et al.* (2015). New approaches for improving outcomes in breast cancer in Europe. Breast 24**:** 321-330.

Dufey E, Sepúlveda D, Rojas-Rivera D, & Hetz C (2014). Cellular Mechanisms of Endoplasmic Reticulum Stress Signaling in Health and Disease. 1. An overview. American Journal of Physiology-Cell Physiology 307**:** C582-C594.

Egger SJ, Willson ML, Morgan J, Walker HS, Carrick S, Ghersi D*, et al.* (2017). Platinum-containing regimens for metastatic breast cancer. Cochrane Database Syst Rev 6**:** CD003374.

Ernst A, Hofmann S, Ahmadi R, Becker N, Korshunov A, Engel F*, et al.* (2009). Genomic and expression profiling of glioblastoma stem cell-like spheroid cultures identifies novel tumor-relevant genes associated with survival. Clin Cancer Res 15**:** 6541-6550.

Eroles P, Bosch A, Pérez-Fidalgo JA, & Lluch A (2012). Molecular biology in breast cancer: intrinsic subtypes and signaling pathways. Cancer Treat Rev 38**:** 698-707.

Feng Y-X, Jin DX, Sokol ES, Reinhardt F, Miller DH, & Gupta PB (2017). Cancer-specific PERK signaling drives invasion and metastasis through CREB3L1. Nature Communications 8**:** 1079.

Feng Y-x, Sokol ES, Del Vecchio CA, Sanduja S, Claessen JHL, Proia TA*, et al.* (2014). Epithelial-to-Mesenchymal Transition Activates PERK–eIF2α and Sensitizes Cells to Endoplasmic Reticulum Stress. Cancer Discovery 4**:** 702.

Fischbach C, Chen R, Matsumoto T, Schmelzle T, Brugge JS, Polverini PJ*, et al.* (2007). Engineering tumors with 3D scaffolds. Nat Methods 4**:** 855-860.

Foidart P, Yip C, Radermacher J, Blacher S, Lienard M, Montero-Ruiz L*, et al.* (2019). Expression of MT4-MMP, EGFR, and RB in Triple-Negative Breast Cancer Strongly Sensitizes Tumors to Erlotinib and Palbociclib Combination Therapy. Clinical Cancer Research 25**:** 1838.

Fribbens C, O'Leary B, Kilburn L, Hrebien S, Garcia-Murillas I, Beaney M*, et al.* (2016). Plasma ESR1 Mutations and the Treatment of Estrogen Receptor–Positive Advanced Breast Cancer. Journal of Clinical Oncology 34**:** 2961-2968.

Friedrich J, Ebner R, & Kunz-Schughart LA (2007). Experimental anti-tumor therapy in 3-D: spheroids--old hat or new challenge? Int J Radiat Biol 83**:** 849-871.

Fry DW, Harvey PJ, Keller PR, Elliott WL, Meade M, Trachet E*, et al.* (2004). Specific inhibition of cyclin-dependent kinase 4/6 by PD 0332991 and associated antitumor activity in human tumor xenografts. Molecular Cancer Therapeutics 3**:** 1427.

Gennari A, & D'Amico M (2011). Anthracyclines in the management of metastatic breast cancer: state of the art. European Journal of Cancer Supplements 9**:** 11-15.

Geutjes E-J, Tian S, Roepman P, & Bernards R (2012). Deoxycytidine kinase is overexpressed in poor outcome breast cancer and determines responsiveness to nucleoside analogs. Breast Cancer Research and Treatment 131**:** 809-818.

Ghersi D, Wilcken N, Simes J, & Donoghue E (2005). Taxane containing regimens for metastatic breast cancer. Cochrane Database Syst Rev**:** CD003366.

Ghosh S, Spagnoli GC, Martin I, Ploegert S, Demougin P, Heberer M*, et al.* (2005). Three-dimensional culture of melanoma cells profoundly affects gene expression profile: a high density oligonucleotide array study. J Cell Physiol 204**:** 522-531.

Gianni L, Eiermann W, Semiglazov V, Manikhas A, Lluch A, Tjulandin S*, et al.* (2010). Neoadjuvant chemotherapy with trastuzumab followed by adjuvant trastuzumab versus neoadjuvant chemotherapy alone, in patients with HER2-positive locally advanced breast cancer (the NOAH trial): a randomised controlled superiority trial with a parallel HER2-negative cohort. The Lancet 375**:** 377-384.

Gibbs JB (2000). Mechanism-Based Target Identification and Drug Discovery in Cancer Research. Science 287**:** 1969.

Gradishar WJ (2012). Taxanes for the treatment of metastatic breast cancer. Breast Cancer (Auckl) 6**:** 159-171.

Griffiths CL, & Olin JL (2012). Triple negative breast cancer: a brief review of its characteristics and treatment options. J Pharm Pract 25**:** 319-323.

Harada M, Morikawa M, Ozawa T, Kobayashi M, Tamura Y, Takahashi K*, et al.* (2019). Palbociclib enhances activin-SMAD-induced cytostasis in estrogen receptor-positive breast cancer. Cancer science 110**:** 209-220.

He L, Kulesskiy E, Saarela J, Turunen L, Wennerberg K, Aittokallio T*, et al.* (2018). Methods for High-throughput Drug Combination Screening and Synergy Scoring. Methods Mol Biol 1711**:** 351-398.

Holbeck SL, Collins JM, & Doroshow JH (2010). Analysis of Food and Drug Administration–Approved Anticancer Agents in the NCI60 Panel of Human Tumor Cell Lines. Molecular Cancer Therapeutics 9**:** 1451.

Honma Y, Kanazawa K, Mori T, Tanno Y, Tojo M, Kiyosawa H*, et al.* (1999). Identification of a novel gene, OASIS, which encodes for a putative CREB/ATF family transcription factor in the long-term cultured astrocytes and gliotic tissue. Brain Res Mol Brain Res 69**:** 93-103.

Hubalek M, Czech T, & Müller H (2017). Biological Subtypes of Triple-Negative Breast Cancer. Breast Care (Basel) 12**:** 8-14.

Huttunen KM, Raunio H, & Rautio J (2011). Prodrugs—from Serendipity to Rational Design. Pharmacological Reviews 63**:** 750.

Isakoff SJ (2010). Triple-negative breast cancer: role of specific chemotherapy agents. Cancer J 16**:** 53-61.

Jacquet E, Lardy-Cléaud A, Pistilli B, Franck S, Cottu P, Delaloge S*, et al.* (2018). Endocrine therapy or chemotherapy as first-line therapy in hormone receptor–positive HER2-negative metastatic breast cancer patients. European Journal of Cancer 95**:** 93-101.

Jamalzadeh L, Ghafoori H, Sariri R, Rabuti H, Nasirzade J, Hasani H*, et al.* (2016). Cytotoxic Effects of Some Common Organic Solvents on MCF-7, RAW-264.7 and Human Umbilical Vein Endothelial Cells. Avicenna J Med Biochem 4**:** 10-33453.

John NW, & John KB (2000). Molecular Targets in Cancer Drug Discovery: Cell-Based Profiling. Current Pharmaceutical Design 6**:** 473-483.

Kern KM, & Schroeder JR (2014). Comparison of Cantharidin Toxicity in Breast Cancer Cells to Two Common Chemotherapeutics. International Journal of Breast Cancer 2014.

Kollmann K, Heller G, Schneckenleithner C, Warsch W, Scheicher R, Ott Rene G*, et al.* (2013). A Kinase-Independent Function of CDK6 Links the Cell Cycle to Tumor Angiogenesis. Cancer Cell 24**:** 167-181.

Kondo N, Takahashi A, Ono K, & Ohnishi T (2010). DNA damage induced by alkylating agents and repair pathways. J Nucleic Acids 2010**:** 543531-543531.

Kondo S, Hino SI, Saito A, Kanemoto S, Kawasaki N, Asada R*, et al.* (2012). Activation of OASIS family, ER stress transducers, is dependent on its stabilization. Cell Death Differ 19**:** 1939-1949.

Lander ES, Linton LM, Birren B, Nusbaum C, Zody MC, Baldwin J*, et al.* (2001). Initial sequencing and analysis of the human genome. Nature 409**:** 860-921.

Lehmann BD, Bauer JA, Chen X, Sanders ME, Chakravarthy AB, Shyr Y*, et al.* (2011). Identification of human triple-negative breast cancer subtypes and preclinical models for selection of targeted therapies. J Clin Invest 121**:** 2750-2767.

Lotfi K, Juliusson G, & Albertioni F (2003). Pharmacological Basis for Cladribine Resistance. Leukemia & Lymphoma 44**:** 1705-1712.

Lü S, & Wang J (2014). Homoharringtonine and omacetaxine for myeloid hematological malignancies. J Hematol Oncol 7**:** 2-2.

Malyutina A, Majumder MM, Wang W, Pessia A, Heckman CA, & Tang J (2019). Drug combination sensitivity scoring facilitates the discovery of synergistic and efficacious drug combinations in cancer. PLOS Computational Biology 15**:** e1006752.

Martin HL, Smith L, & Tomlinson DC (2014). Multidrug-resistant breast cancer: current perspectives. Breast Cancer (Dove Med Press) 6**:** 1-13.

Marzo I, Pérez-Galán P, Giraldo P, Rubio-Félix D, Anel A, & Naval J (2001). Cladribine induces apoptosis in human leukaemia cells by caspase-dependent and -independent pathways acting on mitochondria. Biochem J 359**:** 537-546.

Matutino A, Amaro C, & Verma S (2018). CDK4/6 inhibitors in breast cancer: beyond hormone receptor-positive HER2-negative disease. Ther Adv Med Oncol 10**:** 1758835918818346.

Melber A, & Haynes CM (2018). UPRmt regulation and output: a stress response mediated by mitochondrial-nuclear communication. Cell Research 28**:** 281-295.

Mellor P, Deibert L, Calvert B, Bonham K, Carlsen SA, & Anderson DH (2013). CREB3L1 is a metastasis suppressor that represses expression of genes regulating metastasis, invasion, and angiogenesis. Mol Cell Biol 33**:** 4985-4995.

Milanti A, Metsälä E, & Hannula L (2016). Reducing psychological distress in patients undergoing chemotherapy. Br J Nurs 25**:** S25-30.

Minotti G, Menna P, Salvatorelli E, Cairo G, & Gianni L (2004). Anthracyclines: Molecular Advances and Pharmacologic Developments in Antitumor Activity and Cardiotoxicity. Pharmacological Reviews 56**:** 185.

Pahl HL (1999). Signal transduction from the endoplasmic reticulum to the cell nucleus. Physiol Rev 79**:** 683-701.

Pernas S, & Tolaney SM (2019). HER2-positive breast cancer: new therapeutic frontiers and overcoming resistance. Ther Adv Med Oncol 11**:** 1758835919833519.

Perou CM, Sørlie T, Eisen MB, van de Rijn M, Jeffrey SS, Rees CA*, et al.* (2000). Molecular portraits of human breast tumours. Nature 406**:** 747-752.

Piro LD, Carrera CJ, Carson DA, & Beutler E (1990). Lasting Remissions in Hairy-Cell Leukemia Induced by a Single Infusion of 2-Chlorodeoxyadenosine. New England Journal of Medicine 322**:** 1117-1121.

Pommier Y, Leo E, Zhang H, & Marchand C (2010). DNA Topoisomerases and Their Poisoning by Anticancer and Antibacterial Drugs. Chemistry & Biology 17**:** 421-433.

Porporato PE, Filigheddu N, Pedro JMB-S, Kroemer G, & Galluzzi L (2018). Mitochondrial metabolism and cancer. Cell Research 28**:** 265-280.

Prat A, Pineda E, Adamo B, Galvan P, Fernandez A, Gaba L*, et al.* (2015). Clinical implications of the intrinsic molecular subtypes of breast cancer. Breast 24 Suppl 2**:** S26-35.

R Core Team (2019). R: A language and environment for statistical computing. R Foundation for Statistical Computing: Vienna, Austria.

Raspé E, Coulonval K, Pita JM, Paternot S, Rothé F, Twyffels L*, et al.* (2017). CDK4 phosphorylation status and a linked gene expression profile predict sensitivity to palbociclib. EMBO Mol Med 9**:** 1052-1066.

Reddy D, Kumavath R, Ghosh P, & Barh D (2019). Lanatoside C Induces G2/M Cell Cycle Arrest and Suppresses Cancer Cell Growth by Attenuating MAPK, Wnt, JAK-STAT, and PI3K/AKT/mTOR Signaling Pathways. Biomolecules 9.

Reinert T, Gonçalves R, & Bines J (2018). Implications of ESR1 Mutations in Hormone Receptor-Positive Breast Cancer. Current Treatment Options in Oncology 19**:** 24.

Reynolds CP, Maurer BJ, & Kolesnick RN (2004). Ceramide synthesis and metabolism as a target for cancer therapy. Cancer Lett 206**:** 169-180.

Robinson TJW, Liu JC, Vizeacoumar F, Sun T, Maclean N, Egan SE*, et al.* (2013). RB1 status in triple negative breast cancer cells dictates response to radiation treatment and selective therapeutic drugs. PloS one 8**:** e78641-e78641.

Robson M, Goessl C, & Domchek S (2017). Olaparib for Metastatic Germline BRCA-Mutated Breast Cancer. N Engl J Med 377**:** 1792-1793.

Rose M, Schubert C, Dierichs L, Gaisa NT, Heer M, Heidenreich A*, et al.* (2014). OASIS/CREB3L1 is epigenetically silenced in human bladder cancer facilitating tumor cell spreading and migration in vitro. Epigenetics 9**:** 1626-1640.

Rossing M, Østrup O, Majewski WW, Kinalis S, Jensen M-B, Knoop A*, et al.* (2018). Molecular subtyping of breast cancer improves identification of both high and low risk patients. Acta Oncologica 57**:** 58-66.

Senchenkov A, Litvak DA, & Cabot MC (2001). Targeting ceramide metabolism--a strategy for overcoming drug resistance. J Natl Cancer Inst 93**:** 347-357.

Sherr CJ, & McCormick F (2002). The RB and p53 pathways in cancer. Cancer Cell 2**:** 103-112.

Sigal DS, Miller HJ, Schram ED, & Saven A (2010). Beyond hairy cell: the activity of cladribine in other hematologic malignancies. Blood 116**:** 2884-2896.

Slamon DJ, Leyland-Jones B, Shak S, Fuchs H, Paton V, Bajamonde A*, et al.* (2001). Use of Chemotherapy plus a Monoclonal Antibody against HER2 for Metastatic Breast Cancer That Overexpresses HER2. New England Journal of Medicine 344**:** 783-792.

Sørlie T, Perou CM, Tibshirani R, Aas T, Geisler S, Johnsen H*, et al.* (2001). Gene expression patterns of breast carcinomas distinguish tumor subclasses with clinical implications. Proceedings of the National Academy of Sciences in the United States of America 98**:** 10869-10874.

Tang R, Faussat A-M, Majdak P, Marzac C, Dubrulle S, Marjanovic Z*, et al.* (2006). Semisynthetic homoharringtonine induces apoptosis via inhibition of protein synthesis and triggers rapid myeloid cell leukemia-1 down-regulation in myeloid leukemia cells. Molecular Cancer Therapeutics 5**:** 723.

Tassone P, Tagliaferri P, Perricelli A, Blotta S, Quaresima B, Martelli ML*, et al.* (2003). BRCA1 expression modulates chemosensitivity of BRCA1-defective HCC1937 human breast cancer cells. British journal of cancer 88**:** 1285-1291.

Thorn CF, Oshiro C, Marsh S, Hernandez-Boussard T, McLeod H, Klein TE*, et al.* (2011). Doxorubicin pathways: pharmacodynamics and adverse effects. Pharmacogenet Genomics 21**:** 440-446.

Toogood PL, Harvey PJ, Repine JT, Sheehan DJ, VanderWel SN, Zhou H*, et al.* (2005). Discovery of a Potent and Selective Inhibitor of Cyclin-Dependent Kinase 4/6. Journal of Medicinal Chemistry 48**:** 2388-2406.

Tsesmetzis N, Paulin CBJ, Rudd SG, & Herold N (2018). Nucleobase and Nucleoside Analogues: Resistance and Re-Sensitisation at the Level of Pharmacokinetics, Pharmacodynamics and Metabolism. Cancers (Basel) 10**:** 240.

Turner NC, Neven P, Loibl S, & Andre F (2017). Advances in the treatment of advanced estrogen-receptor-positive breast cancer. Lancet 389**:** 2403-2414.

Vijayaraghavan S, Karakas C, Doostan I, Chen X, Bui T, Yi M*, et al.* (2017). CDK4/6 and autophagy inhibitors synergistically induce senescence in Rb positive cytoplasmic cyclin E negative cancers. Nature communications 8**:** 15916-15916.

Vinci M, Gowan S, Boxall F, Patterson L, Zimmermann M, Court W*, et al.* (2012). Advances in establishment and analysis of three-dimensional tumor spheroid-based functional assays for target validation and drug evaluation. BMC Biology 10**:** 29.

Voelker R (2019). Caution Accompanies New MS Drug. JAMA 321**:** 1659-1659.

Wahba HA, & El-Hadaad HA (2015). Current approaches in treatment of triple-negative breast cancer. Cancer Biol Med 12**:** 106-116.

Wang S, & Kaufman RJ (2012). The impact of the unfolded protein response on human disease. J Cell Biol 197**:** 857-867.

Ward AK, Mellor P, Smith SE, Kendall S, Just NA, Vizeacoumar FS*, et al.* (2016). Epigenetic silencing of CREB3L1 by DNA methylation is associated with high-grade metastatic breast cancers with poor prognosis and is prevalent in triple negative breast cancers. Breast Cancer Res 18**:** 12.

Weaver VM, Petersen OW, Wang F, Larabell CA, Briand P, Damsky C*, et al.* (1997). Reversion of the malignant phenotype of human breast cells in three-dimensional culture and in vivo by integrin blocking antibodies. J Cell Biol 137**:** 231-245.

Witkiewicz AK, Chung S, Brough R, Vail P, Franco J, Lord CJ*, et al.* (2018). Targeting the Vulnerability of RB Tumor Suppressor Loss in Triple-Negative Breast Cancer. Cell Rep 22**:** 1185-1199.

Witkiewicz AK, & Knudsen ES (2014). Retinoblastoma tumor suppressor pathway in breast cancer: prognosis, precision medicine, and therapeutic interventions. Breast cancer research : BCR 16**:** 207-207.

Workman P (2001). Scoring a bull's-eye against cancer genome targets. Current Opinion in Pharmacology 1**:** 342-352.

Wu C, Zhao A, Tan T, Wang Y, & Shen Z (2019). Overexpression of microRNA-620 facilitates the resistance of triple negative breast cancer cells to gemcitabine treatment by targeting DCTD. Exp Ther Med 18**:** 550-558.

Yadav B, Wennerberg K, Aittokallio T, & Tang J (2015). Searching for Drug Synergy in Complex Dose-Response Landscapes Using an Interaction Potency Model. Comput Struct Biotechnol J 13**:** 504-513.

Yakhni M, Briat A, El Guerrab A, Furtado L, Kwiatkowski F, Miot-Noirault E*, et al.* (2019). Homoharringtonine, an approved anti-leukemia drug, suppresses triple negative breast cancer growth through a rapid reduction of anti-apoptotic protein abundance. Am J Cancer Res 9**:** 1043-1060.

Zou Y, Li Q, Jiang L, Guo C, Li Y, Yu Y*, et al.* (2016). DNA Hypermethylation of CREB3L1 and Bcl-2 Associated with the Mitochondrial-Mediated Apoptosis via PI3K/Akt Pathway in Human BEAS-2B Cells Exposure to Silica Nanoparticles. PLOS ONE 11**:** e0158475.

APPENDIX

R script

```
###
# Drug synergy for R. Plett high-throughput screen
# Written by S. Austin Hammond, 9 Mar 2020
# University of Saskatchewan NGSF
###

require(synergyfinder)
set.seed(1)

## example data
#data("mathews_screening_data")
#set.seed(1)
#dose.response.mat <- ReshapeData(mathews_screening_data,data.type = "viability",impute =
TRUE,noise = TRUE,correction = "non")
#PlotDoseResponse(dose.response.mat)

## Doxo HCC1806
# load data and create output directories
x <- read.csv("Doxorubicin_Other_Drugs_HCC1806.csv", stringsAsFactors=FALSE)
system2("mkdir", args="-p doxo_HCC1806/dose_response")
system2("mkdir", args="-p doxo_HCC1806/2D")
system2("mkdir", args="-p doxo_HCC1806/3D")

# make dose-response matrix
dose.response.mat <- ReshapeData(x, data.type = "viability", impute = TRUE, noise = TRUE,
   correction = "part")

# plot dose-response and move plots
PlotDoseResponse(dose.response.mat, save.file = TRUE)
system2("mv", args="*.pdf ./doxo_HCC1806/dose_response/")

# calculate synergy
synergy.score <- CalculateSynergy(data = dose.response.mat, method = "ZIP")

# make 2D and 3D synergy plots, and move to prevent overwriting
PlotSynergy(synergy.score, type = "2D", save.file = TRUE, len = 10,
   legend.start = -50, legend.end = 50)
system2("mv", args="*.pdf ./doxo_HCC1806/2D/")

PlotSynergy(synergy.score, type = "3D", save.file = TRUE, len = 10,
   legend.start = -50, legend.end = 50)
```

```
system2("mv", args="*.pdf ./doxo_HCC1806/3D/")

## Doxo CREB3L1 CL3
# load data and create output directories
x <- read.csv("Doxorubicin_Other_Drugs_HCC1806_HACREB3L1_Cl3.csv",
stringsAsFactors=FALSE)
system2("mkdir", args="-p doxo_CREB3L1/dose_response")
system2("mkdir", args="-p doxo_CREB3L1/2D")
system2("mkdir", args="-p doxo_CREB3L1/3D")

# make dose-response matrix
dose.response.mat <- ReshapeData(x, data.type = "viability", impute = TRUE, noise = TRUE,
   correction = "non")

# plot dose-response and move plots
PlotDoseResponse(dose.response.mat, save.file = TRUE)
system2("mv", args="*.pdf ./doxo_CREB3L1/dose_response/")

# calculate synergy
synergy.score <- CalculateSynergy(data = dose.response.mat, method = "ZIP")

# make 2D and 3D synergy plots, and move to prevent overwriting
PlotSynergy(synergy.score, type = "2D", save.file = TRUE, len = 10,
   legend.start = -50, legend.end = 50)
system2("mv", args="*.pdf ./doxo_CREB3L1/2D/")

PlotSynergy(synergy.score, type = "3D", save.file = TRUE, len = 10,
   legend.start = -50, legend.end = 50)
system2("mv", args="*.pdf ./doxo_CREB3L1/3D/")

## Paclitaxel HCC1806
x <- read.csv("Paclitaxel_Other_Drugs_HCC1806.csv", stringsAsFactors=FALSE)
system2("mkdir", args="-p pacl_HCC1806/dose_response")
system2("mkdir", args="-p pacl_HCC1806/2D")
system2("mkdir", args="-p pacl_HCC1806/3D")

# make dose-response matrix
dose.response.mat <- ReshapeData(x, data.type = "viability", impute = TRUE, noise = TRUE,
   correction = "non")

# plot dose-response and move plots
PlotDoseResponse(dose.response.mat, save.file = TRUE)
system2("mv", args="*.pdf ./pacl_HCC1806/dose_response/")

# calculate synergy
synergy.score <- CalculateSynergy(data = dose.response.mat, method = "ZIP")
```

```
# make 2D and 3D synergy plots, and move to prevent overwriting
PlotSynergy(synergy.score, type = "2D", save.file = TRUE, len = 10,
   legend.start = -50, legend.end = 50)
system2("mv", args="*.pdf ./pacl_HCC1806/2D/")

PlotSynergy(synergy.score, type = "3D", save.file = TRUE, len = 10,
   legend.start = -50, legend.end = 50)
system2("mv", args="*.pdf ./pacl_HCC1806/3D/")

# Paclitaxel CREB3L1 CL3
x <- read.csv("Paclitaxel_Other_Drugs_HCC1806_HACREB3L1_Cl3.csv",
stringsAsFactors=FALSE)
system2("mkdir", args="-p pacl_CREB3L1/dose_response")
system2("mkdir", args="-p pacl_CREB3L1/2D")
system2("mkdir", args="-p pacl_CREB3L1/3D")

# make dose-response matrix
dose.response.mat <- ReshapeData(x, data.type = "viability", impute = TRUE, noise = TRUE,
   correction = "non")

# plot dose-response and move plots
PlotDoseResponse(dose.response.mat, save.file = TRUE)
system2("mv", args="*.pdf ./pacl_CREB3L1/dose_response/")

# calculate synergy
synergy.score <- CalculateSynergy(data = dose.response.mat, method = "ZIP")

# make 2D and 3D synergy plots, and move to prevent overwriting
PlotSynergy(synergy.score, type = "2D", save.file = TRUE, len = 10,
   legend.start = -50, legend.end = 50)
system2("mv", args="*.pdf ./pacl_CREB3L1/2D/")

PlotSynergy(synergy.score, type = "3D", save.file = TRUE, len = 10,
   legend.start = -50, legend.end = 50)
system2("mv", args="*.pdf ./pacl_CREB3L1/3D/")
```